



UCGE Reports
Number 20232

Department of Geomatics Engineering

**The Feasibility of Replacing Precise Levelling with GPS
for Permafrost Deformation Monitoring**

(URL: <http://www.geomatics.ucalgary.ca/links/GradTheses.html>)

by

Li Sheng

October 2005



UNIVERSITY OF CALGARY

THE FEASIBILITY OF REPLACING PRECISE LEVELLING WITH GPS FOR
PERMAFROST DEFORMATION MONITORING

by

Li Sheng

A THESIS

SUBMITTED TO THE FACULTY OF GRADUATE STUDIES
IN PARTIAL FULFILMENT OF THE REQUIREMENTS FOR THE
DEGREE OF MASTER OF SCIENCE IN ENGINEERING

DEPARTMENT OF GEOMATICS ENGINEERING

CALGARY, ALBERTA

October, 2005

© Li Sheng 2005

ABSTRACT

Although several investigations have reported the ability to use GPS to provide several millimetres accuracy to monitor permanent objects, the attainable position accuracy in high latitude areas (~70 degrees) has not been investigated in detail. The challenges for GPS in this area mainly concern two aspects. First, in the far north, no satellites pass overhead of the observation stations, in which case the satellite geometry is not as good compared to mid-latitude cases. Second, increased ionospheric activity is observed in the north compared to mid-latitudes, and this is particularly exacerbated by the low satellite elevations and subsequent increased path-length of the GPS signals. This leads to increased loss of signal (cycle slips) as well as path delays due to the ionospheric activity. In order to investigate the highest attainable accuracy of GPS in the far north, especially for the height component, two GPS campaigns were carried out in a selected area in the summers of 2003 and 2004. Data was then processed to assess the influence of different error sources, such as antenna phase centre variation (PCV), increased ionospheric activity, tropospheric delay, and multipath effects. Precise levelling data was collected on the same benchmarks that were occupied using GPS. All the analysis is based on a comparison between the estimated heights from GPS and the measured heights using precise levelling. By studying the feasibility of replacing precise levelling with GPS for permafrost deformation monitoring, the attainable accuracy of 'GPS levelling' is investigated. At the same time, this research will quantify the stability of monuments in permafrost, and this knowledge will play an important role not only in the future analysis of movement due to oil and gas extraction and hence its affect on the environment, but

also in the analysis of climate change effects in permafrost areas where stable stations over long periods are required.

By analyzing different types of monuments, it was found that the use of solid ground rods founded at 5.5 m or deeper will display a similar movement pattern which is independent of the geological conditions in which they are founded. By processing the collected GPS data using different strategies and the analysis of the impact of different error sources, the best strategy for both data collection and data processing has been developed. With this developed strategy, the attainable accuracy of GPS positioning in the height component was found to be 2 mm with a standard deviation of 8 mm. After applying the error propagation law, the combination of the developed best strategy for ‘GPS levelling’ and the best monument type is capable of detecting 1 cm movement. After applying the same congruency analysis (95% confidence, Fisher test for 1D and assuming a known probability density function [PDF]), the combination of ‘GPS levelling’ with this 1σ observation accuracy of 1 cm is only capable of finding 28 mm movement on an annual basis. It will take 5-6 years to find movement of 5 mm per year. But it can still be used as an early warning system for subsidence higher than expected.

ACKNOWLEDGEMENTS

I would like to express my deepest appreciation for my supervisors, Drs. Matthew Tait and Elizabeth Cannon, for their continued support and encouragement throughout my M.Sc. programme. Without their support, both academic and financial, this thesis would not have been possible.

Second, I would like to thank Matthew Vanderwey, Changbae Yoon, Rinske Van Gosliga, and Jeff Williams for helping collect the data used for this thesis. The experience in the far north of Canada together with all of you will always be a sweet memory in my life.

Third, I would like to acknowledge my friends and fellow graduate students for their all kinds of help: Kongze Chen, Robert Radovanovic, Zhizao Liu, Yufeng Zhang, Haitao Zhang, Qiaoping Zhang, Chen Xu, Bo Zheng, Junjie, Liu, Xiaohong Zhang, Chaochao Wang and Xiaobing Shen, to name a few.

Fourth, I would like to thank Dr. Luiz Fortes from The Brazilian Institute of Geography and Statistics, Dr. Andreas Wieser from Graz University of Technology and Mr. Pierre Fridez from Astronomical Institute University of Berne for answering my questions all the time. They are very valuable contacts for my research.

Last, and most of all, I would like to thank my parents and my sister, who makes everything meaningful.

TABLE OF CONTENTS

APPROVAL PAGE	ii
ABSTRACT	iii
ACKNOWLEDGEMENTS	v
TABLE OF CONTENTS	vi
LIST OF FIGURES	ix
LIST OF TABLES	xii
LIST OF NOTATIONS	xiv
LIST OF ACRONYMS	xvi
CHAPTER 1	1
INTRODUCTION	1
1.1 Introduction.....	1
1.2 Research Objective	6
1.3 Thesis Outline	8
CHAPTER 2	10
GPS, PRECISE LEVELLING AND THEIR ERROR SOURCES	10
2.1 Global Positioning System Overview.....	10
2.2 GPS Time Frame.....	13
2.3 GPS Observations	17
2.4 GPS Error Sources	21
2.4.1 Satellite Orbit Error.....	22
2.4.2 Tropospheric Error.....	24

2.4.3 Ionospheric Error	25
2.4.4 Multipath.....	29
2.5 Precise Levelling and its Error Sources	30
2.6 Deformation Monitoring Overview	35
CHAPTER 3	38
PROJECT BACKGROUND	38
3.1 Subsidence Issue in the Target Area.....	38
3.2 Feasibility Study into Monitoring Deformation in the Niglintgak Region of the Mackenzie Delta	41
3.2.1 <i>Precise Levelling</i>	41
3.2.2 <i>DINSAR</i>	42
3.2.3 <i>CDGPS</i>	43
3.2.4 <i>DGPS</i>	44
3.3 Project Objectives.....	51
CHAPTER 4	53
PRE-RESEARCH FOR THE TARGET AREA.....	53
4.1 Antenna Phase Centre Variation.....	53
4.1.1 Introduction.....	53
4.1.2 Antenna PCV Experiment.....	58
4.2 Multipath.....	63
CHAPTER 5	76
EXPERIMENTAL DESIGN AND DATA PROCESSING	76
5.1 Data Collection in summer 2003	77

5.2 Data Collection in summer 2004	80
5.3 Long-term Stability of Different Survey Monument in Permafrost	82
5.4 Initial Processing.....	84
5.5 Antenna Phase Centre Variation.....	85
5.6 Ionosphere and Satellite Geometry	87
5.6.1 Influence of Enhanced Ionospheric Activities on GPS Receiver Tracking Performance	87
5.6.2 Influence of Enhanced Ionospheric Activities on GPS Positioning Accuracy	91
5.7 Tropospheric Delay Estimation Strategy	95
5.8 Multipath.....	100
5.9 Repeatability Analysis	105
5.10 Developing the Best Strategy.....	107
CHAPTER 6	111
CONCLUSIONS AND RECOMMENDATIONS	111
REFERENCES	116
APPENDIX 1: A SUMMARY OF THE TYPE OF MONUMENT	129

LIST OF FIGURES

Figure 2.1 World PDOP assessment.....	12
Figure 2.2 Double difference concepts.....	20
Figure 2.3 Predicted sunspot number for the current solar cycle	27
Figure 2.4 Typical setup for precise levelling	31
Figure 2.5 Relationship between ellipsoidal, geoid and orthometric heights.....	33
Figure 2.6 A simple model illustrating the variation of gravity anomaly.....	34
Figure 3.1 The distribution of permafrost in Canada and areas of the Niglintgak and Taglu gas reservoirs (Tait <i>et al</i> , 2004).....	39
Figure 3.2 The subsidence bowl anticipated to result from gas extraction from the Niglintgak Island lease (Tait <i>et al</i> , 2004).....	40
Figure 3.3 DOP values and number of available satellites generated from GPS planning tool (top) and GPS data processing (middle) and skyplot (bottom) over 24 hours at INVK station.....	46
Figure 3.4 DOP values and number of available satellites generated from GPS planning tool (top) and GPS data processing (middle) and skyplot (bottom) over 24 hours at PRDS station.....	48
Figure 3.5 Kp index for a quiet day, 14 July, 2004	50
Figure 3.6 Kp index for a day of significant ionospheric disturbance, 25 July, 2004	50
Figure 4.1 PCV description of a GPS antenna.....	55
Figure 4.2 Experimental set-ups for antenna PCV correction error analysis	59
Figure 4.3 Flowchart diagram of multipath mitigation algorithm (Radovanovic, 2000) .	66

Figure 4.4 Receiver clock drift for an Ashtech Z-12 receiver	68
Figure 4.5 Two Day's DD residuals generated by fixing both N1 and S1's coordinates to Day 1's station coordinates estimation	70
Figure 4.6 Multipath correlation coefficients between two consecutive Days.....	71
Figure 4.7 DD residuals for Day 1, Day 2 and that of Day 2 after applying the multipath mitigation algorithm.....	72
Figure 4.8 Power spectral density plots before and after applying the multipath mitigation algorithm.....	73
Figure 5.1 The Inuvik test-bed (Tait <i>et al</i> , 2004).....	78
Figure 5.2 Test-bed with a geodetic GPS receiver set over benchmark 623 (2004 campaign). Vegetation in the area was moderately-dense small trees and bushes, with moss below.....	80
Figure 5.3 Plot of height change with time for benchmark 625 with a missing epoch in the summer 1994 for a) 1987-1995 and b) 1987-2004 (Tait <i>et al</i> , 2004).....	83
Figure 5.4 Auroral Region	88
Figure 5.5 Plots of ionospheric activity from Yellowknife recording station for (a) July 14 and (b) July 25 2004 (Natural Resources Canada website http://www.geolab.nrcan.gc.ca/myservlet/geomag/magnetogram/dataplot_geomag_e.jsp)	93
Figure 5.6 Estimated station height for T625 (above) and T631 (bottom) using different tropospheric parameter estimation strategies.....	97
Figure 5.7 Estimated station height differences for two baselines (INVK to T625 and INVK to T631) using different tropospheric parameter estimation strategies	98

Figure 5. 8 Smoothed residuals for four 12-hour sessions on one station within the tree-line environment 101

Figure 5.9 Day-to-day correlation from the residuals..... 101

Figure 5.10 IF fixed DD residuals for two consecutive days and that of the Day 2 after applying the multipath mitigation algorithm 104

LIST OF TABLES

Table 4.1 Differences in height between pillars (m) estimated with three different antenna configurations using L1 and IF processing strategies with both antenna PCV corrections switched on and off.....	61
Table 4.2 The amplification of noise and multipath for an IF solution compared to an L1 solution (Cannon and Lachapelle, 2003)	62
Table 4.3 Statistics of the DD residuals for Day 1, Day 2 and that of Day 2 after applying the multipath mitigation algorithm	72
Table 4.4 Measured station height differences from 12 hour data	74
Table 4.5 Measured station height differences from 1 hour data	74
Table 5.1 Summary of 2003 / 2004 DGPS campaign and external data collection.....	82
Table 5.2 Effects of various error sources on the standard processing strategy for the 15 km baselines (24 baselines in total) measured in 2003	84
Table 5.3 Station height estimation repeatability for Benchmark 624 (mixed antennas), 635 (mixed antennas), 640 (similar antennas)	86
Table 5.4 Marked unpaired L1/L2 observations and cycle slips reported from	90
Table 5.5 Effect of the variation in cut-off angle, and the use of the EDW, for two 130 km baselines observed on July 14 and July 25 2004. Estimates of height and the mean and standard deviations between these and weekly IGS averages results are shown.....	94
Table 5.6 Tested tropospheric delay estimation strategies	96

Table 5.7 Four days' station coordinates from Bernese for station T631 using mode 3 in Table 5.6. The coordinates for Days 2-4 were given in the difference with respect to the coordinates for Day 1.....	106
Table 5.8 Summarized results for the comparison between GPS height solution and the external accuracy measures for 2003/2004 campaign	108
Table 5.9 Variation in accuracy (and standard deviation of grouped baselines) with occupation length for days of low and high ionospheric activity.	109

LIST OF NOTATIONS

a	the semi-major axis of satellite orbit
e	the eccentricity of satellite orbit
E_k	the mean anomaly of satellite orbit
a_0	the broadcast polynomial coefficients
a_1	the broadcast polynomial coefficients
a_2	the broadcast polynomial coefficients
P	the measured pseudorange in metres
φ	the measured carrier phase in metres
ρ	the true geometric range in metres
c	the speed of light in vacuum in m/s
ΔT^s	the satellite clock error in seconds
ΔT_r	the receiver clock error in seconds
T_r	the signal reception time at the receiver
T^s	the signal transmit time at the satellite
$T^{s'}$	the corrected transmit time
t	the observation epoch
t_{oc}	the epoch to which the coefficients refer
d_{orb}	the satellite orbit error in metres
d_{trop}	the tropospheric delay in metres

d_{ion}	the ionospheric delay in metres
λ	the signal wavelength in m/cycle
N	the integer ambiguity in cycles
$d_{multipath(P)}$	the multipath effect on pseudorange in metres
$d_{multipath(\varphi)}$	the multipath effect on carrier phase in metres
ε_p	the pseudorange measurement noise in metres
ε_φ	the carrier phase measurement noise in metres
μ	the gravitational constant
r^s	the satellite position vector at transmission time
r_r	the receiver position vector at reception time
ω	the earth rotation rate
τ	the transit time of the signal
$\nabla\Delta$	the double difference operator
db	the baseline error
b	the baseline length
I	the first-order carrier phase error caused by the ionosphere
h	the ellipsoidal height
H	the orthometric height
N	the geoidal undulation
δt_{rec}^{est1}	the estimated receiver clock offset on day one
m	the multipath at each receiver for each satellite in metres
n	the carrier phase noise

LIST OF ACRONYMS

ARP	Antenna Reference Point
C/A	Coarse Acquisition
CDGPS	Continuous Differential Global Positioning System
DD	Double Difference
DGPS	Differential GPS
DINSAR	Differential Radar Interferometry
DoD	Department of Defense
DOP	Dilution of Precision
DRMS	Distance Root Mean Square
EDW	Elevation Dependent Weighting
GPS	Global Positioning System
GSD	Geodetic Survey Division
IF	Ionospheric Free
IGS	International GPS Service
NGS	National Geodetic Survey
NRCan	Natural Resources Canada
OCS	Operational Control System
PCV	Phase Centre Variation
PDF	Probability Density Function
PLL	Phase Lock Loop
PPS	Precise Positioning Service
PRN	Pseudorandom Noise

RINEX	Receiver Independent Exchange Format
RMS	Root Mean Square
SA	Selective Availability
SNR	Signal-to-noise-ratio
SPS	Standard Positioning Service
SD	Standard Deviation
TEC	Total Electron Content

CHAPTER 1

INTRODUCTION

1.1 Introduction

Permafrost is a permanently frozen layer at variable depths below the surface in frigid regions of the earth (Muller, 1943). As permafrost thaws, soil volume reduces and subsidence takes place. If the thaw is large scale, water may drain away through the soil, and further subsidence can then take place. Moreover, oil and gas extraction in permafrost areas causes vertical surface displacements that have caused serious environmental issues, such as massive subsidence and land slides (Rempel, 1970). With the development of the oil and gas reserves in the Mackenzie River Delta of the Northwest Territories in Canada, the effects of extraction as the reservoirs depressurise and start to subside has to be carefully monitored.

The area of the Mackenzie River Delta is characterised by continuous permafrost to depths of up to 600 metres (Smith *et al*, 2001). The annual freeze/thaw of the active layer above the permafrost in this area has been observed at the 20 cm level depending on annual snow cover, atmospheric conditions, and vegetation growth, etc. (Mackay *et al*, 1979). In addition, with large portions of the islands between 0.5 and 1.0 m above sea level, the threat of subsidence leading to inundation of such areas could result in both a deepening of the active permafrost layer and the thawing of massive ice. This could potentially lead to subsidence in the order of tens of metres and the loss of substantial portions of land. The complex geological conditions plus remote location of the target area make the planning of a monitoring method very difficult.

A feasibility study into the most appropriate method for deformation monitoring in the target area has been carried out (Tait and Moorman, 2003). The subsidence predicted in this area will occur over a 25-year production cycle, with little movement anticipated in the first 10 years due to glacial pre-stressing and associated rebound. Assuming linear rates of subsidence over this 15 year period, a maximum yearly vertical displacement of around 2.7 cm would occur. A simple congruency analysis resulted in a 1σ observation accuracy of 9.7 mm being required to find significant movement in the central point on an annual basis (ibid). In addition, since the planimetric deformation may impose shear on production platforms, both vertical and planimetric measurements of deformation are desired.

Precise levelling is considered a very accurate method for monitoring subsidence, which is capable of providing accuracies up to 0.2 to 1 ppm of the length of the level route depending on the instrument used (Gili *et al*, 2000). A great deal of the area has large water bodies (>2 km), over which conducting precise levelling measurements is very difficult. In addition, it does not provide planimetric measurements. Therefore, precise levelling is not suitable for monitoring subsidence in the target area.

Based on the previous feasibility study of the most appropriate method for deformation monitoring in the target area, a monument-based DGPS method based on carrier phase processing was recommended. However, for any derived monument-based deformation monitoring method, the stability of the monument is a fundamental requirement, which must be quantified and taken into account in the total error budget (Kenselaar and Quadvlieg, 2001). For the target area which has relatively high heave/settlement, a

relatively large signal is expected. To establish a complete error budget for deformation monitoring in the target area, the long-term stability of different survey monuments in permafrost has to be characterized and quantified.

The Global Positioning System (GPS) was designed by the United States Department of Defense for the purpose of providing continuous and reliable position, velocity and timing information (Parkinson, 1996). The advantages of applying GPS to static applications mainly lies in the autonomous operation of the system and no requirement for survey sites to be inter-visible. Both of these issues have posed serious limitations to traditional survey techniques for precise positioning and deformation monitoring applications (Radovanovic, 2002).

However, many civil applications such as pipeline alignment, offshore oil exploration, and deformation monitoring require accuracies at the sub-metre, even centimetre levels. The position accuracy was further improved for the civilian users to the sub-decimetre through the development of differential techniques (Counselman *et al*, 1972), the use of carrier phase measurements (Collins, 1982) and the use of dual frequency measurements for ionospheric modelling (Raquet, 1998).

A critical aspect of carrier phase positioning is that ambiguities must be resolved to their integer values (Kaplan, 1996). Ambiguity resolution is the key point to achieving very high positioning accuracy. A lot of research has been dedicated to this special area and several algorithms have been developed including FASF (Chen and Lachapelle, 1994)

and LAMBDA (Teunissen and Tiberius, 1994). Although these algorithms provide a rapid ambiguity resolution capability, the success of ambiguity resolution is still limited by the observation errors in the carrier phase observations.

Another key factor that influences the carrier phase positioning accuracy is the difficulty in maintaining phase lock. This can result in non-continuous phase measurements, known as cycle slips. If a cycle slip occurred without detection, it would seriously contaminate the positioning accuracy. A cycle slip must be detected and repaired before the phase data is processed as double difference observations (Hofmann-Wellenhof *et al*, 2001).

Unlike pseudorange-based DGPS, where the dominant accuracy-limiting factor is code multipath and receiver noise, the dominant accuracy-limiting factors for carrier phase based positioning are the differential ionospheric and tropospheric errors and multipath. Through the development of different error modelling techniques the accuracy of the system has been shown to be at the centimetre level and at the millimetre-level in special cases (Beutler *et al*, 2001). This makes it possible to use GPS in demanding applications such as deformation monitoring where vertical movements of less than 1 cm may need to be detected on an annual basis (Tait, 2003).

Multipath effects have to be carefully treated in GPS data processing to achieve very high position accuracy. Several methods for effectively reducing the multipath effect have been developed. Examples include the mitigation of GPS code and carrier phase multipath effects using a multi-antenna system (Ray, 2000), multipath mitigation via day-

to-day correlation analysis (Radovanovic, 2000), and multipath mitigation by making use of signal-to-noise ratio information (Brunner *et al*, 1999). Moreover, by using a chocking antenna during field data collection, multipath effects can be greatly reduced (Lachapelle and Cannon, 2004).

Errors due to antenna phase centre variation (PCV) have also to be taken into consideration when high position accuracy is required (Wübbena *et al*, 2000). Broadly speaking, there are two types of antenna PCV calibration products available: relative PCV calibration and absolute PCV calibration. The most commonly used calibration type is relative PCV calibration, which is available on various web-sites such as NGS and IGS. These type of calibration results are relative to a reference antenna, whose PCV is set to zero. Due to the method adopted in this type of calibration, the results are site dependent, i.e. the results are subject to some site dependent effects such as multipath and the location of the test site (Mader, 1999). Compared with relative PCV calibration, absolute PCV calibration results are site, and reference antenna, independent, but are still not widely used because these types of products have not been published in the public domain.

For longer baselines (>10 km), some error sources will decorrelate with baseline length, such as satellite orbit error, tropospheric delay and ionospheric delay (Lachapelle, 2003). Considering the excellent quality of predicted or precise orbital data available through the International GPS Service (IGS) (less than 5 cm), it is not necessary to investigate the influence of orbital errors on GPS derived coordinates but rather use these services for

static and kinematic GPS surveys (Hartinger and Brunner, 1999). Errors due to tropospheric delay are very hard to model. Mostly, in GPS data processing, tropospheric delay is treated as an additional unknown parameter to be estimated along with the data itself (Beutler *et al*, 2001). For the ionospheric delay, it is deemed that by applying the ionospheric free combination from the dual frequency data, most of the error due to ionospheric delay can be eliminated (Lachapelle, 2003). However, at the same time, the errors due to receiver noise and multipath increases by more than three times (Lachapelle, 2003).

1.2 Research Objective

Although several investigations have reported the ability to use GPS to provide sub-centimetre accuracy to monitor permanent objects, the attainable position accuracy in high latitude areas (~70 degrees) has not been investigated in detail. The challenges for GPS in this area mainly concern two aspects. First, in the far north, no satellites pass overhead of the observation stations, in which case the satellite geometry is not as good compared to mid-latitude cases. Second, increased ionospheric activity is observed in the north compared to mid-latitudes, and this is particularly exacerbated by the low satellite elevations and subsequent increased path-length of the GPS signals. This may lead to increased loss of signal (cycle slips) as well as path delays due to ionospheric activity (Skone *et al*, 2001).

The goal of this research is to investigate the attainable accuracy of GPS, especially for the height component, in the far north. In order to achieve the aforementioned objectives, the following sub-areas are investigated:

- The long-term stability of different survey monuments in permafrost;
- The most appropriate data collection and processing schemes using state-of-the-art GPS data processing software (Bernese) for GPS data collected in the far north of Canada. This processing scheme, including the selection of the observation cut-off angle, the tropospheric model to be used, and the residual tropospheric delay estimation method, will be developed and applied to give a general idea about the attainable accuracy of ‘GPS levelling’ for the target area.
- A multipath mitigation via a day-to-day correlation algorithm will be implemented for the data processing to improve position accuracy.

The appeal of this research is that by studying the feasibility of replacing precise levelling with GPS for permafrost deformation monitoring, the attainable ‘GPS levelling’ accuracy in the far north of Canada will be investigated. At the same time, this research will quantify the stability of monuments in permafrost, which will play an important role not only in the future analysis of movement due to oil and gas extraction and hence its affect on the environment, but also in the analysis of climate change effects in permafrost areas where stable stations over long periods are required.

1.3 Thesis Outline

The thesis begins with a basic investigation into the operation of the GPS system and the nature of the observations it provides, followed by a review of the project background. From this starting point, analysis is carried out on the GPS data collected in the far north of Canada. Different aspects for the data processing are individually studied. Finally, conclusions on the feasibility of replacing precise levelling with GPS for permafrost deformation monitoring are made.

This thesis is organized as follows:

In Chapter 2, both GPS and precise levelling fundamentals are reviewed. The basic equations relating double differenced GPS observables and their unknown parameters are presented. Various differential error sources are introduced. The basic concept for precise levelling is introduced. The main error sources for precise levelling are reviewed and the attainable accuracy for precise levelling is thus provided. An overview of deformation monitoring is given at the end of this section.

Chapter 3 gives an overview of the target area, which the research described in this thesis is related to, and its subsidence issue. Previous feasibility studies of the most appropriate method for subsidence monitoring in the target area are summarized as part of the project background.

Chapter 4 describes pre-research carried out to characterize two types of error sources: antenna phase centre variation and multipath. In this chapter, an introduction is given to

these two types of error sources. Experiments to characterize and/or mitigate these two types of error sources are explained. Experiment results and conclusions are given at the end.

Chapter 5 summarizes the data collected in the summer 2003 and 2004. The study of the long term stability of different survey monument in permafrost is then described, based on the analysis of two newly collected epochs of precise levelling data together with historical data. Investigations into the impact of different error sources on GPS height estimation for the target area are discussed, and a repeatability analysis is used as an external assessment of the quality of the position results. Based on the analysis results presented, the best strategy for the field data collection and data processing is developed. The data processing results using this developed strategy are presented at the end.

Chapter 6 summarizes the conclusions and recommendations obtained from this research.

CHAPTER 2

GPS, PRECISE LEVELLING AND THEIR ERROR SOURCES

The most attractive characteristic of GPS is that the satellites play the role of control points in a network, while GPS receivers are unknown stations. This results in a trilateration problem which deals with only electromagnetic distance measurement observations.

This section introduces the background as well as the mathematical model for GPS observations. The error sources affecting GPS and the method used to mitigate these error sources are presented thereafter. Precise levelling and its error sources are summarized in the second part of this section. An overview of deformation monitoring is given at the end.

2.1 Global Positioning System Overview

“The Navstar Global Positioning System (GPS) is an all-weather, space-based navigation system under development by the Department of Defense (DoD) to satisfy the requirements for the military forces to accurately determine their position, velocity, and time in a common reference system, anywhere on or near the Earth on a continuous basis” (Wooden, 1985). This all-weather global system consists of three segments (Hofmann-Wellenhof *et al*, 2001):

- The space segment consisting of satellites which broadcast signals,
- The control segment steering the whole system,

- The user segment including the many types of receivers and applications.

Theoretically, the GPS constellation consists of 24 operational satellites deployed in six evenly spaced (60 degrees apart) planes (A to F) with an inclination of 55° relative to the equatorial plane and with four satellites per plane. According to the GPS status on May 24, 2005 reported by the U.S. Coast Guard Navigation Center, the current GPS constellation actually consists of 29 operational satellites. The satellites are positioned about 20,000 kilometres above Earth in approximately 12-hour orbits. With this configuration, almost every point on Earth can simultaneously see four to eight satellites above a 15° cut-off elevation at any time of day (Hofmann-Wellenhof *et al*, 2001). The first GPS satellite was launched in 1978. Initial operational capability was established in December 1993 when the full constellation of 24 satellites was completed. In 1995, the U.S. Air Force Space Command formally declared that GPS met the requirements for Full Operational Capability. Figure 2.1 shows the global coverage of the GPS constellation. As can be seen from this figure, GPS constellation does not provide evenly distributed position accuracy all around the world. Some parts of the world may even experience significantly degraded position accuracy (red part).

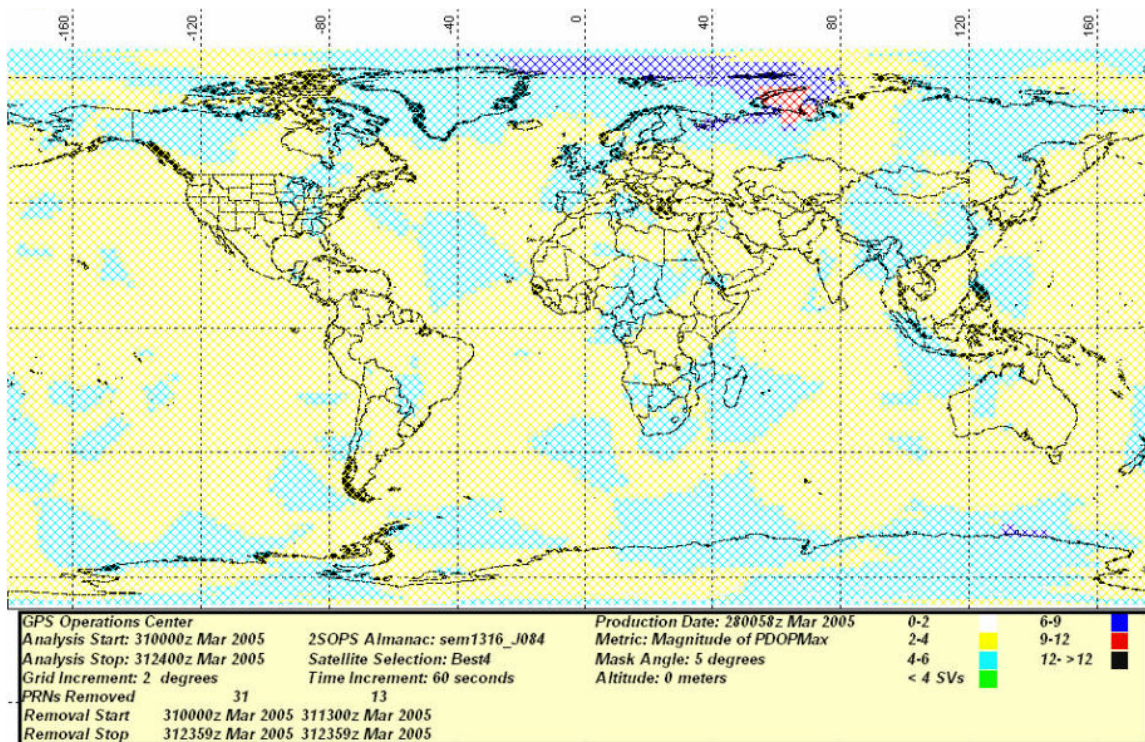


Figure 2.1 World PDOP assessment

(Source: http://www.schriever.af.mil/GpsSupportCenter/reports/uclas_world_dop.jpg)

GPS satellites continuously transmit microwave carrier signals on two frequencies: L1 at 1575.42 MHz and L2 at 1227.60 MHz. One or two pseudorandom noise (PRN) signals, known as the C/A and P codes, are modulated to these two carrier phase signals. The L1 signal is modulated by both the C/A and P codes, while the L2 signal is only modulated by the P code. The C/A code is the basis for the Standard Positioning Service (SPS), and has a chip length of approximately 300 metres. The P code, which has been reserved for U.S. military and other authorized users, provides the signals which are used to support the Precise Positioning Service (PPS). The effective wavelength for the P code is approximately 30 metres. In addition to PRN codes, a 50 Hz data message (known as the

navigation message) is modulated onto the carriers and consists of status information, satellite clock correction information, and satellite ephemerides.

The Operational Control System (OCS) consists of a master control station, monitor stations, and ground control stations. The main tasks of the OCS are: tracking of the satellites for orbit and clock determination and prediction, time synchronization of the satellites, and uploading of the data message to the satellites (Hofmann-Wellenhof *et al*, 2001). There are five monitoring stations located at: Hawaii, Colorado Springs, Ascension Island in the South Atlantic Ocean, Diego Garcia in the Indian Ocean, and Kwajalein in the North Pacific Ocean. Each of these stations continuously measure pseudoranges to all satellites in view and send these ranging measurements to the master control station in Colorado Springs. The master control station processes the ranging measurements in a Kalman filter every 15 minutes to determine satellite orbit and clock corrections. These results form the content of the navigation messages to be uploaded to the satellites (ibid).

2.2 GPS Time Frame

In this section, GPS pseudorange measurements were taken as an example to illustrate the GPS time frame. By comparing the signal received from the satellite with an internally generated signal, a receiver measures the time it takes for the signal to travel from the satellite to the user. Pseudorange measurements are generated by multiplying this time-delay measurement by the speed of light. The observation equation relating the pseudorange measurements with the unknown parameters is given by Parkinson (1996):

$$P = c (T_r - T^s) \quad (2.1)$$

where P is the measured pseudorange measurements in metres, T_r is the signal reception time at the receiver, T^s is the signal transmit time at the satellite and c is the speed of light in a vacuum.

However, Eq. (2.1) only holds true in theory. The effects of the atmosphere on the signal are neglected and it assumes that the transmit time and reception time refer to an absolute time frame. In practice, the transmit time is implicitly embedded in the GPS signal and refers to the satellite's unique time frame. Similarly, the reception time is based on the receiver's time frame, i.e. the receiver's local oscillator.

In the case of the satellite time frame, this time frame refers only to the satellite's onboard clock since it is the clock which drives the frequency synthesizer and code generator required to generate the signal (ICD-GPS-200C, 2003). Since each satellite has its own onboard clock and each one of these clocks slowly drifts over time, the signals simultaneously received from several satellites belong to different time frames and the differences between any two satellites' individual time frame are not constant over time.

In the case of GPS, an "absolute" time frame is derived by averaging the master atomic clocks at five ground monitoring stations (Francisco, 1996). The deviations of each satellite's onboard clock are continuously monitored by these stations, and a prediction model for each satellite's clock error is created based on these deviations (ICD-GPS-200C, 2003):

$$\Delta T^s = a_0 + a_1(t - t_{oc}) + a_2(t - t_{oc})^2 \quad (2.2)$$

where ΔT^s is the satellite clock offset, $a_0, a_1, \text{ and } a_2$ are the broadcast polynomial coefficients, t is the observation epoch and t_{oc} is the epoch to which the coefficients refer.

In addition, the relativistic effects due to the high altitude of the satellites and their high velocity have to be corrected in the satellite transmit time. The corrected transmit time is then given by (ICD-GPS-200C, 2003):

$$T^{s'} = T^s - \Delta T^s + \frac{2\mu^{1/2}}{c^2} e \cdot a^{1/2} \cdot \sin E_k \quad (2.3)$$

where $T^{s'}$ is the corrected transmit time, μ is the gravitational constant, c is the speed of light in vacuum, and a, e, E_k are the semi-major axis, eccentricity and mean anomaly of satellite orbit.

Just as the transmit time refers to the satellite's unique time frame, the measured reception time refers to the receiver's unique time frame. However, unlike the satellites which use high quality atomic clocks, the receivers typically employ low cost quartz oscillators. As a consequence, the clock offsets and drifts for the receivers can be larger than those of the satellites.

Since the GPS receivers make observations to all visible satellites simultaneously, the impacts of the receiver clock offset on all observations are identical. This allows the solving of the receiver clock offset as an additional unknown parameter together with the

receiver coordinates in the least squares adjustment. Since the receiver clock offset drifts over time, a new offset has to be estimated for each epoch.

In practice, since only reception time is explicitly known, one has to derive the transmission time. If the reception time recorded by the receiver is T_r , then the true time of the measurement is $T_r - \Delta T_r$, with ΔT_r being the receiver clock offset. The transmit time can be expressed as:

$$T^s = T_r - \Delta T_r - \frac{\rho}{c} \quad (2.4)$$

where ρ is the true range between the satellite and receiver.

By replacing the true range ρ with the pseudorange measurement, one can derive:

$$T^s = T_r - \Delta T_r - \frac{p + c(\Delta T^s - \Delta T_r)}{c} = T_r - \frac{p}{c} - \Delta T^s \quad (2.5)$$

In Equation (2.5), the pseudorange observation noise is ignored, which is at the several metre level (corresponding to a timing error of about 33 ns). The resulting error in the transmit time calculation when using pseudorange observations contributes less than one centimetre to the satellite position error (Radovanovic, 2002). Since the transmit time usually ranges from approximately 67 ms to 90 ms (Remondi, 1984), a satellite position error of up to 350 m could result if the correction for transmit time is not applied.

It should be emphasized that the transmitted navigation messages provide the user with only a function from which the satellite position can be calculated in WGS84 as a function of the transmission time. Usually, the satellite transmission times are unequal, so

the coordinate system in which the satellite positions are specified changes orientation from one measurement to the next. Therefore, each calculated satellite position has to be corrected for this kind of effect due to earth orientation, or known as the Sagnac effect.

The Sagnac effect can be corrected by adding a rotation factor in the equation for true range calculation. The corrected true range can be expressed as:

$$\begin{aligned} \rho &= \| R_z(\omega \cdot \tau) \cdot r^s - r_r \| \\ &= \sqrt{(x^s \cos \omega \tau + y^s \sin \omega \tau - x_r)^2 + (y^s \cos \omega \tau - x^s \sin \omega \tau - y_r)^2 + (z^s - z_r)^2} \end{aligned} \quad (2.6a)$$

where

$$R_z(\omega \cdot \tau) = \begin{bmatrix} \cos \omega \tau & \sin \omega \tau & 0 \\ -\sin \omega \tau & \cos \omega \tau & 0 \\ 0 & 0 & 1 \end{bmatrix} \quad (2.6b)$$

where r^s and r_r are the satellite and receiver position vector at transmission time and reception time in a non-rotation reference frame. ω is the earth rotation rate, which is known equal to $7292115.1467 \cdot 10^{-11}$ rad s⁻¹. τ is the transit time of the signal.

2.3 GPS Observations

In concept, the GPS observables are ranges which are deduced from measured time or phase differences based on a comparison between received signals and receiver generated signals (Hofmann-Wellenhof *et al*, 2001). There are two basic observations that can be output from GPS receivers: pseudorange and carrier phase.

The difference between these two types of observation is that the pseudorange is generated by correlation between the satellite generated code and the identical copy of the code generated inside the receiver, while the carrier phase is generated by comparing the carrier frequency of the transmitted signal and the receiver generated replica. The carrier phase is a more precise measurement mode. The principle advantage of carrier phase measurement is that the phase of the carrier can be measured to better than 0.01 cycles which corresponds to millimetre precision (Hofmann-Wellenhof *et al*, 2001). On the other hand, the pseudorange measurement noise is currently at the several decimetre level (Langley, 1997).

However, Equation (2.1) only holds true in theory. The pseudorange and carrier phase observations are both corrupted by many error sources such as receiver clock offsets, satellite clock offsets, troposphere delay, ionospheric delay etc. Therefore, the complete equations for pseudorange and carrier phase observations are given by:

$$P = \rho + c(\Delta T^s - \Delta T_r) + d_{orb} + d_{trop} + d_{ion} + d_{multipath(P)} + \varepsilon_P \quad (2.7)$$

$$\varphi = \rho + c(\Delta T^s - \Delta T_r) + d_{orb} + d_{trop} - d_{ion} + \lambda \cdot N + d_{multipath(\varphi)} + \varepsilon_\varphi \quad (2.8)$$

where,

P is the measured pseudorange in metres,

φ is the measured carrier phase in metres,

ρ is the true geometric range in metres,

c is the speed of light in vacuum in m/s,

ΔT^s is the satellite clock error in seconds,

ΔT_r is the receiver clock error in seconds,

d_{orb}	is the satellite orbit error in metres,
d_{trop}	is the tropospheric delay in metres,
d_{ion}	is the ionospheric delay in metres,
λ	is the signal wavelength in m/cycle,
N	is the integer ambiguity in cycles,
$d_{multipath(P)}$	is the multipath effect on pseudorange in metres,
$d_{multipath(\varphi)}$	is the multipath effect on carrier phase in metres,
ε_p	is the pseudorange measurement noise in metres, and
ε_φ	is the carrier phase measurement noise in metres.

In Equations (2.7) and (2.8), satellite orbit error, satellite clock error, receiver clock error, and tropospheric error are frequency independent. The influence of these error sources on pseudorange and carrier phase observations are the same from the same satellite on both frequencies. On the other hand, the ionospheric error is frequency dependent, which is proportional to the inverse of the squared frequency. Furthermore, the influence of ionospheric error on pseudorange and carrier phase observations has the same magnitude but with opposite sign, i.e. the pseudorange observations are delayed by the ionospheric error while carrier phase observations are advanced by the ionospheric error.

In the context of this thesis, the double difference (DD) technique is used. The DD observation equations are therefore discussed here. Figure (2.2) illustrates the typical setup for double differencing.

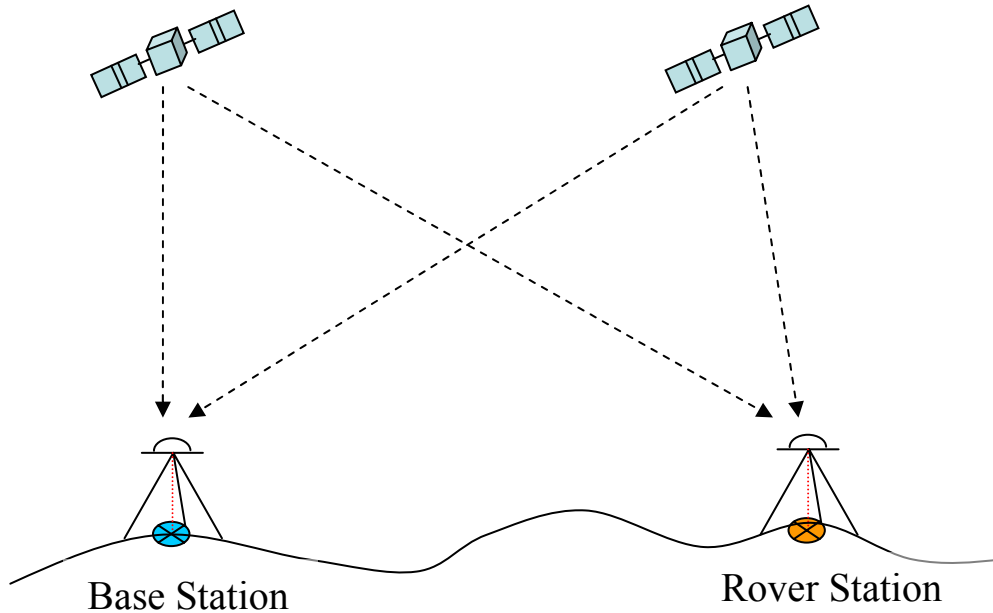


Figure 2.2 Double difference concepts

By differencing between observations to the same satellite from the base and rover GPS receivers, the satellite clock error is cancelled and the orbital, tropospheric, and ionospheric errors are significantly reduced. The reduction of these errors depends on the correlation of these errors in the observation between the base and rover stations. The derived observation after differencing between receivers is known as the single difference (SD). By further differencing the SD observations between different satellites, the double difference observation is derived. After differencing between satellites, the receiver clock error is completely eliminated.

The observation equations for double differenced pseudorange and carrier phase observations are expressed as:

$$\nabla\Delta P = \nabla\Delta\rho + \nabla\Delta d_{orb} + \nabla\Delta d_{trop} + \nabla\Delta d_{ion} + \nabla\Delta d_{multipath(P)} + \nabla\Delta\varepsilon_P \quad (2.9)$$

$$\nabla\Delta\varphi = \nabla\Delta\rho + \nabla\Delta d_{orb} + \nabla\Delta d_{trop} - \nabla\Delta d_{ion} + \lambda \cdot \nabla\Delta N + \nabla\Delta d_{multipath(\varphi)} + \nabla\Delta\varepsilon_\varphi \quad (2.10)$$

where $\nabla\Delta$ is the double difference operator. For a set of observations collected at two receivers observing four satellites, the corresponding differencing matrix, $\nabla\Delta$, is given by:

$$\nabla\Delta = \begin{bmatrix} 1 & -1 & 0 & 0 & -1 & 1 & 0 & 0 \\ 1 & 0 & -1 & 0 & -1 & 0 & 1 & 0 \\ 1 & 0 & 0 & -1 & -1 & 0 & 0 & 1 \end{bmatrix} \quad (2.11a)$$

The original observation vector is formed as:

$$l^T = [P_{1B} \quad P_{2B} \quad P_{3B} \quad P_{4B} \quad P_{1R} \quad P_{2R} \quad P_{3R} \quad P_{4R}] \quad (2.11b)$$

After double differencing, the magnitude of the double differenced satellite orbit error, tropospheric error, and ionospheric error are much smaller than the undifferenced values. However, the noise level of the double difference observations is increased since it is the linear combination of the original observations (Raquet, 1998).

2.4 GPS Error Sources

The error sources have been listed in Equations (2.7) and (2.8). For high precision GPS applications, all these error sources are required to be eliminated or mitigated even after double differencing.

All these error sources can be classified into two categories: spatially correlated errors and site-dependent errors. Spatially correlated errors are those of which the magnitude

increases with baseline length. These errors include satellite orbital error, tropospheric error, and ionospheric error. Site-dependent errors are the errors which are unique to each receiver or its environment. They are not correlated to baseline length and therefore can not be cancelled through DD. These errors include multipath and receiver noise.

As has been discussed previously in this chapter, satellite clock error and receiver clock error will not be repeated here. All the above mentioned error sources will be discussed in the following paragraph.

2.4.1 Satellite Orbit Error

As previously mentioned, to position with GPS, the coordinates of the GPS satellites are generally assumed to be known. These coordinates are normally expressed in terms of an ephemeris, which gives a mathematical description of where a satellite is at a given time (Roulston *et al*, 2000). The satellite orbital error is a result of the discrepancy between the computed coordinate from the ephemeris and its true value.

The effect of satellite orbital error on differential positioning can be given using the following rule of thumb (Beutler, 1992):

$$\frac{db}{b} = \frac{d_{orb}}{\rho} \quad (2.12)$$

where db is the baseline error. b is the baseline length. d_{orb} is the satellite orbit error and ρ is the distance from satellite to the receiver. The computed satellite coordinates from broadcast ephemeris have a standard deviation of approximately 3 m (Roulston *et al*,

2000). Assuming an average satellite-receiver distance of 20200 km, the effect of satellite orbital error on differential positioning is approximately 0.099 parts per million (ppm). It can be concluded that the effect of satellite orbit error on differential positioning for a baseline up to 50 km is approximately 5 mm and thus can be neglected in most cases.

Moreover, the configuration of the satellite orbit has the following effects on GPS positioning (Rizos, 1999):

- Height is a relatively weakly determined component, mainly because there are no satellites below the horizon.
- The East-West (longitude) component is slightly weaker than the North-South (latitude) component because of the motion of satellites (particularly in equatorial regions).

There are two basic types of satellite orbit information: broadcast and post-processed ephemerides. The broadcast ephemerides, which are available in the GPS Navigation Message, are predicted from past tracking information. Therefore, they can be used for real time applications. Post-processed ephemerides are orbit representations valid only for the time interval covered by the tracking data. Obviously this information is not available in real time as there is a delay between the collection of the data, transmission of the data to the computing centre, the orbit determination process and the subsequent distribution to GPS users (Rizos, 1999). Post-processed ephemerides, which come in several forms, are more accurate than broadcast ephemerides. The IGS post-processed ephemerides products demonstrated accuracies well below the metre level to several

centimetres (Roulston *et al*, 2000). Because of the high precision of the post-processed ephemerides, they are widely used in various high precision GPS applications. In the context of this thesis, IGS final orbit product is used for all GPS data processing.

2.4.2 Tropospheric Error

The troposphere is the portion of the atmosphere extending up to 60 km above the Earth's surface. When the GPS signal travels through the troposphere, its path will bend slightly due to the refractivity of the troposphere. The change of the refractivity from free space to the troposphere causes the speed of the GPS signal to slow down, which causes a delay in the GPS signal. This tropospheric delay is a function of temperature, pressure, and relative humidity. Measurement of these quantities at widely spaced (greater than 10 km) monitoring stations would be ineffective owing to their short spatial correlations (Kaplan, 1996).

There are two components in the tropospheric delay: dry and wet component. The effect of these two components on the propagation delay of the GPS signals has quite different characteristics. The dry component causes a delay of around 2.3 m in the zenith direction depending on local temperature, pressure, and humidity. The dry component induced delay is quite stable over time (varies only 1% in a few hours) and thus can be very well predicted using existing models. The wet component of the zenith delay is generally much smaller (between 1 and 80 cm at zenith direction), and is very unpredictable. It may change by as much as 10% to 20% in a few hours (Spilker, 1994).

Generally, tropospheric delay can be modelled very well. It was found that the contribution of the troposphere to the differential positioning error budget varies typically from 0.2 to 0.4 ppm after applying a model (Lachapelle and Cannon, 2004). For baselines up to 25 km, the residual tropospheric delay is approximately 1 cm.

However, to achieve centimetre or even millimetre accuracy, either a tropospheric model must be applied or the residual tropospheric delay must be estimated as an additional parameter. There are quite a number of tropospheric delay models available, e.g. Hopfield (1970, 1972), Saastamoinen (1972), and Lanyi (1984). The Hopfield tropospheric delay model and Saastamoinen tropospheric model are the most frequently used and they give comparable results in most situations. For low elevation satellites, the Saastamoinen model produces slightly better results than the Hopfield model (Spilker, 1994).

2.4.3 Ionospheric Error

The ionosphere is the layer of the atmosphere that extends from 60 to over 1000 km of height above the Earth's surface. At times, the range errors of the troposphere and the ionosphere are comparable, but the variability of the Earth's ionosphere is much larger than that of the troposphere, and it is more difficult to model (Klobuchar, 1996). The first-order carrier phase error I (in metres) caused by the ionosphere is given as (Seeber, 1993; Hofmann-Wellenhof *et al*, 2001):

$$I = -\frac{40.3}{f^2} TEC \quad (2.13)$$

where 40.3 is an empirically derived constant with units of $\text{m}^3/\text{s}^2/\text{electrons}$, TEC

represents the Total Electron Content along the signal path in units of electrons/m², and f is the L1 or L2 carrier frequency.

It can be seen from Equation (2.13) that the magnitude of the ionospheric error depends on the TEC. The TEC values depend on the rate of ionization, recombination and transport processes (Skone, 2001). The rate of ionization in a global sense is a function of the solar activity, which follows cycles of approximately 11 years in duration (Klobuchar, 1996). Figure 2.3 shows the predicted sunspot number for the current solar cycle. The TEC values have been observed to increase by a factor of three during a solar maximum versus a solar minimum (Klobuchar *et al*, 1995). The latest solar maximum occurred during the year 2000-2001. The data set used in this thesis is collected in the summer of 2003 and 2004, approximately three years after the solar maximum, which means there is still a medium ionospheric signature in the data.

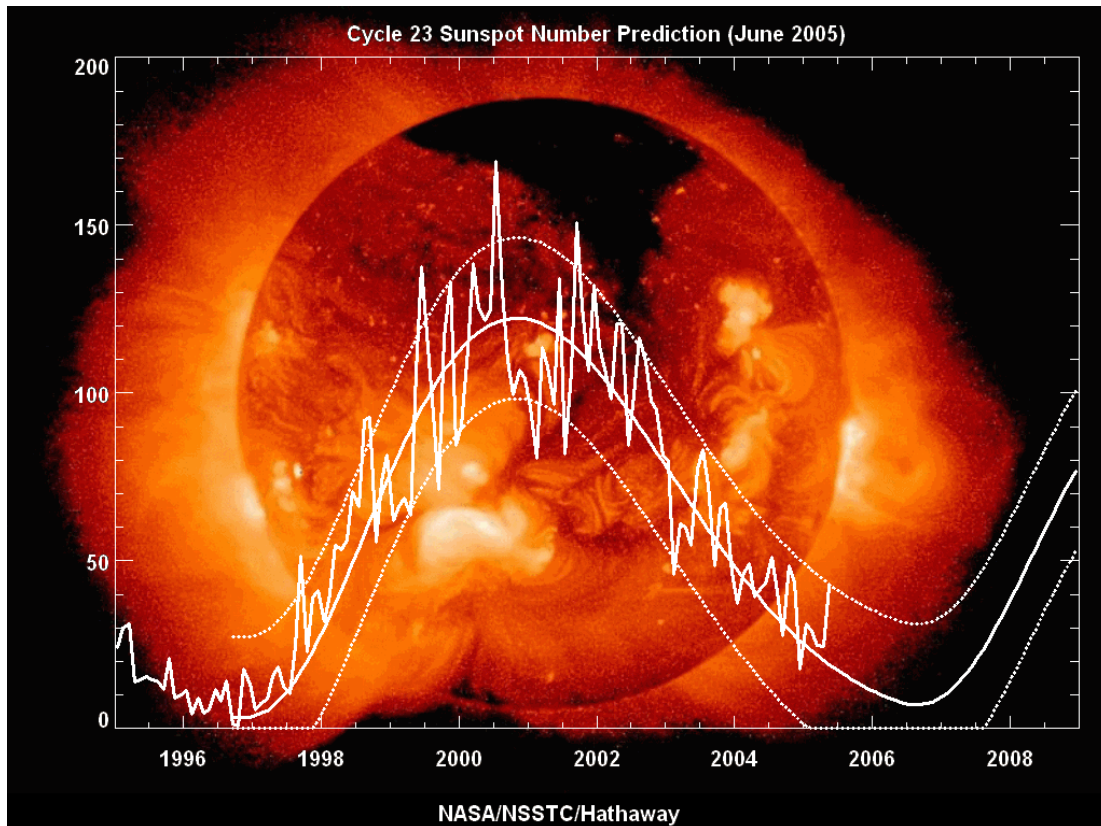


Figure 2.3 Predicted sunspot number for the current solar cycle

(Source: http://science.nasa.gov/ssl/pad/solar/images/ssn_predict_1.gif)

In addition to the large scale variation with solar cycle, the TEC presents the following variation characteristics (Skone, 2003):

- Maximum TEC occurs at 14:00 local time and TEC can be asymmetric with a secondary maximum at 22:00 local time and a minimum before sunrise.
- The lowest TEC values are in the summer (for the Northern Hemisphere) and maximum near the equinoxes (March and October). This is opposite for the Southern Hemisphere, i.e. lowest in the winter and maximum in the summer. The TEC values are 2-3 times higher in winter than in summer.

- The two maxima are at $\pm 10^\circ$ from the magnetic equator, in the region under the so-called equatorial anomaly.

There are some models available to compensate the ionospheric delay. Klobuchar (1986) introduced a model that is being used by the GPS Control Center as part of the navigation message broadcast by the GPS satellites. This model utilizes a cosine function to represent the diurnal ionospheric error. It has been shown to be effective in removing around 50% (RMS) of the total error. This model is helpful for improving SPS performance. However, to achieve centimetre accuracy, it is not sensitive enough and it is not therefore used in carrier phase applications.

Although the ionospheric error is hard to compensate for by applying models, it can be eliminated by making use of its dispersive property. From Equation (2.13), it can be seen that the ionospheric error on L1 and L2 is different and is proportional to the inverse of the square of frequency. This dispersive property allows the formation of a very important carrier phase combination, the ionosphere-free (IF) combination, in which the ionospheric error is removed.

The contribution of residual ionospheric error to differential positioning has been reported by Alves *et al* (2002) to be approximately 2 ppm on geometry-free combination observations on baselines up to 50 km under ionospheric quiet conditions. During the time of solar maximum, the contribution of residual ionospheric error to differential positioning error budget can increase by a factor of three (Lachapelle and Cannon, 2004).

2.4.4 Multipath

Multipath is the interference of a reflected GPS signal with the line-of-sight GPS signal. It distorts the signal modulation and thus degrades the measurement accuracy (Braasch, 1996).

The theoretical maximum multipath bias that can occur in the pseudorange data is approximately half the code chip length or 150 m for C/A code ranges and 15 m for P code. The carrier phase multipath is much smaller than that of the pseudorange, with a maximum magnitude of one quarter of a carrier wavelength, i.e. 5 cm for L1 and 6 cm for L2 (Cannon and Lachapelle, 2003). However, in practical applications, the reflected signal is attenuated to some extent and the typical phase multipath values are more on the order of 1 cm or less (Lachapelle and Cannon, 2004).

Multipath effects have to be carefully treated in GPS data processing to achieve very high position accuracies. Several methods for effectively reducing multipath effect have been developed. Examples include the mitigation of GPS code and carrier phase multipath effects using a multi-antenna system (Ray, 2000), multipath mitigation via day-to-day correlation analysis (Radovanovic, 2000), and multipath mitigation by making use of signal-to-noise ratio information (Brunner *et al*, 1999). Moreover, by using a chokering antenna in the field data collection, multipath effects can be greatly reduced (Lachapelle and Cannon, 2004).

The multipath mitigation via day-to-day correlation was considered to be the most effective method for mitigation multipath for static GPS data. This method will be

implemented and used for the data processing in this thesis to improve station positioning accuracy (See chapter 5).

2.5 Precise Levelling and its Error Sources

Early levelling was done with crude instruments that had a provision for sighting along a water surface or by some mechanical application of a plumb line (Berry, 1976). Today, more sophisticated equipment enables levelling to achieve very high accuracies. This new equipment depended on the invention of three important items: (1) the telescope invented by a Dutch optician by the name of Lippershey in 1608; (2) the reticle with cross wires and the ocular invented by Johann Kepler in 1611 and (3) the level vial invented by Melchisedech Thevenot in 1666 (Gareau, 1986). Moreover, by applying laser technology in the instrument and the improvement in manufacturing techniques of the invar rod in recent days, the performance of the levelling is significantly improved.

Levelling provides a means of accurately measuring of the height difference between two points that are some tens of metres apart. A level is setup on a tripod and levelled so that the line of sight is horizontal. A precise graduated rod is held vertically over the first point and a reading is made from the level, which is called a backsight. Another rod is then held vertically over the second point and a further reading is made, which is called a foresight. The difference between the two readings is the difference in height between the two points. Figure (2.4) illustrates the typical setup for precise levelling.

There are a large number of potential error sources for levelling (Gareau, 1986). But many of these are only significant for precise levelling over long distances. For levelling over short distances, there are only two worth mentioning: collimation error, and error due to refraction. Collimation error occurs when the collimation axis is not truly horizontal when the instrument is level. The error due to refraction is caused by the ray path passing through atmospheric layers of different refractive index which results in a bending ray from the level to the rod. However, the effect of these error sources can be reduced or eliminated by using equal sight lengths for fore- and backsights.

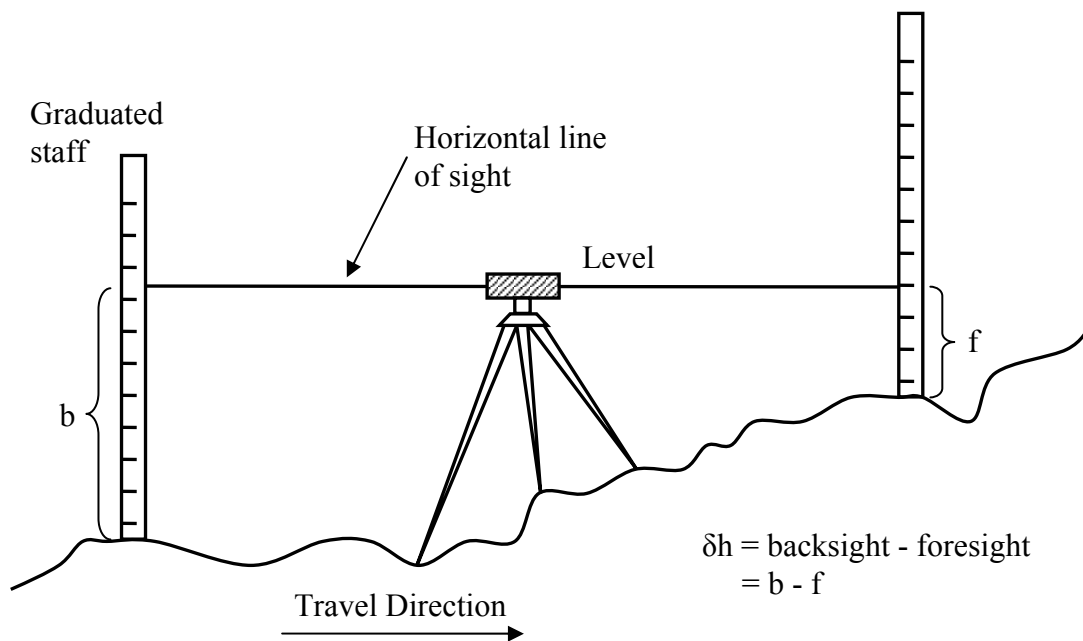


Figure 2.4 Typical setup for precise levelling

Overall, precise levelling is the most precise method for monitoring local vertical deformations. This technique can provide a vertical component precision of 0.2 to 1 ppm of the length of the level route (Gili *et al*, 2000). However, the drawback of this

technique is obvious at the same time. First, precise levelling can only provide information in one dimension. Second, levelling must be initiated from a stable monument located outside the deformation area in most cases. The result may be that the level route goes up to several kilometres, which makes the levelling work laborious, often slow, and subject to the propagation of levelling errors. These reduce the overall effectiveness of this technique. However, for some potential relative networks, trend signal analysis (Kenselaar and Quadvlieg, 2001) allows a network that is constrained using one of the unstable benchmarks in the test area.

It is important to note that the heights obtained from levelling are orthometric heights while the heights obtained from GPS are ellipsoidal heights. The relationship between these two height types is given by (Heiskanen and Moritz, 1967):

$$h - H - N = 0 \quad (2.14)$$

where h is the ellipsoidal height, H is the orthometric height and N is the geoidal undulation obtained from a regional gravimetric geoid model or a global geopotential model. The relationship of the two height types are also illustrated in figure (2.5):

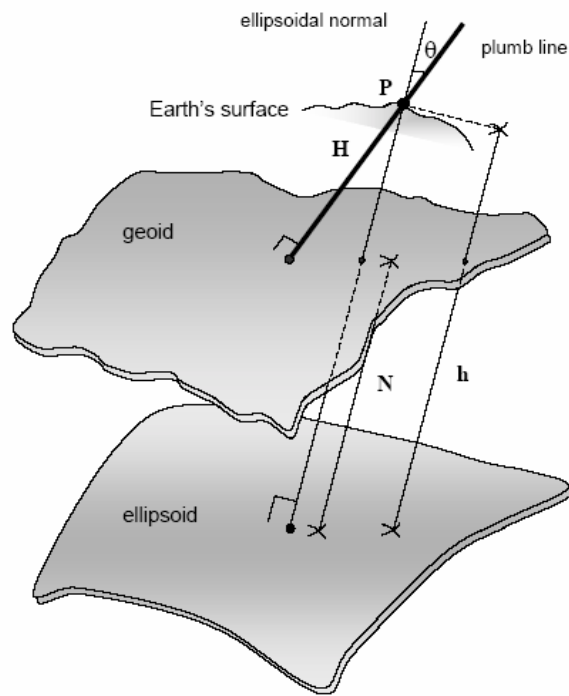


Figure 2.5 Relationship between ellipsoidal, geoid and orthometric heights

(Fotopoulos, 2003)

When comparing heights obtained from GPS and heights obtained from precise levelling, one has to note that they belong to different height systems. However, for a very small area (a circle with a diameter of 70 metres), the magnitude of change of N is quite small and thus can be neglected. Consider the variation in gravitational acceleration that would be observed over a simple model. For this model, let's assume that the only variation in density in the subsurface is due to the presence of a small ore body. Let the ore body have a spherical shape with a radius of 10 metres, buried at a depth of 25 metres below the surface, and with a density contrast to the surrounding rocks of 0.5 grams per centimetre cubed (see Figure 2.6). The maximum value of the gravity anomaly is quite small, 0.025 mGals (1 Gal = 1 cm/sec², 1 Gal = 1,000 milligals) for this example. This maximum

variation of gravity anomaly transferred into the variation of geoid undulation is only 2-3 mm. Therefore, the variation of geoid undulation within a small area (a circle with a diameter of 70 metres) can be neglected. Because of the high accuracy of precise levelling in height component, levelling results can be used as ground truth to examine the performance of GPS levelling in a small area (a circle with a diameter of 70 metres).

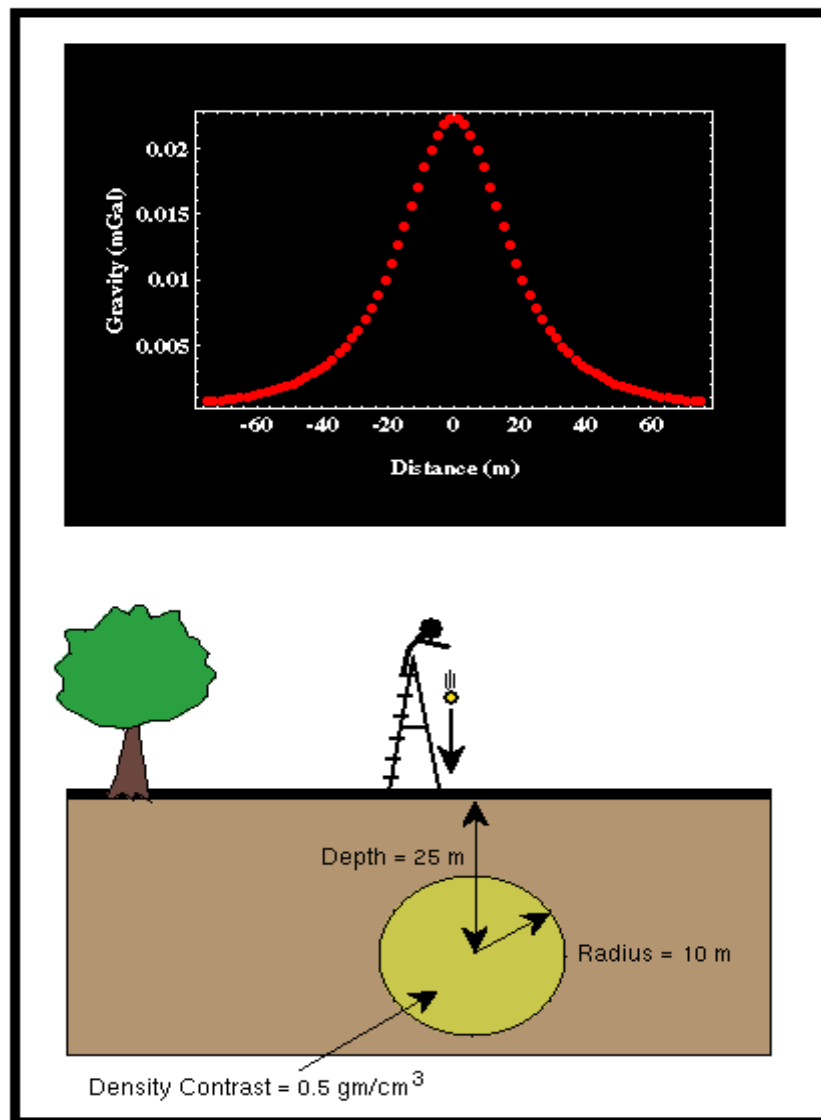


Figure 2.6 A simple model illustrating the variation of gravity anomaly

(Source: <http://gretchen.geo.rpi.edu/roecker/AppGeo96/lectures/gravity/simpmod.html>)

2.6 Deformation Monitoring Overview

Deformation monitoring is used for many applications, including monitoring of large structures such as dams and bridges, steep slopes and embankments, and measuring terrain subsidence due to sub-surface mineral extraction (Caspary, 1987). A deformation survey measures the change of the target object or area with respect to time using a network of points. It is assumed that the measurements are made faster than the deformation process itself and repeated measurements are often done to determine temporal trends. This is done using different geodetic methods for a one-, two- or three-dimensional monitoring.

There are two types of monitoring networks depending on the distribution of points. If the stations around and close to the object, called reference points, can be located on points that will remain stable throughout the period of deformation monitoring, these can be used for network datum definition (Tait, 2004). This is known as an absolute (or reference) monitoring network (Tait, 2004). In this case, movements of the target object or area are determined with respect to the reference points.

A second type of network is called a relative network (Biacs, 1989). In this case, there is no assumption regarding the stability of any survey stations whereby all the points in the network may move. It means none of the points can be used for datum definition. The obvious choice for the datum in a relative network is inner constraints (Tait, 2004). Therefore, the derived point coordinates are solely based on observations. All the points are treated as object points and only relative movements with respect to the centroid of network can be estimated.

For a relative network, it is not possible to model absolute rigid body movements, which is required for most deformation monitoring applications (Casparly, 1987). In this case, it is necessary to turn the relative network into an absolute monitoring network. The most important task in this case is to define points which are stable over time that can be used as reference points. Test statistics can be introduced to test the stability of network points, which are known as congruency tests (Tait, 2004). There are three stages: Global congruency test, congruency testing of partial networks, and the detection of movement of points (Tait, 2004). These tests are based on the information from individual epoch coordinate estimates and, critically, on the variance-covariance of the estimates. Thus the sensitivity of the test relies upon the quality of the observations, the shape of the network and the network datum (Tait, 2004).

GPS deformation monitoring applications have shown that it is capable of monitoring sub-centimetre deformations when using carrier phase measurements (e.g. Hartinger and Brunner, 1998). There exist many applications to apply GPS for high accuracy positioning and deformation monitoring. In most cases, such applications are of small spatial extent (<10 km) (Radovanovic, 2000). These applications include bridge monitoring (Wieser and Brunner, 2002), dam deformation monitoring (Hudnut, 1996), structure deformation monitoring under wind load (Guo and Ge, 1997), and landslide monitoring (Hartinger and Brunner, 2000).

The attainable accuracy for a GPS-based deformation monitoring system is limited by many location dependent errors. Recent work on the effects of location dependent variables such as satellite geometry (Meng *et al*, 2004), tropospheric effects (Roberts and Rizos, 2004), and ionospheric effects (Janssen *et al*, 2001) have mitigated these errors by employing an optimised strategy for data capture and processing.

Furthermore, Continuous GPS monitoring techniques have shown great success in many long-term deformation monitoring applications, for instance the Continuous GPS monitoring of structural deformation at Pacoima Dam (Hudnut *et al*, 2001). In addition, there are those that have been established in sub-arctic areas, for instance the SWEPOS system (Hedling *et al*, 2001). The advantage of the Continuous GPS monitoring technique is that it allows continuous study of all the site-dependent errors and offers real-time positioning information. In addition, no human interference is needed in this case.

Overall, GPS has shown very good performance in many deformation monitoring applications. Examples include the Pacoima Dam deformation monitoring system which has shown that GPS can provide real-time positioning accuracies of 1 cm in horizontal, 2 cm in vertical and post-processed positioning accuracies of 2-4 mm in horizontal and 6-8 mm in vertical (Hudnut and Behr, 1998). Also, a bridge deformation monitoring system developed by the Graz University of Technology has shown that the precision of the GPS results is about 2 mm for the horizontal coordinates and 4 mm for the height (Wieser and Brunner, 2002).

CHAPTER 3

PROJECT BACKGROUND

This chapter gives an overview of the target area, where the research described in this thesis is related to, and its subsidence issue. Previous feasibility studies of the most appropriate method for subsidence monitoring in the target area are summarized as part of the project background. The problems to be investigated are reiterated as project objectives at the end of this chapter.

3.1 Subsidence Issue in the Target Area

Oil and gas extraction in permafrost (continuously frozen soil) areas causes vertical surface displacements that have in the past caused serious environmental issues, such as massive subsidence and land slides (Rempel, 1970). To avoid potential environmental disasters during oil and gas extraction, such vertical subsidence has to be accurately monitored.

The target area, Niglintgak Island, lies approximately 150 kilometres north of Inuvik at a latitude of 69° 20' North and a longitude of 135° 20' West. Figure 3.1 shows a map of Canada highlighting both the area of interest, and the distribution of permafrost. Much of the subsidence is expected to form beneath the Kumak Channel to the south of the island (Figure 3.2).

The target area is characterized by continuous permafrost to depths of up to 600 m (Smith *et al*, 2001). The annual freeze/thaw of the active layer above the permafrost in this area has been observed at the 20 cm level (Mackay *et al*, 1979), with a wide variation in timescale dependant on such factors as annual snow cover, atmospheric conditions, and vegetation growth.

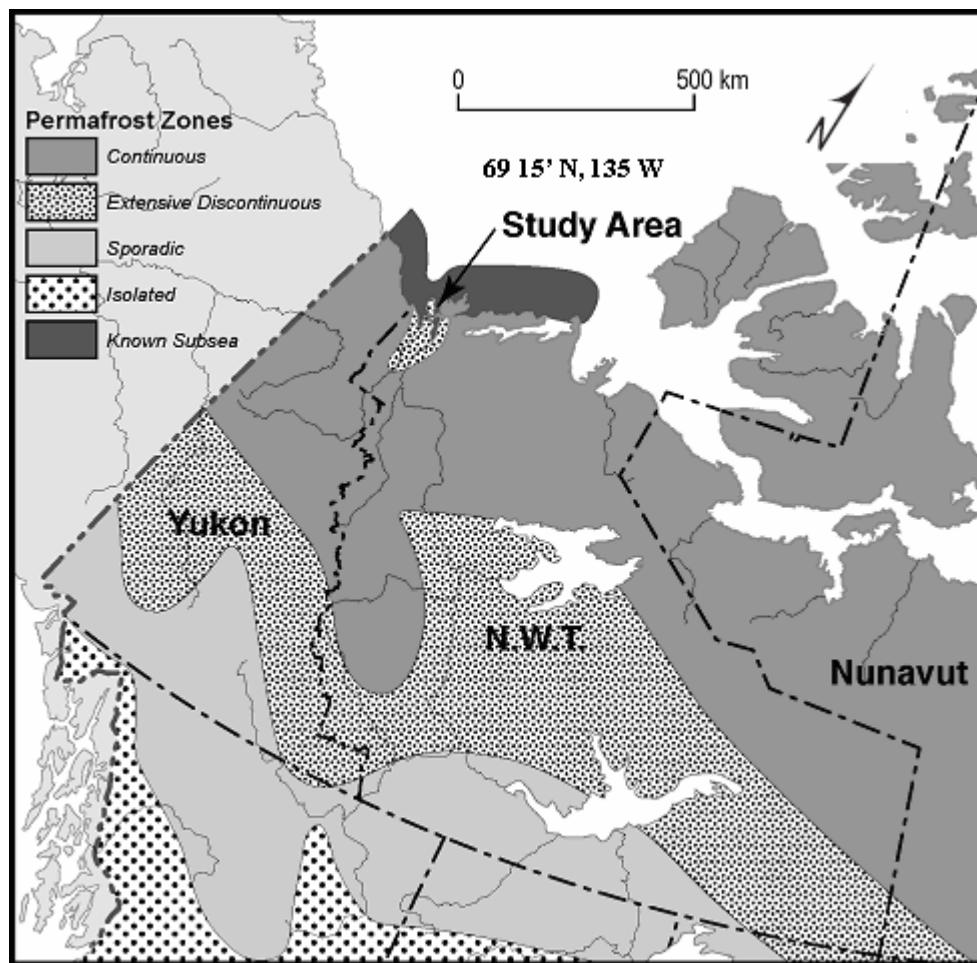


Figure 3.1 The distribution of permafrost in Canada and areas of the Niglintgak and Taglu gas reservoirs (Tait *et al*, 2004)

With large portions of the islands at between 0.5 and 1.0 m above sea level, the threat of subsidence leading to the inundation of such areas could result in both a deepening of the active permafrost layer and the thawing of massive ice. This could potentially lead to subsidence in the order of tens of metres and the loss of substantial portions of land.

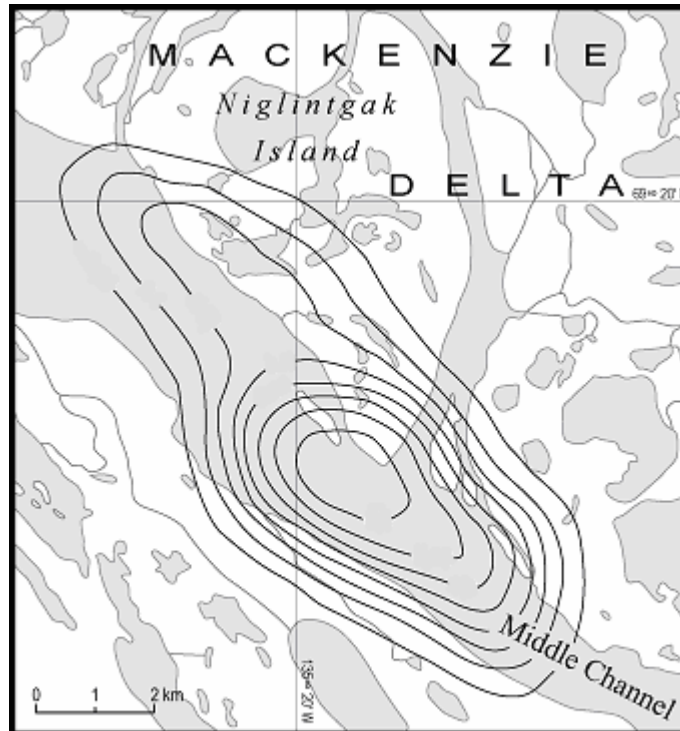


Figure 3.2 The subsidence bowl anticipated to result from gas extraction from the Niglintgak Island lease (Tait *et al*, 2004)

The subsidence predicted in this area will occur over a 25-year production cycle, with little movement anticipated in the first 10 years due to glacial pre-stressing and associated rebound. A simple congruency analysis (95% confidence, Fisher test for 1D and assuming a known probability density function [PDF]) resulted in a 1σ observation

accuracy of 9.7 mm being required to find significant movement in the central point on an annual basis (Tait and Moorman, 2003). The problem of positioning stations away from the critical areas (the submerged centre of the subsidence bowl, for instance) requires that the position accuracy be better than 5 mm (1 sigma).

3.2 Feasibility Study into Monitoring Deformation in the Niglintgak Region of the Mackenzie Delta

Several possible methods of monitoring permafrost subsidence in the target area have been investigated (Tait and Moorman, 2003). These methods include precise levelling, Differential Interferometric Synthetic Aperture Radar (DINSAR), Continuous Differential Global Positioning System (CDGPS), and DGPS.

3.2.1 Precise Levelling

Precise levelling has been examined as a potential solution in both absolute and relative networks for the deformation monitoring of the target area. For an absolute network, it was already recommended that a sea-level gauge be installed to monitor for storm and tide influences on the Kumak Channel, so a datum can be established for an absolute network (Tait and Moorman, 2003). For a relative network, trend signal analysis allows a network to be constrained using one of the unstable benchmarks in the test area. Trend signal analysis has so far been estimated only for extraction from reservoirs with a depth/diameter ratio of 1 (the depth/diameter ratio for the target area is around 0.1), although work is progressing to characterise the trend signal for several irregular reservoirs (Tait and Moorman, 2003).

Despite the high accuracy of precise levelling for height measurement, there are several drawbacks of applying precise levelling for the target area. Since a great deal of the area has large water bodies (>2 km), over which to make precise levelling measurement is very difficult. In addition, it does not provide planimetric measurements at all, which is insufficient for monitoring horizontal movements. For the above reasons, precise levelling is not recommended in this case.

3.2.2 DINSAR

DINSAR has the potential to detect sub-centimetre vertical movements (Wang and Li, 1999). However, the feasibility study noted two problems with DINSAR for monitoring in the Mackenzie Delta (Tait *et al*, 2004):

1. DINSAR relies on the reflection of microwave radiation remaining constant for the area of study. If the scattering properties of the area change between satellite acquisitions due to changes in surface wetness or vegetation growth, this alters the phase of the returned radiation. Such phase alteration with time, known as temporal decorrelation, makes deformation analysis difficult or impossible. Even in regions with less vegetation than the Mackenzie Delta, it was found that between RADARSAT-1 images with a 24 day separation there was too little coherence to generate measurements of vertical displacement (Moorman and Vachon, 1998; Moorman *et al*, 2003).

2. If a deformation map of the area can be generated using DINSAR, this map is of the surface of the permafrost. In the Mackenzie Delta the active layer of the permafrost has been observed to cause heave and settlement of up to 20 cm on an annual basis (Mackay et al, 1979). This is influenced by climatic conditions, vegetation cover, and soil type. This makes estimating true subsidence from measurement of the elevation of the surface itself impossible without an adequate model of the active layer heave. Permafrost models are anticipated to be accurate to 1-2 cm (Tait and Moorman, 2003).

Since the planimetric deformation may impose shear on production platforms, both vertical and planimetric measurements of deformation are desired in this case. In the case of DINSAR, the planimetric accuracy is much lower than vertical measurement accuracy. It can not provide the desired full 3 dimensional monitoring, which makes it less attractive in this case.

3.2.3 CDGPS

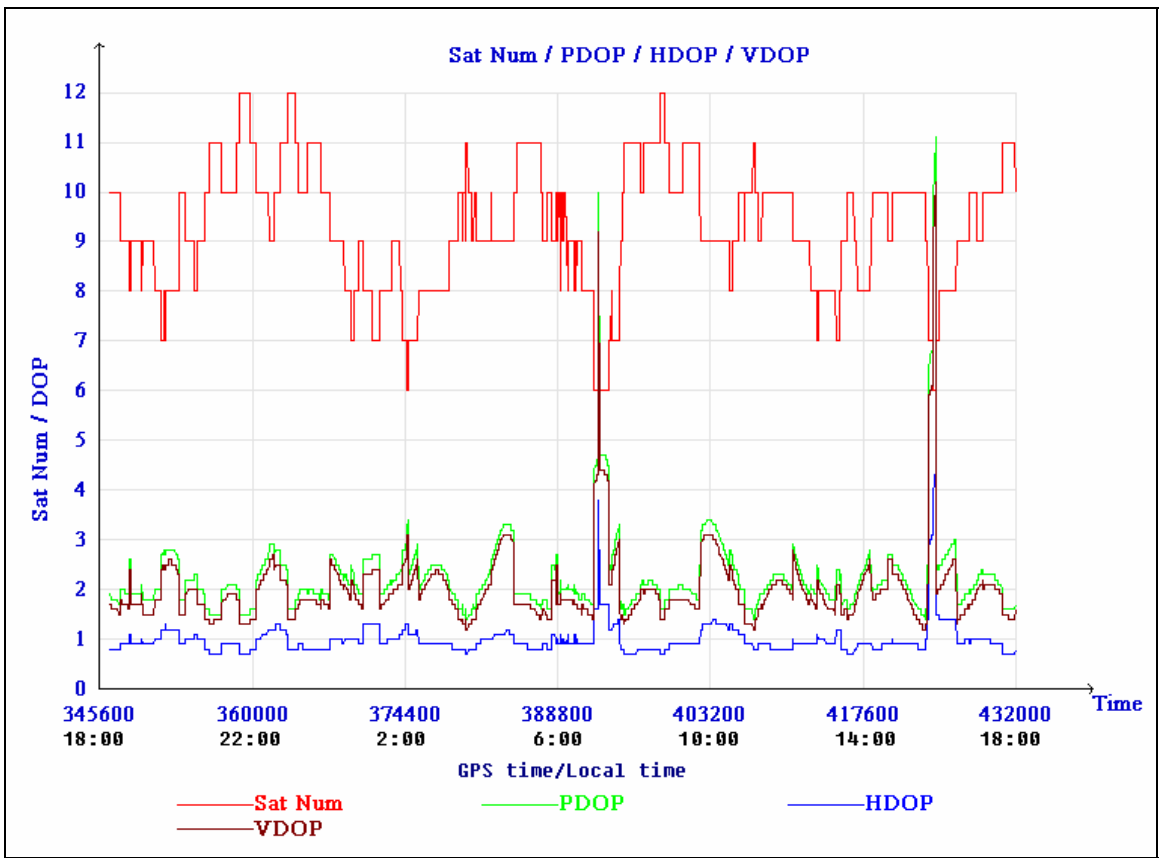
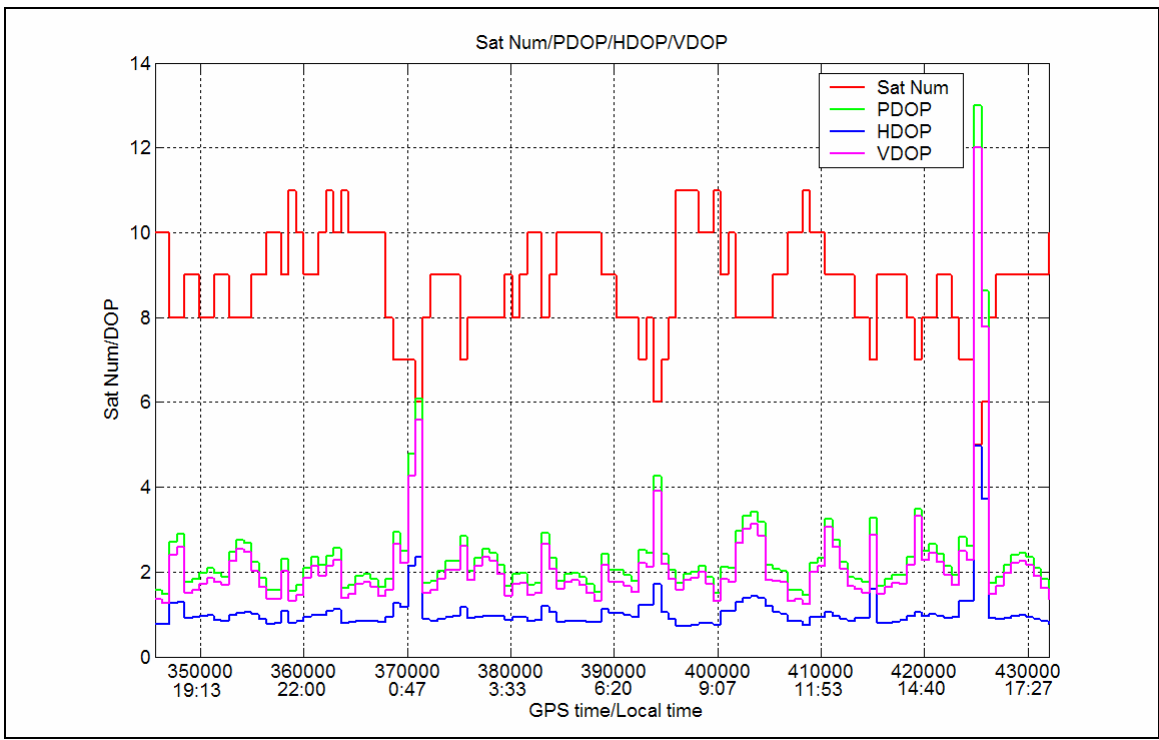
Recognizing the success of Continuous GPS monitoring technique (see Section 2.6), it was also assessed for application in the target area. For continuous monitoring, several factors have to be taken into consideration: power supply for GPS receivers, internet availability to upload data to the server, infrastructure for maintenance, and animal activity. In addition, because the target area is in the far north of Canada, weather is a big issue, including high winds and extreme cold. Additional devices are generally needed to prevent GPS antennas from icing. The requirements for continuous GPS monitoring are

hard to meet in the target area. This approach was considered unfeasible since implementing a relatively large number of such stations, together with the problem of lack of communications in the target area, presented serious logistical and cost issues (Tait and Moorman, 2003).

3.2.4 DGPS

DGPS is a well established fully 3-dimensional measurement method which allows the estimation of deformation parameters at the centimetre level and at the millimetre-level in special cases (Hartinger and Brunner, 1998; Beutler *et al*, 2001). Phase-Centre-Variation of the receiving antenna and multipath effects have been identified in the past as the major station-dependent causes of errors in precise engineering measurement using DGPS (Wübbena *et al*, 2000). However, DGPS also has challenges specific to the target area. In particular, the effects of ionospheric activity and relatively poor satellite geometry in the Arctic region might also contribute to the error budget over longer baselines, even when using an ionosphere-free combination during processing.

In order to illustrate the satellite geometry in the target area, the number of available satellites, dilution of precision (DOP) values (PDOP, HDOP, and VDOP), and the skyplot over 24 hours at the INVK station generated from a GPS planning tool as well as from original data processing for the date of Jul 8th, 2004 are plotted and shown in Figure 3.3. The elevation cut-off angle was set to 10 degrees.



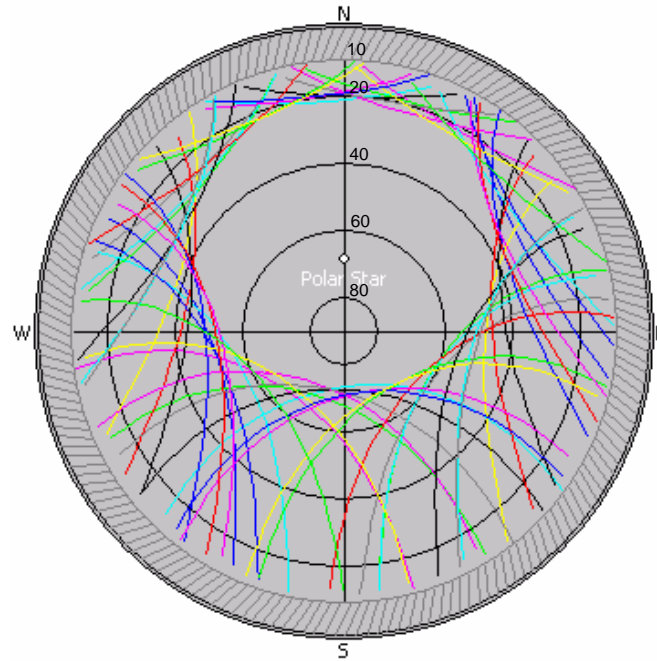
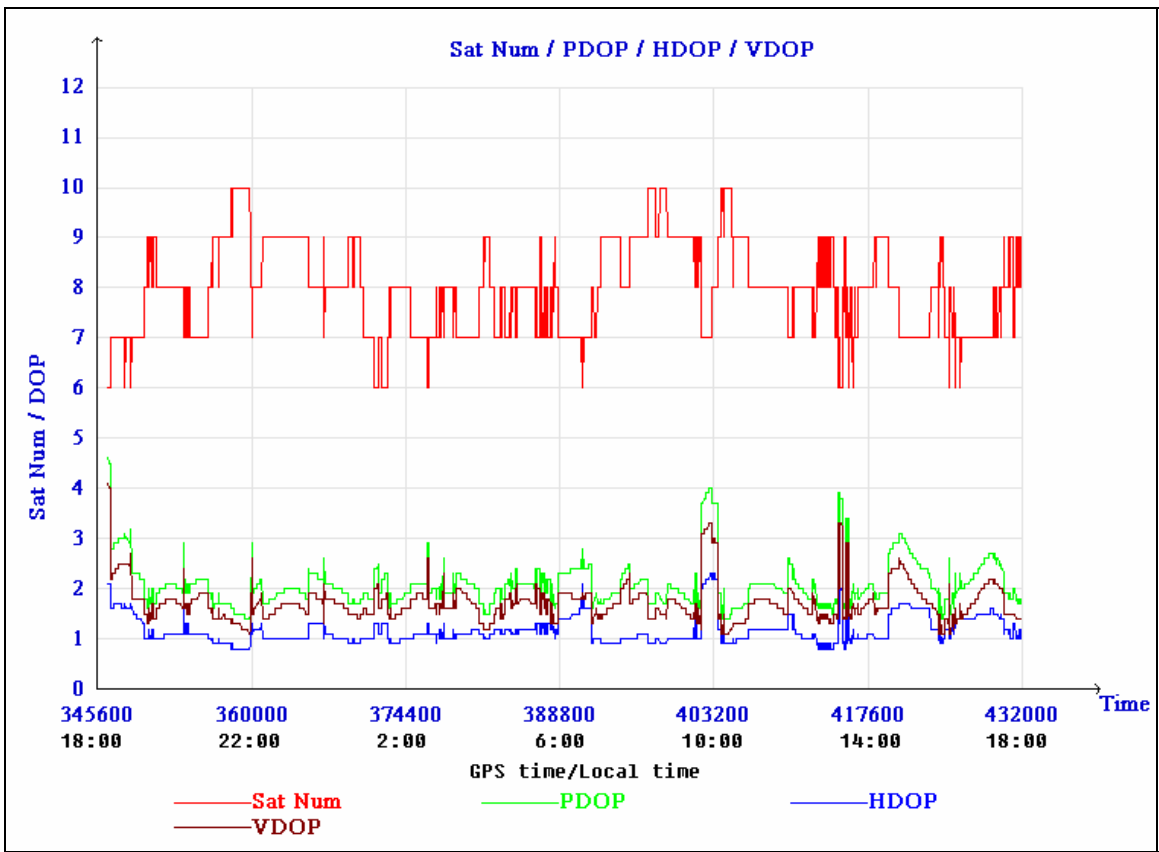
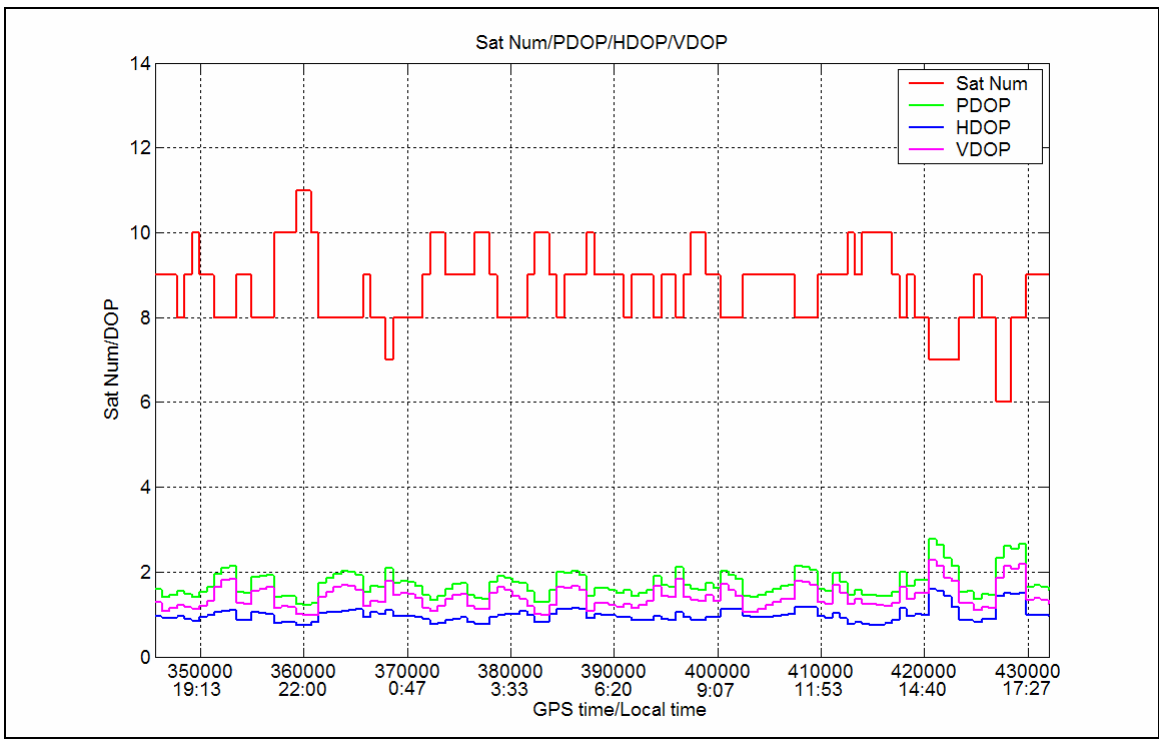


Figure 3.3 DOP values and number of available satellites generated from GPS planning tool (top) and GPS data processing (middle) and skyplot (bottom) over 24 hours at INVK station

For comparison purposes, the number of available satellites, DOP (PDOP, HDOP, and VDOP) values generated from GPS planning tool as well as original data processing and the skyplot over 24 hours at another, mid-latitude, IGS station near Calgary, PRDS, were plotted and shown in Figure 3.4. Elevation cut-off angle was again set to as 10 degrees.



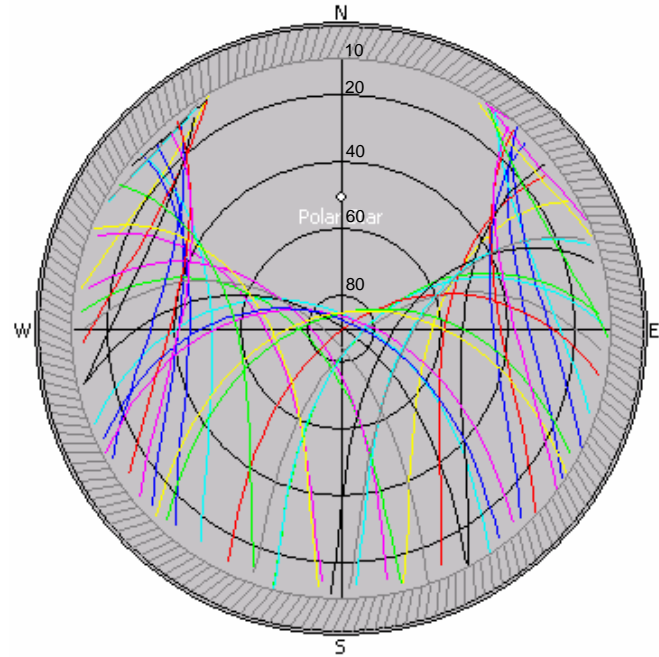


Figure 3.4 DOP values and number of available satellites generated from GPS planning tool (top) and GPS data processing (middle) and skyplot (bottom) over 24 hours at PRDS station

By looking at the skyplot and DOP values over these two stations, two observations were made:

1. There are no satellite passes overhead the INVK station and the elevation angle of the highest available satellite is approximately 75 degrees. This is not the case for the PRDS station. According to Meng *et al* (2004), an optimal constellation to minimize the DOP values is given by a GPS satellite passing directly overhead of the observation station, with other satellites scattered around the horizon with associated low elevation angles. With the current GPS constellation, the target area will experience degraded satellite geometry than that of a mid-latitude area.

2. The horizontal DOP (HDOP) values for these two stations are at the same level, around 1, except for several spikes at INVK station. The vertical DOP (VDOP) values for PRDS station are slightly better than INVK station. Most of the VDOP values at INVK station are between 2 and 3, while most of the VDOP values at PRDS station are below 2. The VDOP value at INVK station may even go up to 10 sometimes. Besides, the VDOP values at the PRDS station have much less variations than that of the INVK station.

The level of global ionospheric activity can be quantified using the conventional space weather index K_p . This index is based on measurements of magnetic field variations at 13 approximately equally longitude-spaced sub-auroral stations to produce the planetary K_p index at three-hour intervals, with values ranging from 0 (quiet) to 9 (extreme) (Skone, 2003). Such indices provide an approximate measure of global ionospheric activity at higher latitudes. Figure 3.5 shows the K_p index for a quiet day (14 July, 2004) and Figure 3.6 shows a day of significant ionospheric disturbance (25 July, 2004).

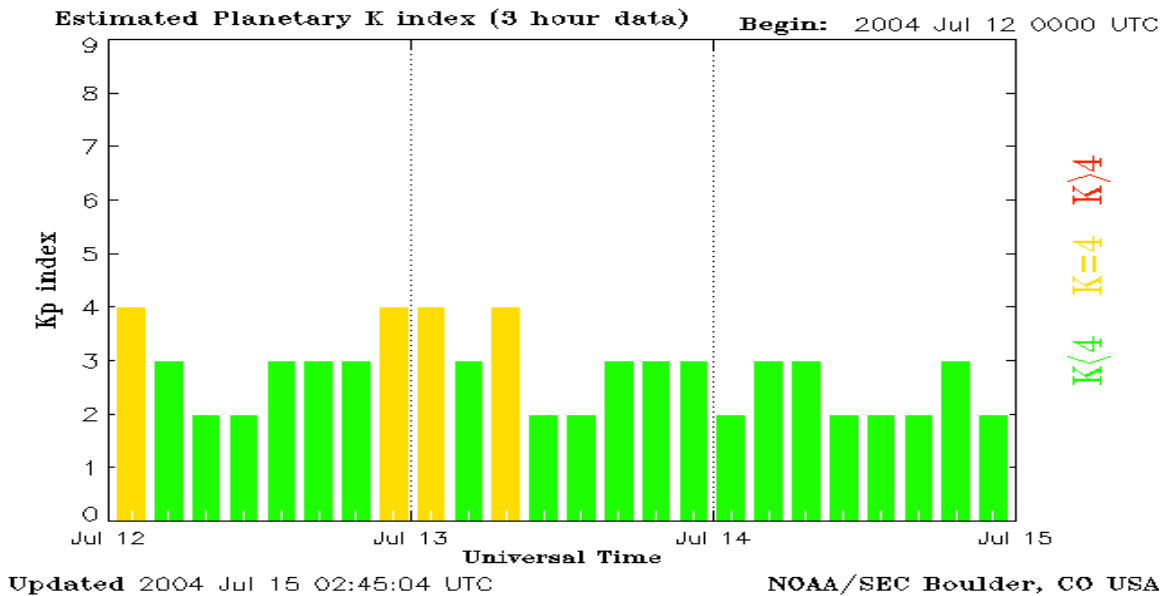


Figure 3.5 Kp index for a quiet day, 14 July, 2004

(Source: http://www.sec.noaa.gov/ftpmenu/plots/2004_plots/kp.html)

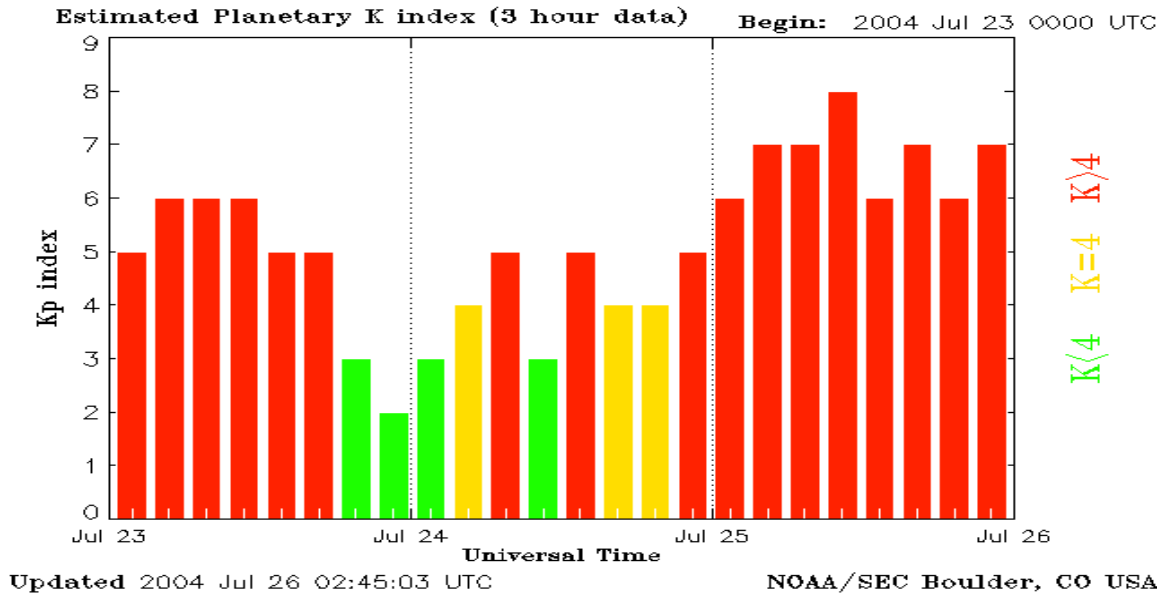


Figure 3.6 Kp index for a day of significant ionospheric disturbance, 25 July, 2004

(Source: http://www.sec.noaa.gov/ftpmenu/plots/2004_plots/kp.html)

3.3 Project Objectives

The overall goal of this project was to analyse and reduce the location dependent errors in the use of DGPS levelling in the north of Canada, as other researchers have done in different environments (Section 2.6). In addition, for any derived monument-based deformation monitoring method, the stability of the monument is a fundamental requirement, which must be quantified and taken into account in the total error budget (Kenselaar and Quadvlieg, 2001). For the target area, an area of relatively high heave/settlement, a relatively large signal is expected. To establish a complete error budget for the deformation monitoring in the target area, the long-term stability of different survey monument in permafrost has to be characterized and quantified.

The challenges for GPS in the target area mainly lie on two aspects. First, in the far north, no GPS satellites pass overhead of the observation stations and all the satellites scatter around the horizon, in which case the satellite geometry is degraded compared to the mid-latitude case. Another site-specific problem occurs due to the increased ionospheric activity in the north compared to mid-latitudes, and this is particularly exacerbated by the low angle of the satellites and subsequent increased path-length of the GPS signals. This leads to increased loss of signal (cycle slips) as well as path delays due to ionospheric activity (Skone *et al*, 2001).

In order to assess the ability of GPS for deformation monitoring in the target area, the attainable accuracy of GPS, especially height component, in the target area has to be examined. The impact of different error sources influencing GPS positioning accuracy has to be examined. These error sources include: tropospheric delay, antenna phase centre

variation, ionospheric delay and multipath. In addition, the impact of satellite geometry on GPS positioning accuracy is to be examined.

CHAPTER 4

PRE-RESEARCH FOR THE TARGET AREA

Prior to carrying out the field campaign in the target area, some initial research was carried out in order to characterize two types of error sources: antenna phase centre variation and multipath. In this chapter, an overview of these error sources is given, and experiments undertaken to characterize and/or mitigate these two types of error sources are described.

4.1 Antenna Phase Centre Variation

4.1.1 Introduction

Differential GPS solutions are obtained from a baseline vector which extends from a station with known coordinates and constrained to a station whose position is to be determined. Once a baseline vector is determined, it is assumed to be a vector between the antenna phase centres of the base and rover stations. However, the phase centre of a GPS antenna is neither a physical point nor a stable point (Mader, 1999). For any given GPS antenna, the phase center will change with the changing direction of the signal from a satellite. Ideally, most of this PCV depends on satellite elevation. Azimuthal effects are only introduced by the local environment around each individual antenna site (Mader, 1999).

These phase centre variations affect the antenna offsets that are needed to connect GPS measurements to physical monuments. If this variation is ignored, the measured baseline

will be between the average phase centres of the two antennas. These average phase centre locations are a weighted average of all the individual phase centers for each of the measurements included in the solution through least squares estimation. Antenna phase centre variation has become, besides tropospheric and multipath errors, the most limiting factor to achieve a breakthrough to the next accuracy level for precise GPS measurements (Wübbena *et al*, 2000). Ignoring these phase centre variations can lead to up to 10 cm vertical errors (Mader, 1999).

A full description of GPS antenna phase centre behaviour contains information on (Wübbena *et al*, 2000):

- Antenna Reference Point (ARP)
- 3D mean phase center offset referring to the ARP
- PCV for L1 and L2 with respect to the given offsets

Figure 4.1 illustrates the relationship between the ARP, mean offset and phase centre variation. The dimension arrows in this figure illustrate how the antenna PCV was related to the ARP.

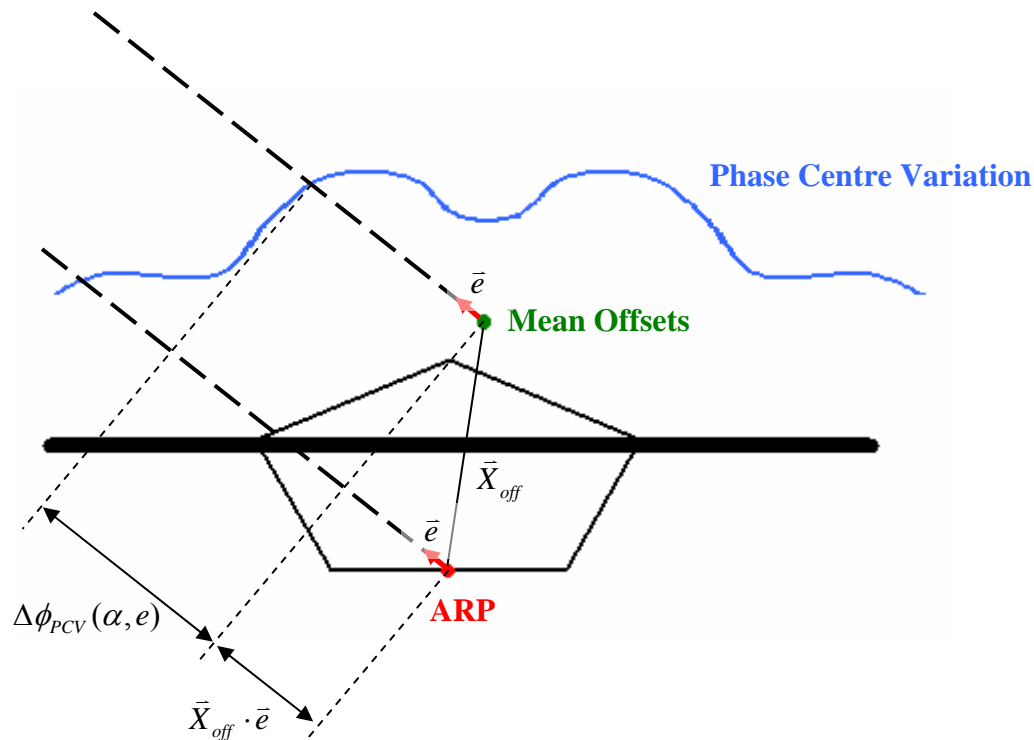


Figure 4.1 PCV description of a GPS antenna (Wübbena *et al*, 2000)

The antenna phase centres are the theoretical points in space where the carrier phase signals are measured to. Due to the imperfections in manufacturing, the phase centre appears to move depending on the direction of the incoming signals. This movement of the phase centre is called the phase centre variation. There exist several methods for antenna phase centre calibration: relative field calibration, absolute chamber calibration, and absolute field calibration (Menge *et al*, 1998).

Relative Field Calibration

The most common calibration method for antenna phase centre variation is relative field calibration as used in most commercial GPS software packages. Two antennas are mounted on two pillars separated by a short distance (approximately 5 m). Both antennas

are connected to GPS receivers which use a Rubidium oscillator as an external frequency standard. Because the PCV is determined using L1 or L2 single differences rather than double differences, the receiver clock error can not be cancelled out. The Rubidium oscillator is used to mitigate the receiver clock error variation. Using single differences will determine the PCV directly rather than from different satellites at different elevations. A 10 degree cutoff angle was used for tracking GPS signals by most agencies that carried out this type of calibrations (Mader, 1999).

The antenna PCV is determined separately for L1 and L2. To calibrate the antenna PCV, a reference antenna is selected, typically the JPL D/M+crT antenna, for which the PCV of this reference antenna are set to zero and the offsets are also fixed. The calibration is then referenced to this antenna. In the first stage of the calibration, a second JPL D/M+crT is mounted on the test pillar, so the L1 and L2 phase centre of this antenna on the test pillar can be determined. These positions are then used as a priori information for the L1 and L2 antenna phase centres of the remaining test antennas. From the solution of the test antennas, the difference from the a priori position can be calculated which can then be used to calculate the location of the test antenna phase center relative to the reference antenna.

The drawback of this type of calibration is as follows: Firstly, the antenna PCV for the reference antenna is set to zero, which is not true in reality. Secondly, the calibration is with respect to a particular circumstance (i.e. the product is dependent on the satellite constellation, the location of the test site and the multipath effects of the test site). Lastly,

since the 10 degree cutoff angle was used for tracking GPS signals during the calibration procedure, the relative field calibration products provide no information for satellites below 10 degree. With these drawbacks, the corrections are not sufficient for networks with differently orientated antennas (large extent networks), especially for the situation when two JPL D/M+crT antennas are used (Mader, 1999). There will be no corrections for the antenna PCV in this case. However, the product of relative field calibration is still widely used by most GPS data processing packages (Mader, 1999).

Absolute Chamber Calibration

Absolute chamber calibration is another solution to the antenna phase centre variation problem whereby the test antenna is precisely moved within an anechoic chamber with artificial GPS signals being used (Wübbena *et al*, 2000). Difficulties for this type of calibration may be the precise definition of the reference point, the mechanical precision of the entire mechanical setup and, possibly, remaining multipath. Since a point source rather than a constellation of sources are used, it is hard to achieve a very high number of observations for a well covered antenna hemisphere. Another issue here is the lack of knowledge about the discrepancy between the attributes of the GPS signals transmitted in the chamber room and in the real world, i.e., it may not fully simulate the circumstances in field conditions.

Absolute Field Calibration

The latest technology is to calibrate the absolute antenna PCV in the field (Wübbena *et al*, 2000). The goal of absolute field calibration is to separate the multipath effect from the

calibration results and to make it independent from a reference antenna and the test station (location, satellite constellation in view on that station, etc.).

The realization is based on the use of a rotating antenna and the use of special observation differences (i.e. sidereal Day difference). To achieve the rotation of the antenna, an automatic precise robot was developed, which is able to rotate the antenna around a fixed point (i.e. the nominal phase centre). The multipath effect is eliminated (in fact greatly reduced) by post processing, making use of the property of multipath Day-to-Day correlation. However, by sidereal Day difference, the antenna PCV was eliminated in this procedure. The antenna PCV is re-introduced by rotation and tilt of the antenna. The PCV difference between the no rotation/tilt on the reference Day and the rotation/tilt on the second is used as input for PCV determination.

The rotation/tilt of the orientation of the antenna not only re-introduced the antenna PCV, it also makes the coverage of the antenna's hemisphere consistent and homogeneous even with observations at the horizon. In this way, station dependencies were excluded. No station dependence can be seen from the plot, like the northern hole and observations down to elevation zero. Unfortunately, even with great advantage of this calibration method, the product is not widely used.

4.1.2 Antenna PCV Experiment

Since only relative field antenna PCV calibration products are available at the processing time, they are used in all the analysis carried out in this thesis. In order to evaluate the

effectiveness of these types of antenna PCV products, the following experiments were carried out on the roof of the engineering building at the University of Calgary with the aim of isolating the effect of PCV error from other error sources such as multipath, troposphere, and ionosphere.

Three sessions of data were captured, each of a 12-hour period and with the start and end of the sessions at the same time of the Day, so that the effects of multipath were approximately the same in each data set. Two monumented, force-centring, pillars (Figure 4.2) were used as the stations. To exclude the possible influence of errors in antenna height measurement, all GPS antennas were mounted directly onto the pillars and the antenna height was set to zero during processing.

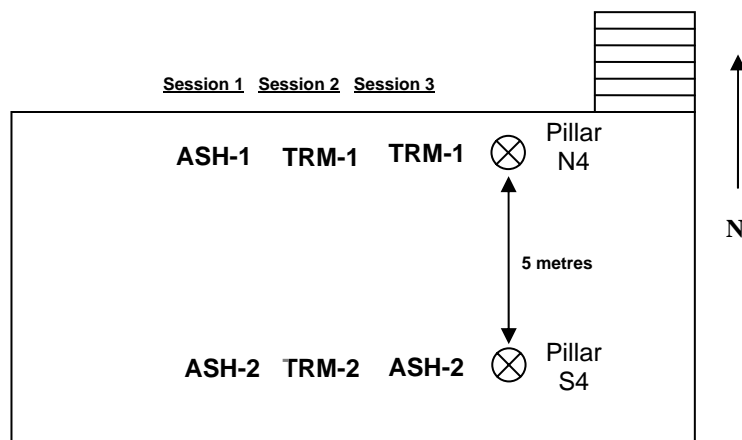


Figure 4.2 Experimental set-ups for antenna PCV correction error analysis

In the first session, two Ashtech antennas (ASH700718B) were set up on the pillars. In the second session, two Trimble antennas (TRM22020.00+GP) were set up on the pillars. In the third session, one Ashtech and one Trimble antenna were set up on the pillars,

respectively. The coordinates of pillar N4 were held fixed for all scenarios. In order to investigate the impact of antenna PCV corrections on GPS positioning accuracy (especially in height component) in different scenarios, the baselines were processed with Bernese using both L1 and ionosphere-free (IF) frequency combinations with both antenna PCV corrections on and off. The estimated station height difference between pillar N4 and S4 in different scenarios were summarized in Table 4.1.

Even though in the case when the PCV corrections were switched off, the antenna PCV error still can be cancelled out for this very short baseline when the same type of antenna types were used. But if different types of antenna were used, the impact of antenna PCV error becomes evident. In order to investigate the impact of PCV corrections, the estimated station height difference between pillar N4 and S4 in different scenario were compared as followed. As can be seen from Table 4.1, by switching the PCV corrections on and off, the disagreement in relative height estimations for session 1 and session 2 of 1-2 mm (L1 solution compared with L1 solution, IF solution compared with IF solution). When coming to the mixed antenna type scenario (session 3), the disagreement in relative height estimations between the same type of solution when the PCV corrections switched on and off of 6-20 mm.

Still the effectiveness of the relative field antenna PCV calibration products used in this thesis is of interest. Therefore the relative height estimations between the scenarios when PCV corrections switched on were compared as followed. The results given in Table 4.1 show a disagreement in relative height estimations between the scenarios of 1.4 mm to 12

mm with PCV corrections on. In the absence of other noise (the RMS of the residuals was 3-4 mm in each case) this was assumed to stem from un-calibrated PCV effects, especially in the mixed antenna case.

Table 4.1 Differences in height between pillars (m) estimated with three different antenna configurations using L1 and IF processing strategies with both antenna PCV corrections switched on and off

	PCV corrections ON		PCV corrections OFF	
	L1	IF	L1	IF
Session 1	-0.0039 m	-0.0027 m	-0.0049 m	-0.0025 m
Session 2	-0.0024 m	-0.0059 m	-0.0035 m	-0.0075 m
Session 3	-0.0059 m	-0.0144 m	0.0004 m	-0.0335 m

The IF solution gives the biggest differences, which is in agreement with previous work that shows this frequency combination to exacerbate the effects of an incorrect PCV model (Wübbena *et al*, 2000). Although it does not make sense to process such a short baseline with IF, the project baselines were all processed this way, and so the effects were of interest. Since the baseline is so short, the ionospheric-free combination amplifies noise without the benefit of removing ionospheric errors. The amplification of noise and multipath for an IF solution compared to an L1 solution was given in Table 4.2.

Table 4.2 The amplification of noise and multipath for an IF solution compared to an L1 solution (Cannon and Lachapelle, 2003)

Error	L1 Error (m)	IF Error (m)	Ratio $\frac{IF}{L1}$
SV Position	$\nabla\Delta\delta\rho_{sv}$	$\nabla\Delta\delta\rho_{sv}$	1
Receiver Position	$\nabla\Delta\delta\rho_{rec}$	$\nabla\Delta\delta\rho_{rec}$	1
Troposphere	$\nabla\Delta\delta\rho_{trop}$	$\nabla\Delta\delta\rho_{trop}$	1
Ionosphere	$-\frac{1}{f_1^2}\nabla\Delta\delta\rho_{iono}$	0	0
Multipath	$\nabla\Delta m$	$\frac{\lambda_{IF}}{\lambda_1}\nabla\Delta m\sqrt{\frac{f_1^2+f_2^2}{f_1^2}}$	3.227
Noise	$\nabla\Delta\varepsilon$	$\frac{\lambda_{IF}}{\lambda_1}\nabla\Delta\varepsilon\sqrt{\frac{f_1^2+f_2^2}{f_1^2}}$	3.227

As can be seen from Table 4.1, with PCV corrections on, if an L1 solution is used, the estimated station height differences between different antenna configurations are only 1.4-3 mm, which is near the level of the receiver noise. It can not really separate uncorrected antenna PCV from receiver noise in this case. However, when looking at the IF solution, the effect of mixed antennas is obvious. As can be seen, the difference between the estimated station height difference between sessions 1 and 2, in which the same type of antenna is used for each session but different types of antennas between sessions, was only 3.3 mm. Since the same types of antennas were used, the uncorrected antenna PCV can be cancelled out for this short baseline (5 m) in the double difference processing like other error sources such as receiver clock offset, ionospheric delay, and

tropospheric delay. When it comes to the mixed antenna type scenario, the problem of uncorrected antenna PCV is evident. The estimated station height differences between sessions 1 and 3 and sessions 2 and 3 are 11.9 mm and 8.6 mm, respectively. It can be concluded that the estimated station height error introduced by mixed antenna type in the IF solution for this 5 m baseline was at 1 cm level. The main phase centre offset component is vertical (up), which ranges from several centimetres to several tens of centimetres, but there are also small horizontal offsets (north and east), which is generally at millimetre level, that can be applied. There are actually two phase centres in an antenna – one for the L1 frequency and the other for L2, and each phase centre has a different offset.

4.2 Multipath

Multipath is another error source of interest, which can cause residuals of up to $\frac{1}{4}$ of the GPS signal wavelength (approximately 5 cm on L1) (Ray, 2000). A brief introduction of this type of error source can be found in Chapter 2, Section 2.4.4. There exist many different methods for multipath identification and mitigation (see Section 2.4.4). In the case of static GPS applications, multipath mitigation via Day-to-Day correlation can be deemed as the most effective method. In this section, multipath mitigation via a Day-to-Day correlation algorithm developed by Radovanovic (2000) was implemented and tested under different conditions.

4.2.1 Multipath Mitigation via Day-To-Day Correlation Algorithm

Since multipath is caused by reflections in the receiver environment, they will repeat under identical reflection geometries (Ray, 2000). Therefore, since GPS orbits repeat every sidereal Day, the multipath error for a static baseline will be the same every 23 hours 56 minutes.

In the case of very short baselines (<1 km), GPS error sources such as the tropospheric and ionospheric delay as well as orbital errors are highly correlated and therefore can be almost completely cancelled when forming double differences. At the same time, receiver and satellite clock offsets cancel in the double differencing process. Thus, the double differences of carrier phases between receivers a, b and satellites i, j can be written as:

$$\nabla\Delta\Phi_{ab}^{ij} = \nabla\Delta\rho_{ab}^{ij} + \nabla\Delta m_{ab}^{ij} + \nabla\Delta n_{ab}^{ij} + \lambda\nabla\Delta N_{ab}^{ij} \quad (4.1)$$

where Φ is the measured carrier phase in metres, ρ is the true range from a receiver to a satellite in metres, m is the multipath at each receiver for each satellite in metres, n is the carrier phase noise, λ is the signal wavelength in metre/cycle, N is the integer ambiguity for each satellite-receiver pair in cycles, and $\nabla\Delta$ is the double difference operator.

Furthermore, if the coordinates of the monitoring stations are known on one day (from a long GPS campaign for instance), then these coordinates can be used to calculate the theoretical ranges from a receiver to a satellite (For information on how to calculate satellite coordinates, refer to Section 2.2). The calculated theoretical ranges can then be used in Equation 4.1 to generate a “multipath signature” for the Day. Since multipath

repeats every Day, this generated signature can be used to correct the data collected on the next Day.

The procedure described above can be analysed using the standard model for carrier phase:

$$\Phi = \rho + \frac{c}{\lambda} \delta t_{sat} - \frac{c}{\lambda} \delta t_{rec} + m + n + N \quad (4.2)$$

where δt_{sat} and δt_{rec} are the satellite and receiver clock offset, respectively, c is the speed of light, and λ is the wavelength of the GPS carrier (19 cm for L1). By denoting quantities measured on different Days by their superscripts, this procedure described above can be analysed using the following equation:

$$\begin{aligned} \Phi_{clean} &= \Phi^2 - (\Phi^1 - \rho^1 - \delta t_{rec}^{est1}) \\ &= (\rho^2 + \frac{c}{\lambda} \delta t_{sat}^2 - \frac{c}{\lambda} \delta t_{rec}^2 + m^2 + n^2 + N^2) \\ &\quad - \left(\begin{array}{l} \rho^1 + \frac{c}{\lambda} \delta t_{sat}^1 - \frac{c}{\lambda} \delta t_{rec}^1 + m^1 + n^1 + N^1 \\ -\rho^1 - \frac{c}{\lambda} \delta t_{rec}^{est1} \end{array} \right) \\ &= \rho^2 + \frac{c}{\lambda} (\delta t_{sat} - \delta t_{rec} + \delta t_{rec}^{est1}) + \partial n + \partial N \end{aligned} \quad (4.3)$$

where δt_{rec}^{est1} is the estimated receiver clock offset on Day 1. Since the multipath error is correlated from day to day, the m term is cancelled out. The δt_{sat} and δt_{rec} terms will be cancelled out after forming double differences. The flowchart diagram of the mitigation algorithm generated by Radovanovic (2000) is described below in Figure 4.3.

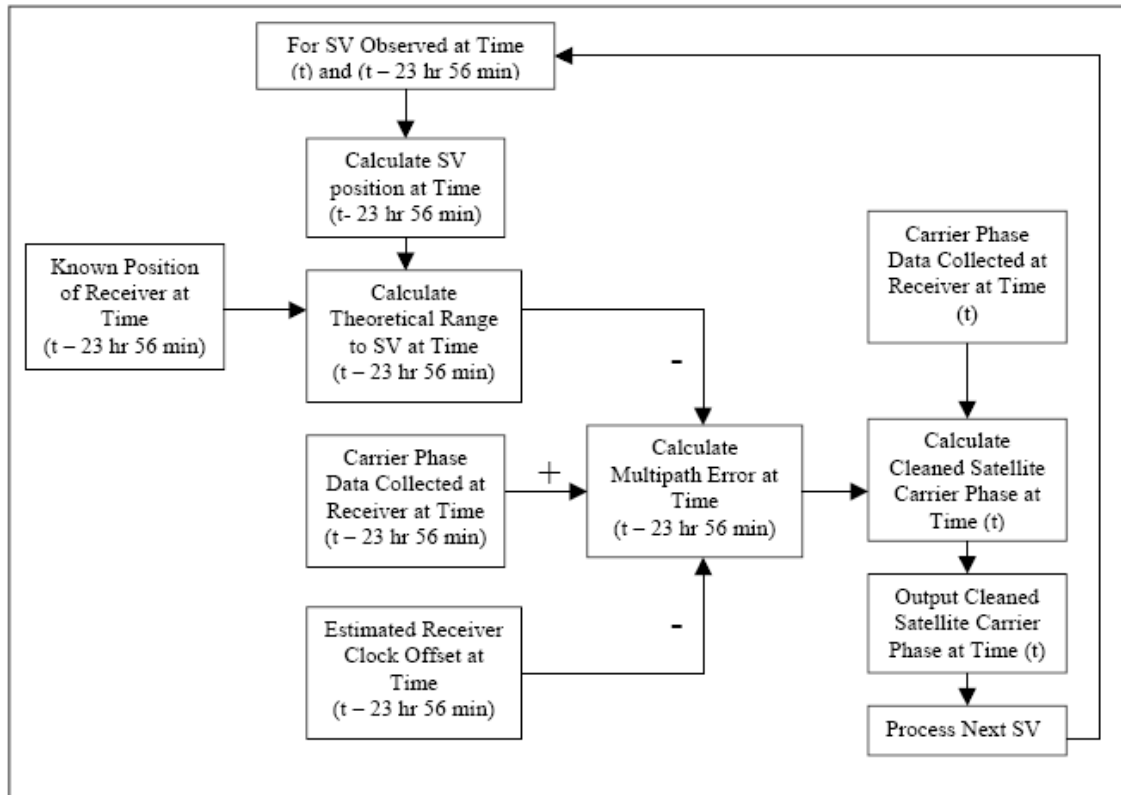


Figure 4.3 Flowchart diagram of multipath mitigation algorithm (Radovanovic, 2000)

The above algorithm works on a satellite-by-satellite and station-by-station basis. First of all, the known positions of each receiver are calculated previously (from a day-long GPS processing campaign, for example). Since the multipath mitigation algorithm operates directly on each carrier phase measurements, these calculated known positions have to be corrected to the antenna phase centre of each station to be used to calculate the theoretical range to each satellite. Secondly, for each observation epoch on Day 1, the receiver clock offset is estimated, the satellite position is calculated from an ephemeris file. Since both the receiver position and satellite position is available, the theoretical range from the receiver to each satellite can be calculated. Based on Equation (4.3), the “multipath signature” -- $(\Phi^1 - \rho^1 - \delta t_{rec}^{est1})$ can be calculated for each epoch on Day 1. Thirdly, for

each epoch on Day 2, the epoch time is deducted by 23 hr 56 min to locate the calculated multipath signature on Day 1, which will be used to correct the carrier phase measurement of the current epoch on Day 2. Fourthly, the cleaned carrier phase measurements on Day 2 are output to a file with RINEX format. Finally, the above described procedure is carried out on each epoch and each satellite.

The δt_{rec}^{est1} term is included such that the receiver clock offset of the cleaned observation will be approximately the same as that of the Day two observation. In some GPS receivers (such as the Ashtech Z-12), it allows the drift of the receiver clock error to grow to 1 ms before resetting the clock. Figure 4.4 illustrates the drift properties of the receiver clock of an Ashtech Z-12 receiver which was estimated through least squares batch processing. If the δt_{rec}^{est1} term is not included, the clock jump information in the data on Day 1 will remain in the cleaned phase observations after going through the procedures described in Equation (4.3), which can cause problems for data processing with the cleaned phase observation on Day 2. In this case, the clock jump information for Day 1 and Day 2 were mixed together, which will cause problem for the GPS software to detect them. Again, this term will cancel out in a single difference between satellites.

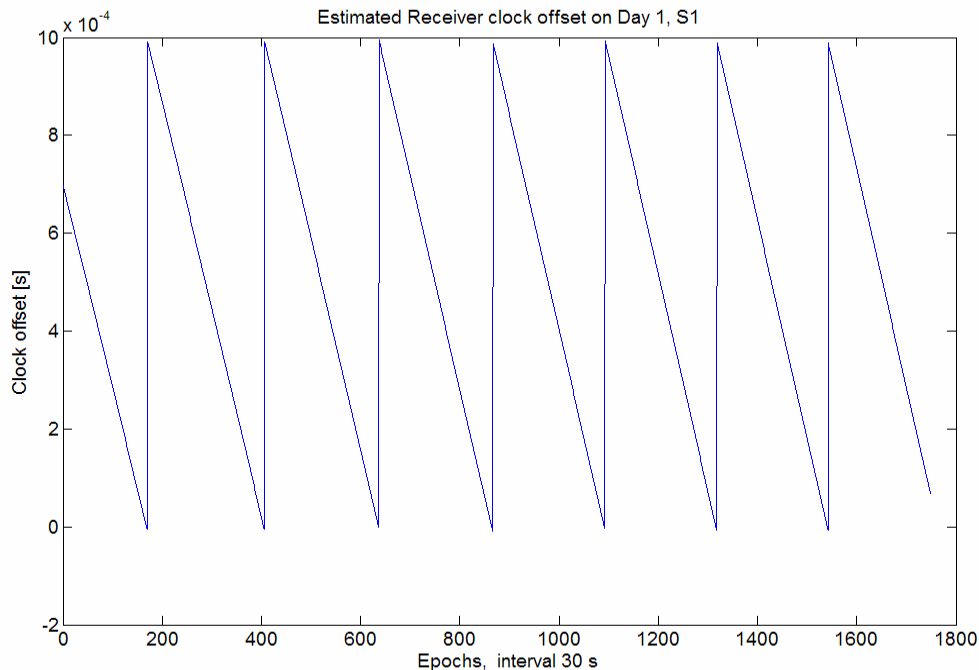


Figure 4.4 Receiver clock drift for an Ashtech Z-12 receiver

The above described multipath mitigation algorithm has been implemented as a pre-processor which operates on individual raw RINEX data files and outputs “clean” data in RINEX format.

With the mitigation algorithm developed by Radovanovic (2000), some test results has been reported. For his test results, the multipath mitigation algorithm can improve epoch-by-epoch position accuracies from 25% to 40%. The improvement in accuracy mainly depends on the magnitude of the multipath effect in the raw GPS data, i.e. for low multipath environment, the multipath mitigation algorithm is less effective, while for strong multipath environment, the effectiveness of the multipath mitigation algorithm is evident. Moreover, if the data is first corrected using the multipath mitigation algorithm and then the position estimates are averaged, the final accuracy improves by about 50%.

4.2.2 Test of the Mitigation Algorithm

In order to examine the success of the described algorithm, the following test procedures were carried out on the roof of the engineering building at the University of Calgary. Two Ashtech Z-12 receivers were mounted on pillars N1 and S1 separated by approximately 5 metres. About 12 hours of 15 s sampling interval dual-frequency data was collected at the same time of Day at both stations.

The IGS station PRDS (approximately 25 km from the test site) was included here to derive station coordinates for N1 and S1. By processing two 25 km baselines using all 12 hours worth of data in Bernese 4.2, the station coordinates for N1 and S1 were derived and used as input as the reference coordinates in the multipath mitigation algorithm. After the reference coordinates were derived, the test was then carried out on the 5-metre baseline between N1 and S1. In later data processing, the coordinates of N1 were held fixed to the derived reference coordinates and the station coordinates of S1 were to be estimated.

Prior to testing the multipath mitigation algorithm, the repeatability of the multipath error was examined. First, the station coordinates of N1 were held fixed to the above derived reference coordinates and the station coordinates of S1 on Day 1 were estimated on this 5-metre baseline. Then, the L1 fixed double difference residuals were generated for both Days 1 and 2 by fixing the station coordinates of N1 and S1 to the estimated station coordinates on Day 1. Figure 4.5 shows the DD residuals for the satellite pair PRN1/11. As can be seen, the multipath errors are highly correlated between days. In all

the analysis carried out for multipath mitigation algorithm, the relative field antenna PCV calibration products have been applied.

In order to better quantify the Day-to-Day correlation of multipath, the correlation coefficients between two Day's DD residuals were generated. The resulting plots for satellite PRN1/11 are shown in Figure 4.6. The peak of the correlation coefficient (93%) occurs with a 4 minute offset. Thus the correlation time of two consecutive Days is 23 hr 56 min (1 sidereal Day).

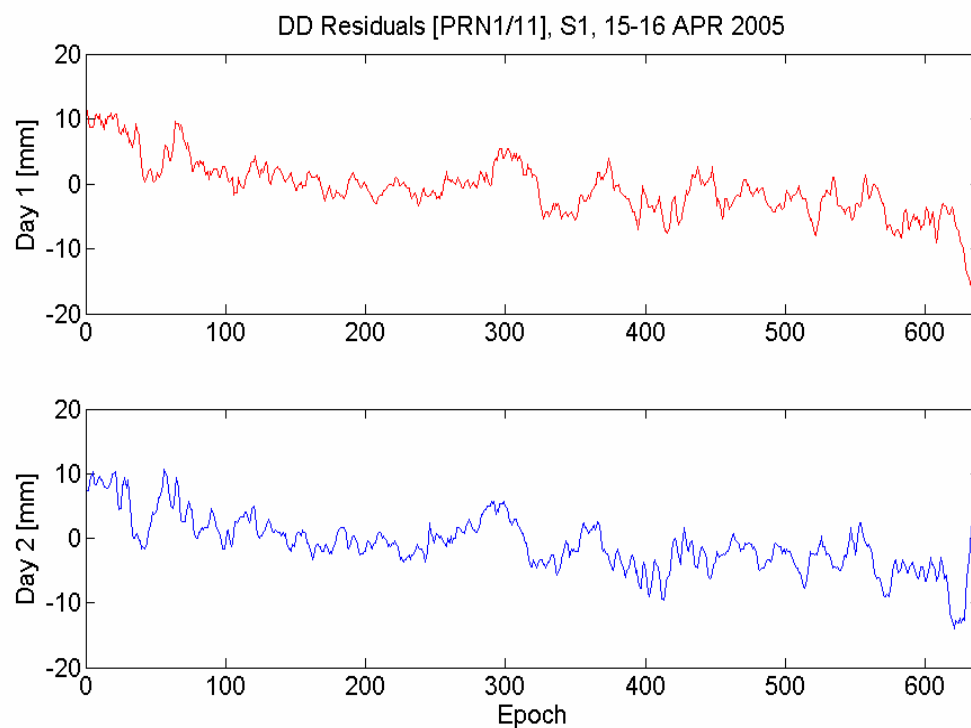


Figure 4.5 Two Day's DD residuals generated by fixing both N1 and S1's coordinates to Day 1's station coordinates estimation

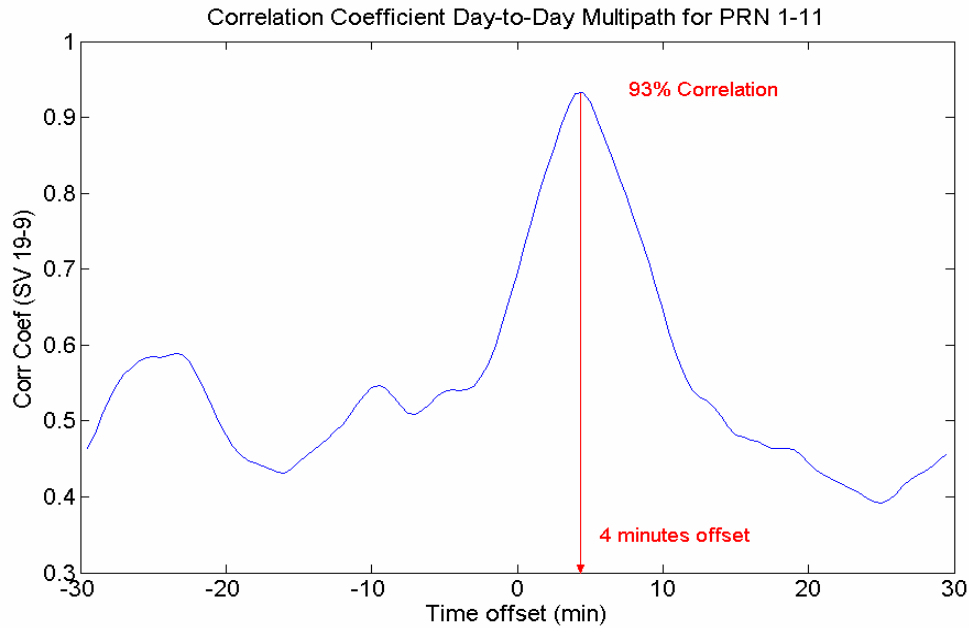


Figure 4.6 Multipath correlation coefficients between two consecutive Days

The Day 2 data was then corrected using the multipath mitigation algorithm using the two Days' worth of data. The corrected data was then used to generate DD residuals and calculate station coordinates of the S1 station on Day 2. Figure 4.7 shows the DD residuals for Day 1, Day 2 and that of Day 2 after applying the multipath mitigation algorithm. Statistics of the DD residuals are summarized in Table 4.3. As can be seen, the RMS of the DD residuals is reduced by 52%. In addition, most of the periodic signal in the DD residuals has been removed. To better understand this improvement, the power spectral density plots before and after applying the multipath mitigation algorithm are shown in Figure 4.8. This clearly shows that the low frequency signals in the DD residuals have been removed. This is important since it means that the behaviour of the DD residuals are now more white noise-like and can be more easily smoothed.

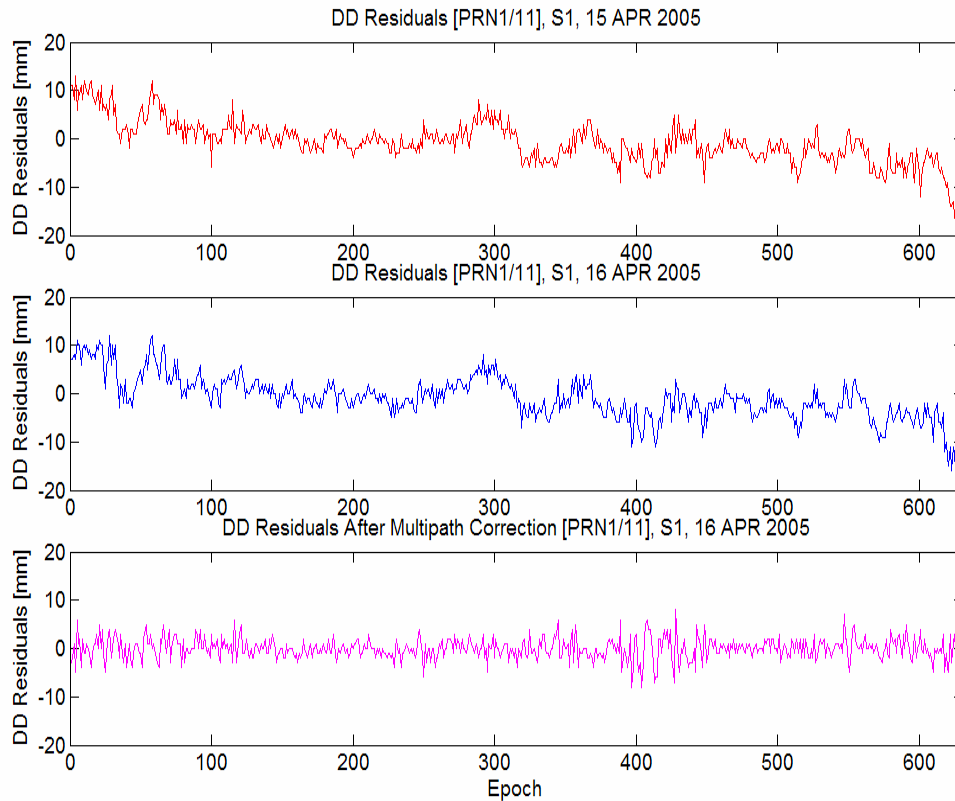


Figure 4.7 DD residuals for Day 1, Day 2 and that of Day 2 after applying the multipath mitigation algorithm

Table 4.3 Statistics of the DD residuals for Day 1, Day 2 and that of Day 2 after applying the multipath mitigation algorithm

	Day 1	Day 2	Day 2 corrected
Mean (mm)	-0.6	-0.7	0.0
RMS (mm)	4.5	4.7	2.2

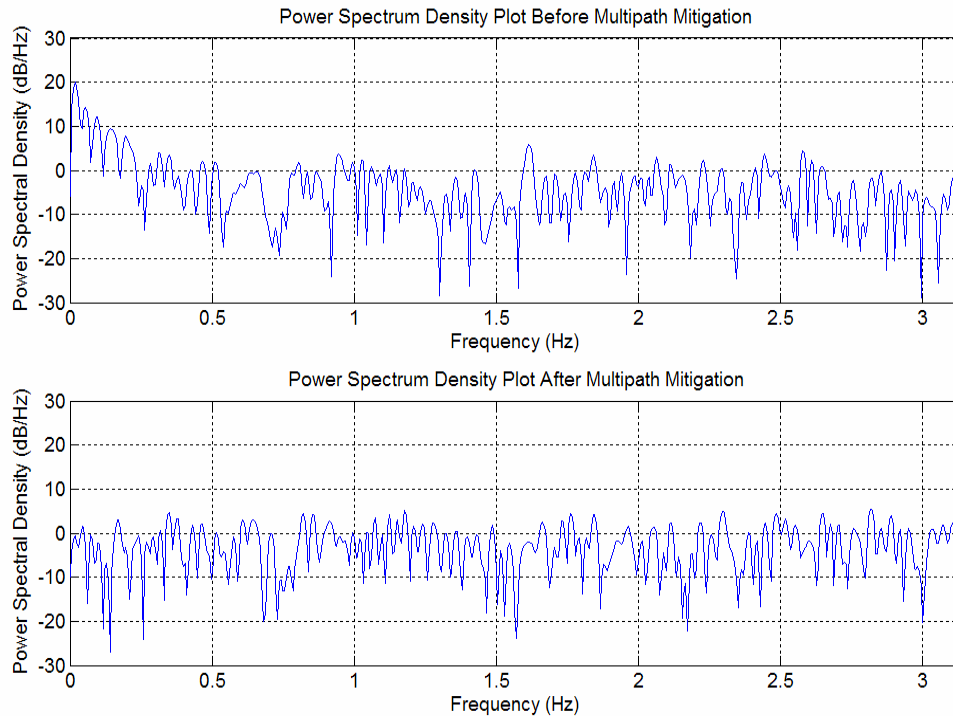


Figure 4.8 Power spectral density plots before and after applying the multipath mitigation algorithm

The results were also compared in the position domain. Before performing the test, the height difference between N1 and S1 was measured using an optical level. The measured height difference was 2.98 cm between these two stations. This height difference was then used as truth to check the correctness of the multipath mitigation algorithm. Then the original 12 hour data on Day 2 was processed using the Bernese software. Finally, the corrected 12 hour data on Day 2 was processed in Bernese. The measured station height differences between N1 and S1 from the optical level, processing using the original GPS data, and processing using the cleaned GPS data are summarized in Table 4.4.

Table 4.4 Measured station height differences from 12 hour data

	Optical level	Original GPS data	Cleaned GPS data on Day 2
Height Difference	2.98 cm	2.98 cm	2.99 cm

As can be seen from Table 4.4, all three methods give comparable results. Since Bernese adopts batch processing methods for data processing, which can be deemed as averaging epoch by epoch solutions over time, the multipath errors can still be averaged out if the occupation time is long enough. The above result shows that averaging (or long term filtering) is as efficient as the above described multipath mitigation algorithm.

A comparison was also made using 1 hour worth of data. The measured station height differences between N1 and S1 from optical level, processing using the original 1 hour GPS data, and processing using the cleaned 1 hour GPS data are summarized in Table 4.5.

Table 4.5 Measured station height differences from 1 hour data

	Optical level	Original GPS data	Cleaned GPS data on Day 2
Height Difference	2.98 cm	2.55 cm	2.87 cm

As can be seen from the table, if the occupation length is not long enough, averaging or long term filtering is not as effective as before. On the other hand, the multipath mitigation algorithm still gives satisfactory results (~1 mm) in this case. It is worth noting that the multipath mitigation algorithm in this case gave slightly degraded results. This is

because the satellite geometry starts to play its part in the results. It can be further expected that this multipath mitigation algorithm can be even more effective for the epoch-by-epoch solution case. Since this is not related to the work presented in this thesis, this will not be discussed here.

CHAPTER 5

EXPERIMENTAL DESIGN AND DATA PROCESSING

Recent work in DGPS on the effects of location dependent variables such as satellite geometry (Meng *et al*, 2004), tropospheric effects (Roberts and Rizos, 2004), and ionospheric effects (Janssen *et al*, 2001) have mitigated these errors by employing an optimised strategy for data capture and processing. The project described in this thesis therefore investigated the location-dependent errors for this region, such as satellite geometry, ionospheric effects, tropospheric effects and multipath, and the mitigation of these errors through different field and processing approaches, based on the expectation of an episodic campaign of DGPS measurements. Two GPS campaigns were carried out in the target area to address these specific issues and precise levelling was used to gather observations of the test points at a higher accuracy to provide ‘ground truth’ with which to compare the DGPS results after data analysis and the application of different error mitigation schemes. The aim of the project was to find the most accurate DGPS levelling solution on baselines up to 130 km for this region.

This chapter first summarises the data collected in the summers of 2003 and 2004. A study of the long term stability of different survey monument in permafrost was carried out based on the analysis of two newly collected epochs of precise levelling data together with historical data. GPS data processing was then carried out to investigate the impact of different error sources on GPS height estimation for the target area. The repeatability result analysis was used as an external assessment of the quality of the position results.

Based on the results, the best strategy for the field data collection and data processing was developed and is presented at the end of the chapter.

5.1 Data Collection in summer 2003

In the summer of 2003, GPS data as well as precise levelling measurements were collected at the Geodetic Survey of Canada (GSD) survey monument test-bed (approximately 15 km from the INVK IGS station) in Inuvik, Northwest Territories to establish the error budget for “GPS levelling” in the target area.

In 1987 the GSD established a long-term monitoring test-bed at the (then) Navy base in Inuvik. The objective was to establish the stability of different types of survey monuments in areas of continuous permafrost. The test-bed (Figure 5.1) comprised seven different types of monuments (see Appendix 1 for a description of the monuments) in a rough circle of diameter 70 metres, in an area described at the time as ‘wide open’. In addition, benchmarks were placed in a link traverse along Navy Road to an area of upland 3 km to the south of the test-bed. The monuments were measured by GSD using differential levelling, twice a year (winter and summer campaigns) between summer 1987 and winter 1995, with a missing epoch in summer 1994. The measurements were then discontinued.

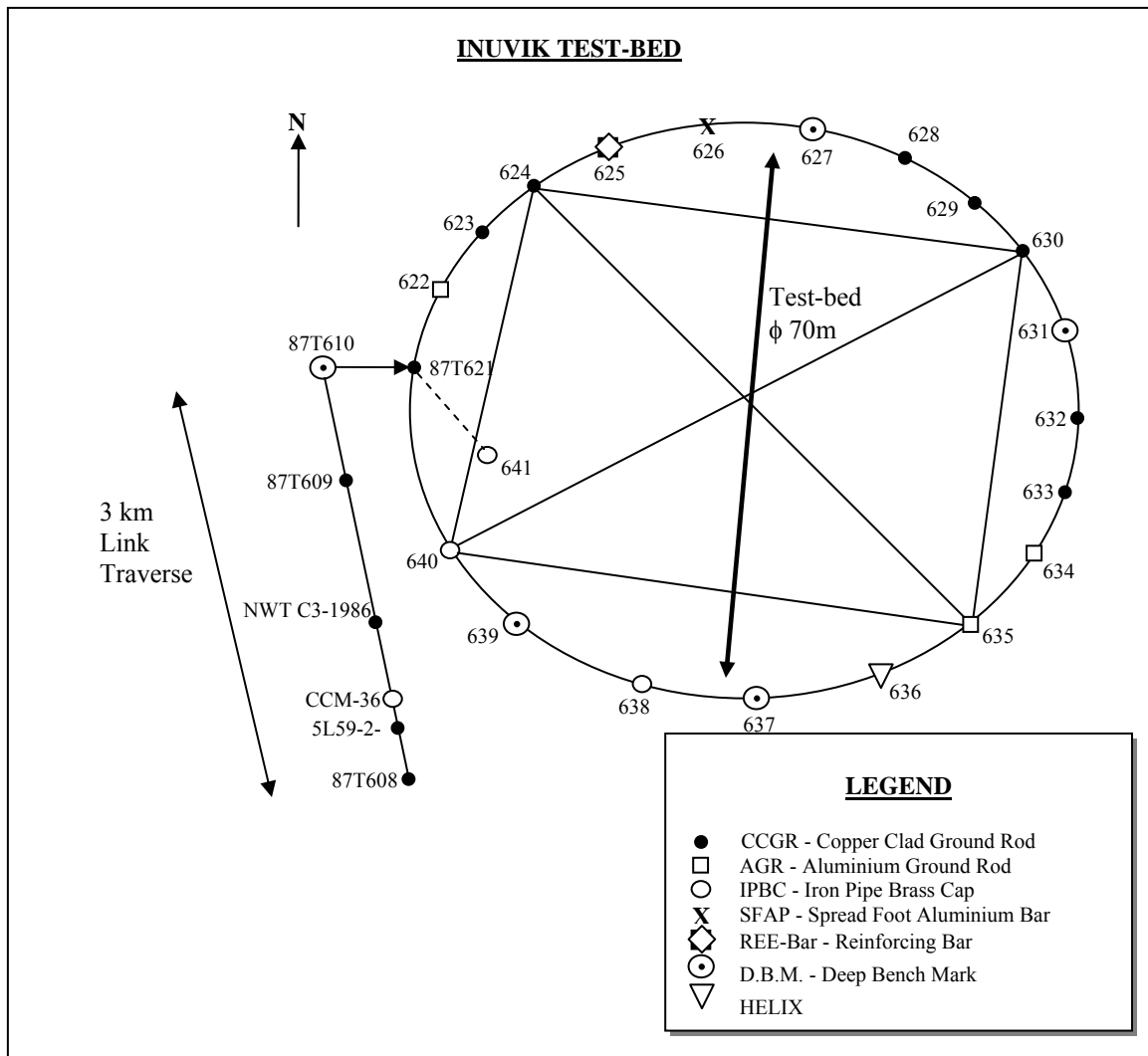


Figure 5.1 The Inuvik test-bed (Tait *et al*, 2004)

By visiting the test-site, some physical changes were observed to have taken place in the area (Tait *et al*, 2004):

- The area was no longer ‘wide open’ but was covered in denser vegetation (Figure 5.2).
- Benchmarks 626 and 633 were unstable in height over the time period of the measurement (they could be moved 1-2 cm by hand pressure alone).

- The benchmark at 608 had clearly been struck, presumably by earth-moving equipment from the recent building in the immediate area. Other monuments on the link traverse had been destroyed (CCM36, the cap had been sheared from this steel pipe, presumably by snowplough) or were unstable (NWT C3-1986, a brass-capped monument was in a swampy area by Navy Road and unstable during measurement).

Four GPS receivers, including two Ashtech Z-12 GPS receivers with ASH700718B antennas and two Trimble 4000SSI GPS receivers with TRM22020.00+GP antennas, were used for data collection. All the GPS antennas were attached to a ground plane. The equipment used at the INVK station was an Ashtech UZ-12 receiver connected with an Ashtech 701945C_M choke ring antenna. Twenty-one monuments in this test-bed were occupied during 6 sessions for 12 hours each with a sampling frequency of between 15-30 seconds depending on the on-board memory of the receiver. The GPS data was collected all using 5 degree cut-off angles. Three of the monuments were re-occupied for similar periods of the day.

Observations of external accuracy were made of the relative heights of the stations using differential levelling. The instrument used was a Leica 3003 digital level with a 3 m solid Invar levelling rod. Misclosure of the circle observations was 0.05 mm, excluding 626 and 633 that could not be satisfactorily measured. Levelling the double-run between 610 and 621 gave a similar misclosure of 0.07 mm. The levelling result shows an order of

magnitude better precision than expected from DGPS levelling judged as being sufficient to be used as ‘ground truth’ with which to compare the DGPS results.



Figure 5.2 Test-bed with a geodetic GPS receiver set over benchmark 623 (2004 campaign). Vegetation in the area was moderately-dense small trees and bushes, with moss below.

5.2 Data Collection in summer 2004

In the summer 2004, another field campaign was carried out at the test site. Some changes were made on the data collection scheme and are listed as follows:

1. Only Ashtech Z-12 receivers were used for the data collection for the 2004 campaign. Still, all the antennas were attached with a ground plane.

2. The GPS data was collected all using 0 degree cut-off angles and 30 sec sampling intervals. The 0 degree cut-off angle was selected to allow the analysis of the influence of different cut-off angles on height estimation. Since the sampling interval used for the INVK station was 30 sec, only a 30 sec sampling interval for data collection was needed. Based on the onboard memory size of the Ashtech Z-12 receiver used, using a 30 sec sampling interval allows for the storage of 12 hours of data.

3. Data was collected on the same benchmark for the same period of time on two consecutive days in order to allow for multipath mitigation via day-to-day correlation analysis and repeatability analysis.

Applying the newly developed data collection scheme, new GPS data was collected at the INVK test-bed through July 8th-15 and July 24th-27, 2004. Levelling measurements were made using an optical level (NA2) as an external check for the GPS height estimation. Table 5.1 summarizes the 2003 and 2004 DGPS campaigns and external data collection.

Table 5.1 Summary of 2003 / 2004 DGPS campaign and external data collection

Length (km)	Rover type (s)	Choke ring	# of stations occupied	Occupation length (h) / sampling frequency (s)	# re-occupied	External comparison
15 (2003)	Ashtech Z12 Trimble 4000SSI	N	21	12 / 15-30	3	Differential levelling (Reduced level estimated accuracy 0.02mm 1 σ)
15 (2004)	Ashtech Z12	N	6 (twice)	12 / 30	6 (twice)	Differential levelling (RL 1.1mm 1 σ)
130	Ashtech UZ12	Y	2	12 / 30 (Data from CDDIS)	N/A	IGS weekly average coordinates

5.3 Long-term Stability of Different Survey Monument in Permafrost

Since it was desirable to have both vertical and planimetric measurements of deformation, a monumented solution using DGPS observations was recommended (Tait and Moorman, 2003). However, this method relies on the measurement station to remain stable for 20-30 years. A stability study of seven different types of monuments had been carried out at the Inuvik test-bed (see Section 5.1 for a full description of the Inuvik test-bed).

In the summers of 2003 and 2004, two new epochs of GPS and precise levelling observations were made. These newly collected height difference measurements, together with the historical data (height difference measurements collected from 1987 to 1995)

provided by GSD, were then each processed using parametric least-squares estimation for direct comparisons. Figure 5.3 shows the height change with time on benchmark 625.

An initial analysis of the stability of the monuments was made by classifying all the monuments into three groups according to the depth of their foundation. However, variance tests on the in-group and between-group variations showed increasingly inconsistency as the foundation depth increased (Tait *et al*, 2005). In order to derive a linear relationship between depth of foundation and monument stability, individual factors (including geological and active layer qualities and type of monument) that might affect the stability of the monuments were then examined.

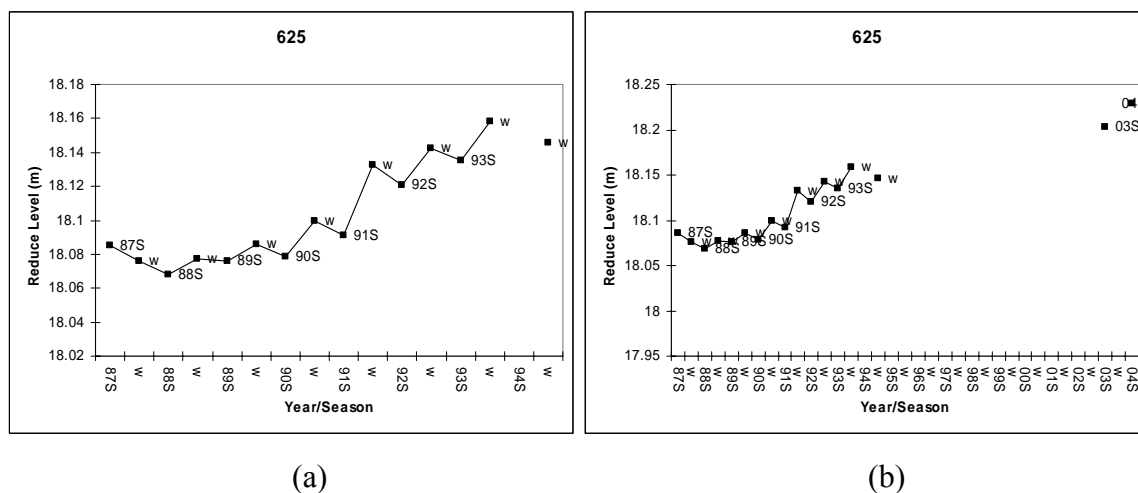


Figure 5.3 Plot of height change with time for benchmark 625 with a missing epoch in the summer 1994 for a) 1987-1995 and b) 1987-2004 (Tait *et al*, 2005)

A factor analysis of the geological and active layer qualities was restrained by the incompleteness and inconsistency of the data sets (Tait *et al*, 2005). By analyzing different types of monuments, it was found that the use of solid ground rods founded at 5.5 m or deeper will display a similar movement pattern which is independent of the geological conditions in which they are founded (Tait *et al*, 2005).

5.4 Initial Processing

Data collected from the 2003 Inuvik campaign was first processed using Bernese 4.2, using a standard processing strategy (Mode 1, Table 5.2) and then reprocessed by changing one of the options (Modes 2 and 3). All the other options were kept the same, including cut-off angle which was 15°.

Table 5.2 Effects of various error sources on the standard processing strategy for the 15 km baselines (24 baselines in total) measured in 2003

Processing Mode	Standard deviation of differential height compared to levelled values (mm)	Mean of the absolute value (mm)
Mode 1. Standard Processing Strategy: <ul style="list-style-type: none"> • Including PCV correction (from IGS tables) • Using IGS precise orbit • 12 hours time span • Saastamoinen model and cosZ mapping function 	15.2	12.4
Mode 2. Set antenna PCV corrections to zero	30.5	23.6
Mode 3. Processing using Broadcast orbit	16.0	13.1

For these 15 km baselines, the dominant error source for carrier phase differential GPS is the ionospheric delay. In order to remove ionospheric errors, the final results are all given for the ionosphere-free (IF) fixed solution. Comparison of the different solutions (L1, L2, and IF) to the levelling results shows that the IF fixed solution gave the best result. Therefore, in Mode 1, 2 and 3, IF fixed solution were used to generate the results.

Since the precise levelling measurements are given in station height differences, the estimated station heights from GPS data were then used to calculate station height differences in order to compare the result with precise levelling directly. The standard deviation of the differences between GPS derived height differences and levelled values are calculated and listed in Table 5.2. The mean value of the absolute value of above mentioned differences are also calculated.

The mean value is not calculated directly here because it does not give any information on the “GPS levelling” accuracy. Since all the benchmark forms were aligned on a circle, the sum of the height difference is actually the “GPS levelling” misclosure on the circle, which is very close to zero.

As can be seen from Table 5.2, the effect of PCV correction is significant as expected, and errors using broadcast orbital ephemeris display the insignificant affect anticipated in theory.

5.5 Antenna Phase Centre Variation

In the 2003 GPS campaign, three benchmarks on the test-site were re-occupied with a different antenna (Trimble TRM22020.00+GP and Ashtech 700718 antennas), as well as with the same type. On examination of the repeatability of the station height estimation, those stations occupied by the same types of antenna gave agreement within 2 mm, while the stations occupied by the different types of antenna was around 3 cm (see Table 5.3).

The station height estimation was generated by IF fixed solution in Bernese by including antenna PCV corrections (relative calibration products from IGS) in the data processing.

The bias in the differential heights was presumed to partially come from uncorrected antenna PCV. Processing was repeated using the Trimble Total Control software (including antenna PCV corrections) with similar results, indicating that a residual error in PCV correction is a common occurrence.

Table 5.3 Station height estimation repeatability for Benchmark 624 (mixed antennas), 635 (mixed antennas), 640 (similar antennas)

Benchmark name	624	635	640
1st measure (m)	14.2477	16.4382	14.0703
2nd measure (m)	14.2153	16.4700	14.0688
Difference (m)	0.0324	-0.0317	0.0016

In order to characterize the impact of the uncorrected antenna PCV on GPS positioning, the previous antenna PCV experiment was carried out (see Chapter 4, Section 4.1.2). In the context of the experiment, the estimated station height error introduced by mixed antenna types in the IF solution for this 5 m baseline was at the 1 cm level. It should be noted that the 3 cm disagreement found by examining the repeatability of the estimated station height at the test-site was not solely due to the uncorrected antenna PCV. For the 15 km baseline, the tropospheric delay error at the base and rover station decorrelates. The residual tropospheric delay goes into the station height estimation as well, which

contributes to the 3 cm disagreement. In addition, only two types of antennas (TRM22020.00+GP and ASH700718) were used in the antenna PCV experiment carried out on the roof of the engineering building, while three types of antenna (TRM22020.00+GP, ASH700718, and ASH701945C_M) were involved in the 2003 summer field campaign. In this case, the uncorrected antenna PCV for the ASH701945C_M antenna may have magnified the impact of the antenna PCV on positioning accuracy.

Based on the above analysis, only one type of receiver/antenna was used for the 2004 summer campaign in order to avoid the potential problem arising by the use of mixed antenna types.

5.6 Ionosphere and Satellite Geometry

5.6.1 Influence of Enhanced Ionospheric Activities on GPS Receiver Tracking Performance

The target area lies within the auroral region (Figure 5.4). The auroral region is typically located between 65 and 75°, where the visible aurora occurs overhead (Rostoker and Skone, 1993). These regions are characterised by enhanced energetic electron precipitation (Skone, 2001). The associated irregularities in electron density lead to rapid phase and amplitude fluctuations when GPS signal travel through the ionosphere, known as scintillation effects (Skone, 2001).

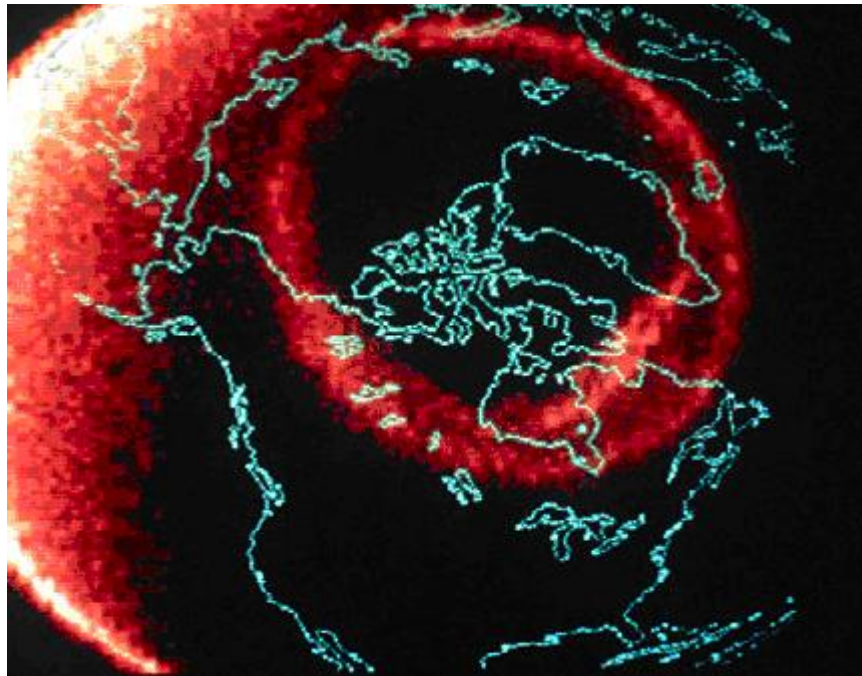


Figure 5.4 Auroral Region

(Source: <http://www.geomatics.ucalgary.ca/faculty/SSkone/SSkone.html>)

GPS receiver tracking performance can be degraded during the above mentioned storm events (Knight *et al*, 1999; Nichols *et al*, 1999). Rapid phase variations (phase scintillations) cause a Doppler shift in the GPS signal, which may exceed the bandwidth of the phase lock loop (PLL), resulting in a loss of phase lock (Leick, 1995). Additionally, amplitude fades can cause the signal-to-noise-ratio (SNR) to drop below the receiver threshold, resulting in loss of code lock (Skone, 2001).

These effects have a larger impact on tracking loops employing codeless and semi-codeless technologies (to extract the encrypted L2 signal) versus full code correlation (Skone, 2001). In particular, codeless and semi-codeless tracking loops experience losses of 27-30 and 14-17 dB, respectively, compared with full code correlation mode, and

therefore are more susceptible to the effects of amplitude fading (Cannon and Lachapelle, 2003). Availability of the L2 signal is particularly important for positioning applications requiring the formation of ionosphere-free combination.

The receiver performance can be quantified in terms of both the number of cycle slips detected and the number of observations missing during reacquisition periods. It is necessary to consider the number of missing observations as an additional statistic in order to accurately reflect the range of the receiver performance (Skone, 2001). When loss of tracking happens, a reacquisition period is required for the receiver to re-track the GPS signal. During this time period, observations may be missing during data dropouts. The longer the reacquisition periods needed for receivers, the more observations will be missing. In such cases only one cycle slip will be detected, but the impact on positioning applications is significant in terms of data dropouts (Skone, 2001).

Table 5.4 shows the marked unpaired L1/L2 observations and cycle slips reported from Bernese for the GPS data collected in 2003. As can be observed in Table 5.4, the Ashtech Z-12 receiver has a better performance than the Trimble 4000SSI receiver. The tracking loop of the Ashtech Z-12 receiver employs semi-codeless technology, while the tracking loop of the Trimble 4000SSI receiver employs codeless technology (Skone and de Jong, 2000). The performance of these two types of receiver coincides with the aforementioned conclusion. The performance of the L1 tracking loop is better than the L2 tracking loop, since the L1 tracking loop employs full code correlation technology, in which case no

power loss is encountered. In addition, due to nature of codeless/semi-codeless technique, the number of cycle slips between L1 and L2 are 100% correlated.

Table 5.4 Marked unpaired L1/L2 observations and cycle slips reported from
Bernese for the GPS data collected in 2003

Session	Baseline	# L1 unpaired	# L2 unpaired	# L1 cycle slip	# L2 cycle slip	Rover Receiver Type
03-0723	INVK-T630	22	6	89	89	Ashtech Z-12
	INVK-T640	78	1	1	1	Trimble 4000SSI
	INVK-T635	73	0	199	199	Trimble 4000SSI
	INVK-T624	25	8	88	88	Ashtech Z-12
03-0724	INVK-T631	0	1	15	15	Ashtech Z-12
	INVK-T641	25	0	15	15	Trimble 4000SSI
	INVK-T636	0	0	45	45	Ashtech Z-12
	INVK-T625	22	0	90	90	Trimble 4000SSI
03-0725	INVK-T632	18	12	82	82	Ashtech Z-12
	INVK-T621	134	4	136	136	Trimble 4000SSI
	INVK-T637	92	3	541	541	Trimble 4000SSI
	INVK-T626	9	6	244	244	Ashtech Z-12
03-0726	INVK-T633	11	1	32	32	Ashtech Z-12
	INVK-T622	71	1	36	36	Trimble 4000SSI
	INVK-T638	64	1	48	48	Trimble 4000SSI
	INVK-T627	10	1	48	48	Ashtech Z-12
03-0727	INVK-T634	33	26	140	140	Ashtech Z-12
	INVK-T623	180	4	194	194	Trimble 4000SSI
	INVK-T639	152	4	248	248	Trimble 4000SSI
	INVK-T628	29	14	250	250	Ashtech Z-12
03-0728	INVK-T635	66	12	137	137	Ashtech Z-12
	INVK-T624	404	5	352	352	Trimble 4000SSI
	INVK-T640	365	7	407	407	Trimble 4000SSI
	INVK-T629	58	3	299	299	Ashtech Z-12

Most of the cycle slips reported by Bernese were actually due to the resetting of the receiver clock. In some GPS receivers, it allows the receiver clock offset to grow to 1 ms before resetting the clock (see Section 4.2.1). This kind of property depends on the receiver design.

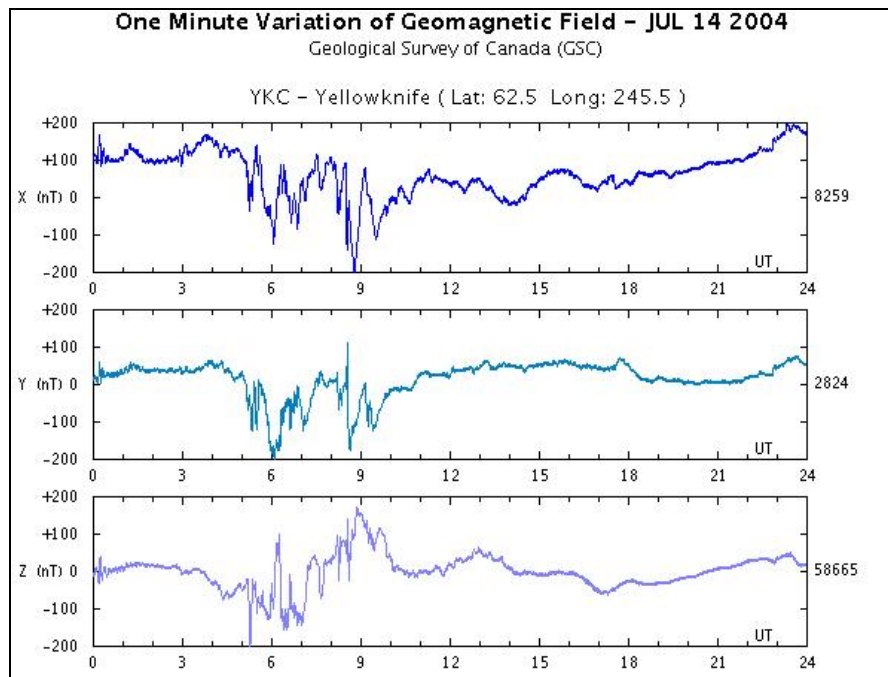
By examine the Kp index for each session listed in Table 5.4, enhanced ionospheric activities was experienced ($K_p > 4$) during the data collection of session 03-0725, 03-0727, and 03-0728. Correspondingly, more unpaired L1 and L2 observations (especially unpaired L1 observations) were reported in Table 5.4 for these three sessions. This impact is more obvious on Trimble 4000SSI receivers, which adopt codeless tracking technique.

For the above mentioned reason, only the Ashtech Z-12 receivers adopting semi-codeless tracking technique were used in the 2004 campaign. The use of semi-codeless receivers for the 2004 15 km and 130 km baselines gave approximately 30-40 cycle-slips per 12-hour session at 15° elevations. These data were used in all the following analyses.

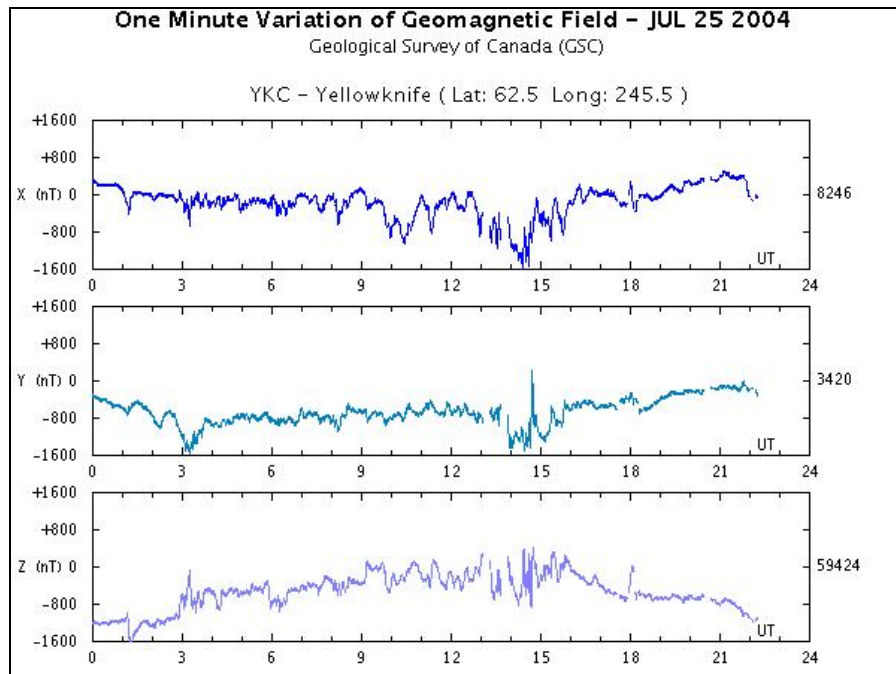
5.6.2 Influence of Enhanced Ionospheric Activities on GPS Positioning Accuracy

This section examines whether or not the most effective processing of the baselines observed using the IF solution, together with the usual Elevation Dependent Weighting (EDW) measures associated with path delay correction, are effective during an ionospheric event. The balance between reducing errors in longer paths and maintaining the best satellite geometry was also of interest.

In order to assess the most appropriate strategy for processing data observed during an ionospheric event, two 15 km baselines were chosen from the 2004 campaign that each had 12-hour observations in both a quiet ionospheric period and during an ionospheric event. These periods were assessed using the one-minute variation of geomagnetic field for the Yellowknife station, the closest station to the test area (approximately 1100 km). The dates chosen were July 14 and 25, the assessments of which are shown in Figures 5.5a and 5.5b.



(a)



(b)

Figure 5.5 Plots of ionospheric activity from Yellowknife recording station for (a) July 14 and (b) July 25 2004 (Natural Resources Canada website

http://www.geolab.nrcan.gc.ca/myservlet/geomag/magnetogram/dataplot_geomag_e.jsp)

The estimated planetary K indices for these two days have also been shown in Section 3.2.4. However, such indices only provide an approximate measure of global ionospheric activity at higher latitudes. To assess the ionospheric activity in the target area, local magnetic field data (at least local in a global sense) was needed. Thus, the one-minute variation of geomagnetic field data at the Yellowknife station (the closest available station for the target area) for a quiet day (July 14 2004) and a day of significant ionospheric disturbance (July 25 2004) were used. Clearly there are large magnetic field fluctuations at high latitude in Canada on July 25. Variations of 500-1000 nT indicate a

storm event. An event of such magnitude has a frequency of approximately 10-12 times per year and duration of around 24 hours (Skone, 2003).

The baselines were processed at different cut-off angles to determine whether there was a ‘best’ configuration of processing in these conditions. The 2004 15 km baselines were processed for both days with EDW both activated and switched off. The results demonstrated no major advantages gained through the application of EDW during the July 14 dataset, and a worsening of the result using EDW during the 25 July session. In terms of path length versus geometry, external accuracy assessments displayed an increasing accuracy from 0° until the 15° cut-off was reached, followed by a reduction in accuracy. In the longer baselines (130 km), with larger expected differences in atmospheric delays at the stations, the same trend was evident (Table 5.5).

Table 5.5 Effect of the variation in cut-off angle, and the use of the EDW, for two 130 km baselines observed on July 14 and July 25 2004. Estimates of height and the mean and standard deviations between these and weekly IGS averages results are shown.

Cut-off angle (degrees)	Estimated heights (GPS) in metres				12 hour session height TUKT– weekly average (m)	
	July 14 EDW on	July 14 EDW off	July 25 EDW on	July 25 EDW off	mean	1σ
0	-1.5313	-1.5348	-1.5440	-1.5357	-0.0074	0.0070
5	-1.5461	-1.5363	-1.5494	-1.5357	-0.0129	0.0074
10	-1.5415	-1.5339	-1.5358	-1.5299	-0.0063	0.0040
15	-1.5321	-1.5283	-1.5249	-1.5253	0.0014	0.0018

20	-1.5228	-1.5220	-1.5233	-1.5230	0.0062	0.0025
Average height estimated	-1.5348	-1.5311	-1.5355	-1.5300		

Note: IGS height difference = -1.5308m for July 14 and -1.5272m for July 25

5.7 Tropospheric Delay Estimation Strategy

When processing GPS data, the tropospheric delay is typically predicted using empirical models, such as models developed by Saastamoinen (1972) and Hopfield (1970). By using these models, standard or measured ground meteorological data, such as temperature, pressure and humidity, must be provided. However, even when accurate meteorological data is available, the predicted tropospheric delay from these models still does not have a high accuracy. The residual tropospheric delay can be the largest remaining error source in dual-frequency precision positioning (Collins and Langley, 1997).

Since tropospheric delay is a spatially dependent error source, it can not be completely removed by forming double differencing for long baselines. The differential tropospheric delay may be significant depending on the meteorological conditions in base and rover stations (ranging from 1-3 ppm in extreme conditions). Yunck (1993) pointed out that the tropospheric delay error in the vertical component far exceeds the inherent geometric weakness of GPS.

In order to obtain the highest precision, the residual zenith tropospheric delay is usually estimated along with other unknowns such as station coordinates. At high elevation angles, the error in the estimated tropospheric zenith delay is virtually absorbed into the height component. To investigate its influence on GPS height estimation, the data was processed in Bernese using different tropospheric delay estimation methods. The tested strategies were as shown in Table 5.6. For all these tropospheric delay estimation methods, the elevation dependent weighting scheme was switched off.

Table 5.6 Tested tropospheric delay estimation strategies

Processing Mode Options	1	2	3	4	5	6	7	8
A priori tropospheric model	Saas	Saas	Saas	No	No	Saas	Saas	Saas
Mapping function	cosZ	cosZ	cosZ	Neill	Neill	cosZ	Neill	cosZ
Estimate residual zenith delay every	2 h	2 h	2 h	2 h	2 h	1 h	2 h	2 h
A priori sigma for absolute/relative zenith delay (m)	1/5	1/0.012	1/0.012	1/0.012	1/0.012	1/0.012	1/0.012	1/0.012
Estimate residual tropospheric zenith delay parameter for base station	No	No	Yes	No	Yes	Yes	Yes	No
Estimate residual tropospheric zenith delay parameter for rover station	Yes	Yes	Yes	Yes	Yes	Yes	Yes	No

The estimated station heights for T625 and T631 using the above eight different tropospheric parameter estimation strategies are shown in Figure 5.6. The estimated

station height differences between T625 and T631 from two baseline solutions (INVK to T625 and INVK to T631) using these strategies are shown in Figure 5.7. The measured station height difference between T625 and T631 from levelling is -1.4779 m, with an expected accuracy of around 2-3 mm.

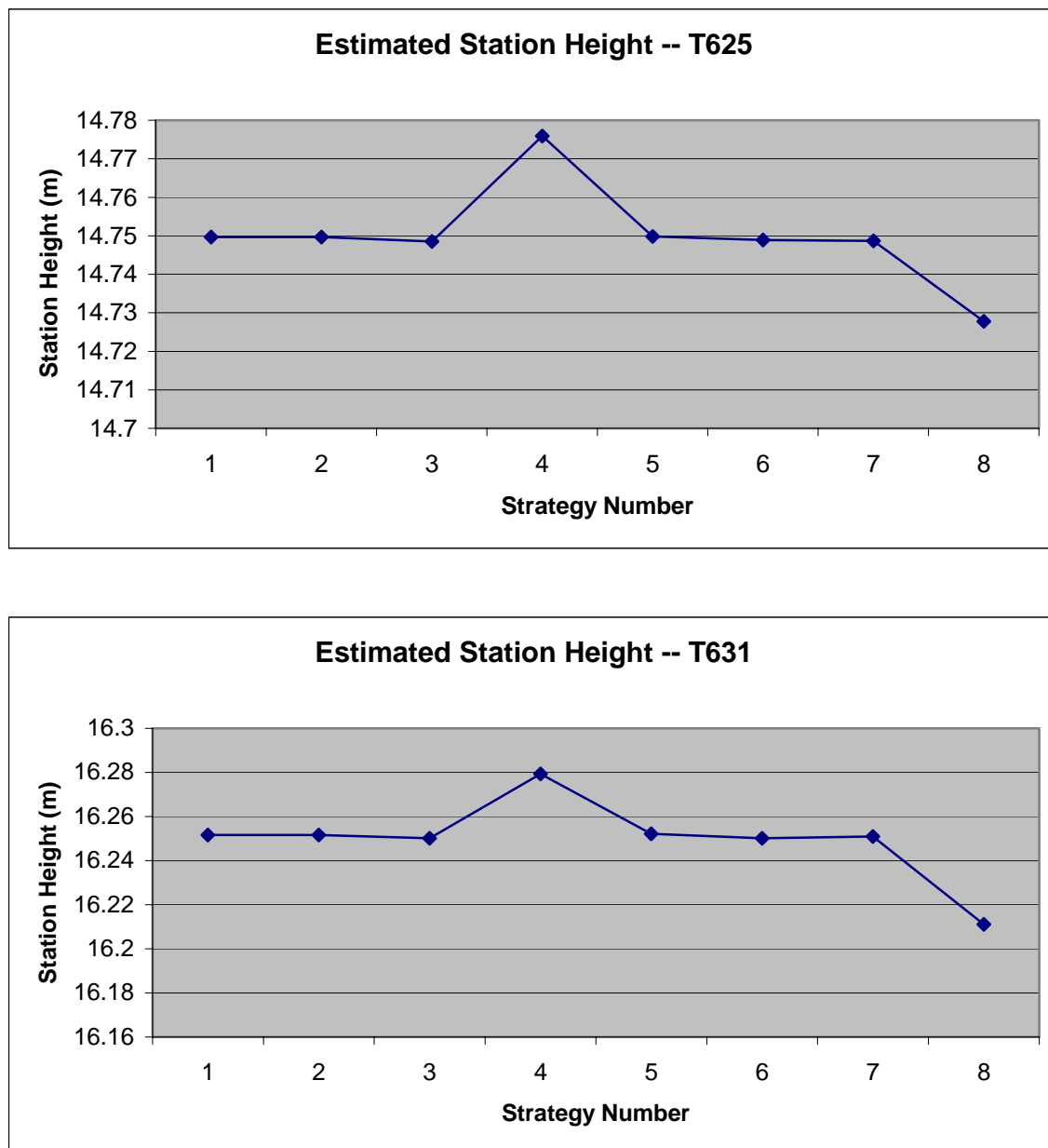


Figure 5.6 Estimated station height for T625 (above) and T631 (bottom) using different tropospheric parameter estimation strategies

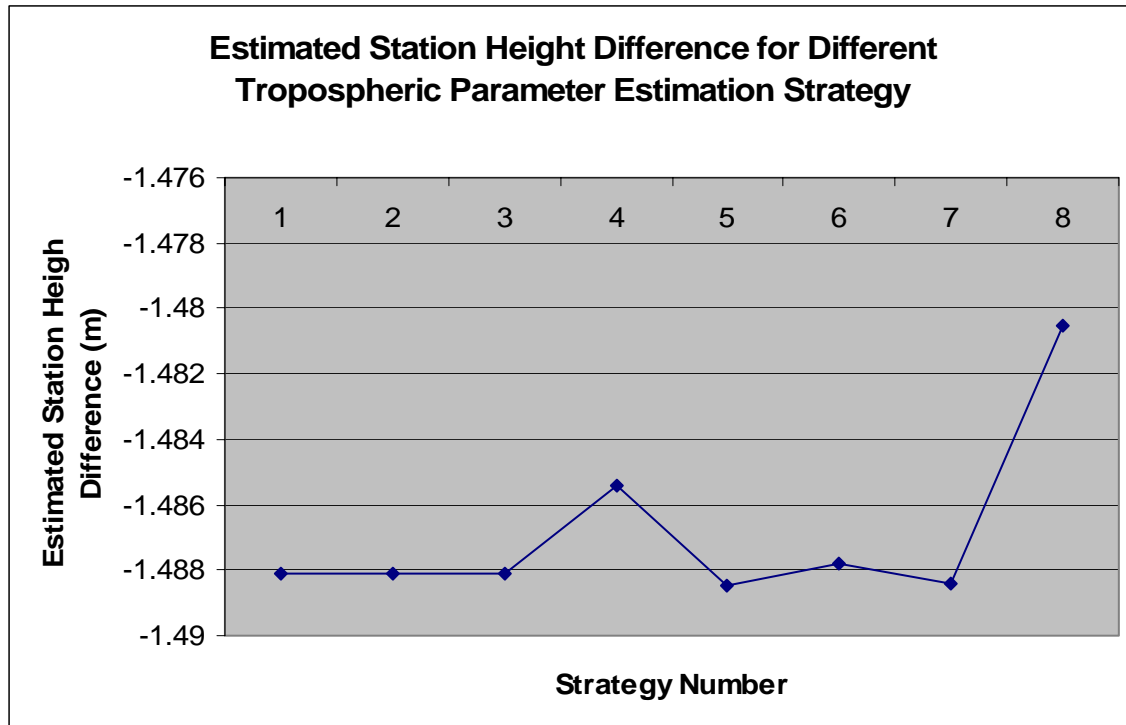


Figure 5.7 Estimated station height differences for two baselines (INVK to T625 and INVK to T631) using different tropospheric parameter estimation strategies

However, since true absolute height information for stations T625 and T631 is lacking, it is difficult to tell which tropospheric parameter estimation strategy gives the best result. Based on the processing results for different processing options, several observations were made:

- The results show that there was no significant difference between the Saastamonien model combined with $\cos Z$ mapping function, and no *a priori* model with the Neill mapping function (with only a 2 mm difference in the estimated station height). These two sets of tropospheric models and mapping functions are the recommended combination by the Bernese group.

- The *a priori* sigma value for absolute zenith delay constrains individual tropospheric parameters to the *a priori* model value. While the *a priori* sigma value for the relative zenith delay constrains the difference between two subsequent tropospheric parameters of the same station to zero. In other words, the absolute *a priori* sigma defines the variation of each individual tropospheric parameter with respect to the value given by the *a priori* model and the relative *a priori* sigma defines the variation of these tropospheric parameters over time. By observing the result, the selection of absolute/relative *a priori* sigma had no significant influence on the height estimates. However, it has a great influence on the estimated tropospheric parameters. The recommended value in Bernese is 5 m for both absolute and relative *a priori* sigma, and 0.012 m is the relative *a priori* sigma value used by some other researchers (Hoyle, 2004). If high precision tropospheric parameters are to be estimated, the absolute and relative *a priori* sigma values have to be carefully selected.
- Estimating residual zenith delay on both the base and rover station gave better results, especially when using the no *a priori* model with the Neill mapping function.
- High resolution estimation (for example every half an hour) for residual zenith delay parameters is not recommended since this may absorb other error sources, such as multipath and noise, into the height estimate, with 1-2 hours recommended

in most cases. In all cases for this project, 2-hours resolution was used except in the case of the 1-hour session where a 1-hour resolution was employed.

- Interestingly, based on the estimated station height difference results, estimating station height without estimating residual tropospheric parameters gives the best result (2 mm difference compared to the levelling result). However, when looking at the estimated station height, the result from Strategy 8 was biased from the other results. In this case, the estimated station height difference may have delivered incorrect information.

Based on similar analyses of all 15 baselines, the most appropriate strategy was determined to be tropospheric estimation Mode three in Table 5.6 in all cases. This tropospheric delay estimation strategy was then used in all the following analysis.

5.8 Multipath

In order to characterize the multipath signal in the collected data, the IF fixed solution double difference residuals from the same satellite-pair during four 12-hour sessions (same period of time on four consecutive days) on one of the benchmarks in the test site were plotted (Figure 5.8). These double difference residuals have been smoothed to reduce noise using a 3-epoch moving-average filter that improved the correlation statistics (shown in Figure 5.9). Day-to-day correlation was found to be in the range of 0.5 – 0.7 at around 4 minutes (a sample rate of 30 seconds was necessary since that is the rate of the IGS base-station).

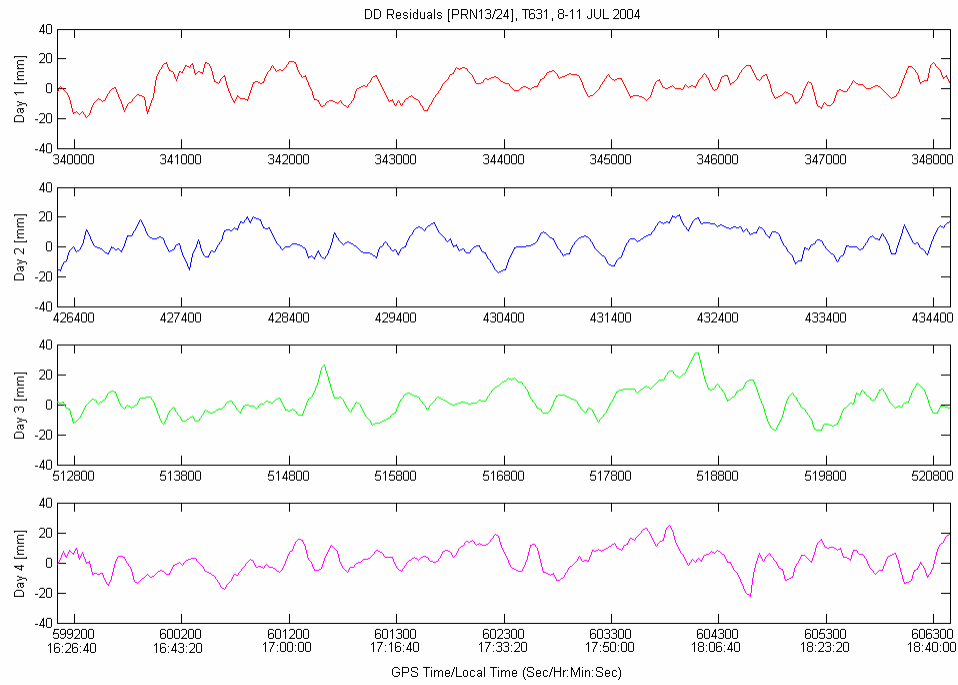


Figure 5.8 Smoothed residuals for four 12-hour sessions on one station within the tree-line environment

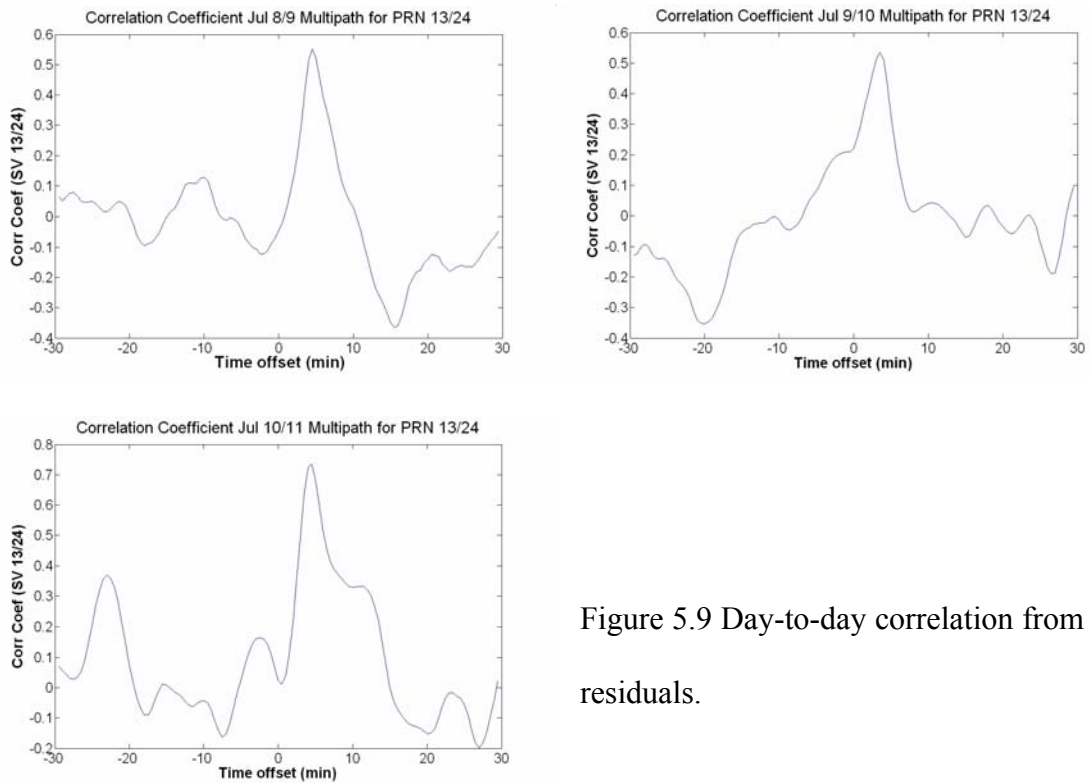


Figure 5.9 Day-to-day correlation from the residuals.

The calculated correlation coefficient is not as high as expected. There may be several reasons for this. First of all, the reported double difference residuals may contain other errors beside multipath error, such as residual tropospheric error. Second, as can be seen from Figure 5.2, there do not appear to be strong reflectors at the test site. Reflections are mainly from the ground and trees, in which case the satellite-reflector-antenna geometry is not stable over time. Last, the correlation time for two consecutive days is 23 hr 55 min 48 sec (one sidereal day) in theory. Radovanovic (2000) reported that this correlation period is stable to ± 10 seconds. Since only data of 30 seconds sampling rate were used, a correlation time of 4 minutes is reasonable in this case.

The developed multipath mitigation via the day-to-day correlation algorithm shown in Section 4.2 was then applied to the data collected at the test site. However, the assumptions made in the developed multipath mitigation algorithm no longer stand true. When applied to the 15 km baselines, the double differenced tropospheric and ionospheric errors can not be neglected in Equation (4.1). As shown in Equation (5.1), the output from the multipath mitigation algorithm now becomes:

$$\begin{aligned}
\Phi_{clean} &= \Phi^2 - (\Phi^1 - \rho^1 - \delta t_{rec}^{est1}) \\
&= (\rho^2 + \frac{c}{\lambda} \delta t_{sat}^2 - \frac{c}{\lambda} \delta t_{rec}^2 - I^2 + T^2 + m^2 + n^2 + N^2) \\
&\quad - \left(\begin{array}{l} \rho^1 + \frac{c}{\lambda} \delta t_{sat}^1 - \frac{c}{\lambda} \delta t_{rec}^1 - I^1 + T^1 + m^1 + n^1 + N^1 \\ -\rho^1 - \frac{c}{\lambda} \delta t_{rec}^{est1} \end{array} \right) \\
&= \rho^2 + \frac{c}{\lambda} (\partial t_{sat} - \partial t_{rec} + \delta t_{rec}^{est1}) - (I^2 - I^1) + (T^2 - T^1) + \partial n + \partial N
\end{aligned} \tag{5.1}$$

where I^1 and I^2 are the ionospheric error in metres on Days 1 and 2, respectively, and T^1 and T^2 are the tropospheric errors in metres on Days 1 and 2. All the other terms have been previously explained.

Fortunately, since IF combinations were used for data processing on the 15 km baselines, the difference between two day's ionospheric error, $(I^2 - I^1)$, can be eliminated. On the other hand, the difference between two day's tropospheric error, $(T^2 - T^1)$, cannot be easily eliminated. Thus, the whole term, $(T^2 - T^1)$, was treated as an unknown parameter to be estimated together with station coordinates. However, no tropospheric model can be applied during data processing in this case. Therefore, no *a priori* model and Neill mapping function were used for data processing. Figure 5.10 show the IF fixed DD residuals for two consecutive days and that of Day 2 after applying the multipath mitigation algorithm for satellite pair PRN20/25 on benchmark T625.

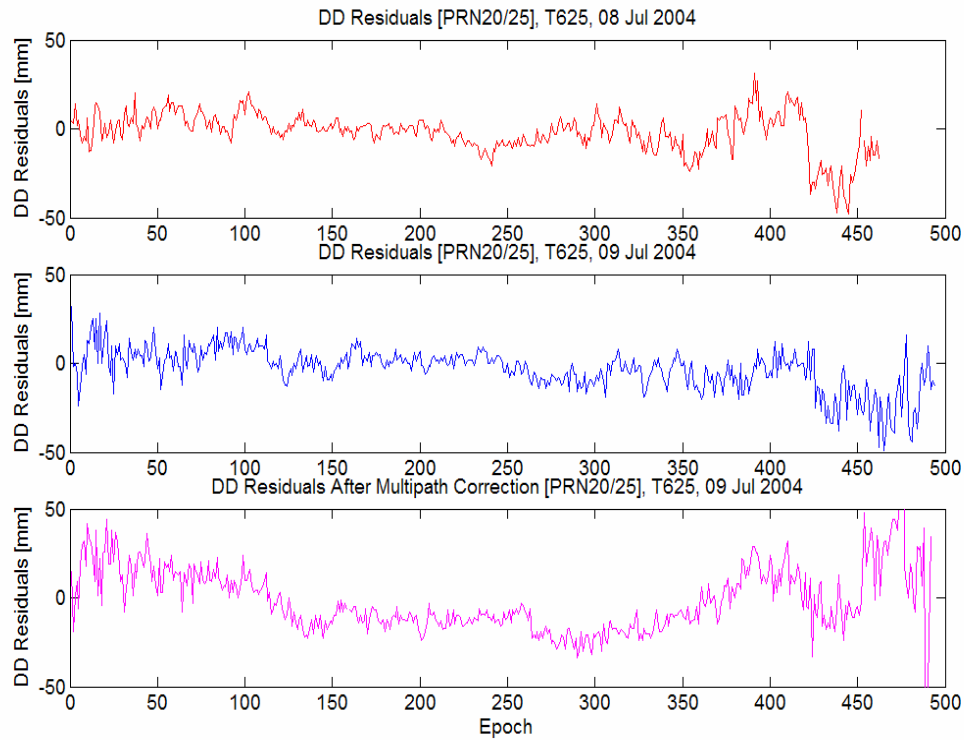


Figure 5.10 IF fixed DD residuals for two consecutive days and that of the Day 2 after applying the multipath mitigation algorithm

As can be seen from Figure 5.10, the residuals after applying the multipath mitigation algorithm have been contaminated, which means the multipath mitigation algorithm implied incorrect multipath corrections to the original Day 2 GPS data. The problem becomes complicated because the tropospheric and ionospheric errors cannot be completely removed after double differencing when encountering long baselines (>1 km depending on local atmospheric conditions). Further research is needed to assess these impacts on various baselines.

As has been discussed in Section 4.2, averaging (or long term filtering) over a long period of time is another efficient method for carrier phase multipath mitigation. It can be expected that the impact of multipath on the positioning accuracy became insignificant after batch processing over 12-hours worth of data. This is confirmed by calculating the mean value of the generated IF fixed DD residuals for each satellite pair. All the mean values are less than 1 mm.

5.9 Repeatability Analysis

In the summer 2004 campaign, all the measured benchmarks were occupied twice. Moreover, there was always one GPS receiver held fixed to connect between sessions. Therefore, four of the six measured benchmarks were occupied four times. A repeatability analysis can be used as an external check for GPS positioning accuracy in the target area.

Table 5.7 summarizes the four days' station coordinates from Bernese for station T631 using mode 3 in Table 5.6. The coordinates for Days 2-4 are given as differences with respect to the estimated coordinates for Day 1. Since it is unlikely that any deformation happened during this four-day period, the repeatability of the estimated station coordinates represents the GPS position accuracy in the target area.

As can be seen from the table, the variation of the four days station coordinates estimation is below 1 cm. In particular, the horizontal variation of the estimated station coordinates is less than 2 mm. Throughout this thesis, since no horizontal ground truth

was gathered for the measured benchmarks, the analysis is unable to determine the planimetric positioning accuracy of GPS in the target area. The repeatability analysis provides an accuracy measure for GPS positioning. On the other hand, the variation of the estimated station coordinates in the height component is slightly larger, at around 7 mm. This is in agreement with the results when using precise levelling as an external accuracy measure for the GPS estimated station height in Section 5.9 (see Table 5.8).

Table 5.7 Four days' station coordinates from Bernese for station T631 using mode 3 in Table 5.6. The coordinates for Days 2-4 were all given in the difference with respect to the coordinates for Day 1 in metres.

	Day 1	Day 2	Day 3	Day 4
X (m)	-1627743.9304	+0.0005	-0.0002	+0.0020
Y (m)	-1699512.0374	+0.0005	+0.0002	+0.0010
Z (m)	5908272.8158	+0.0008	-0.0039	-0.0069
Lat	68 24 52.272771	+0.0009	-0.0014	-0.0005
Lon	-133 45 51.607776	+0.0001	-0.0003	+0.0007
Height (m)	16.2421	+0.0005	-0.0036	-0.0072

From the above repeatability analysis, it can be concluded that the positioning accuracy of GPS in the target area is approximately 2 mm in the horizontal and 7 mm in the vertical.

5.10 Developing the Best Strategy

From the foregoing results and analysis, the proposed strategy for field survey and data processing would be:

1. Processing using mode 3 (Table 5.6),
2. Using the same type of rover antenna throughout the campaign to avoid uncorrected PCV effects,
3. Using GPS receivers adopting semi-codeless tracking technology to avoid significant loss of track problem in the target area,
4. Using a 15° cut-off angle, which gave the best balance between satellite geometry and errors due to different path lengths for both 15 km and 130 km baselines on days of both low- and high- ionospheric activity,
5. EDW correction switched off, since it was found to have insignificant or even deleterious effects on the levelling results.

After processing all collected data using the most appropriate strategy developed in Section 4.3, the results were compared with the levelling measurements collected in the summer 2004. For comparison purposes, the processing results from both the 2003 and 2004 campaigns were shown in Table 5.8.

By examining the GPS height estimation using precise levelling results, the attainable accuracy of GPS positioning in the height component by adopting the developed best strategy for data collection and processing was found to be 2 mm with a standard deviation of 8 mm. As has been found in the stability analysis of different survey

monuments, the best monument type (conclusion 1) changes only 5-10 mm over 17-year period of time (Tait *et al*, 2004). After applying the error propagation law, the combination of the developed best strategy for ‘GPS levelling’ and the best monument type is capable of detecting 1 cm movement. After applying the same congruency analysis (95% confidence, Fisher test for 1D and assuming a known probability density function [PDF]) as that in Section 3.1, the combination of ‘GPS levelling’ with this 1σ observation accuracy of 1 cm is only capable of finding 28 mm movement on a annual basis. It will take 5-6 years to find movement of 5 mm per year. But it can still be used as an early warning system for subsidence higher than expected.

Table 5.8 Summarized results for the comparison between GPS height solution and the external accuracy measures for 2003/2004 campaign

Observation set	# of baselines	External accuracy measures	Difference with external accuracy measures	
			Mean (mm)	Standard deviation (mm)
2003 (15km)	26	Differential levelling (Reduced level estimated accuracy 0.02mm 1σ)	0.7	12.8
2004 (15km)	24	Differential levelling (RL 1.1mm 1σ)	2.0	8.5
2004 (130km)	2	IGS weekly average coordinates	1.5	3.5

With this strategy applied, there might still be a balance to be struck between the length of occupation (and processing period), the time required to average the residual path

effects that exist, and the levelling accuracy. Table 5.9 shows the results of processing using the recommended strategy for the 15 km and 130 km baseline data from days of low and high ionospheric activity. Columns under each baseline length show the mean and standard deviation differences compared to differential levelled results (15 km) and weekly average IGS height coordinates (130 km).

Table 5.9 Variation in accuracy (and standard deviation of grouped baselines) with occupation length for days of low and high ionospheric activity.

Occupation length (hours)	15 km (low)		15 km (high)		130 km (low)		130 km (high)	
	Mean (mm)	Sd (mm)	Mean (mm)	Sd (mm)	Mean (mm)	Sd (mm)	Mean (mm)	Sd (mm)
12	1.7	-	-1.9	-	2.2	-	2.7	-
6	2.4	2.2	-2.7	2.6	-2.1	0.4	2.6	7.7
4	2.7	2.7	-2.3	2.3	-2.0	1.2	2.6	5.2
3	1.9	2.7	-3.1	3.1	-2.7	1.4	2.3	6.2
2	2.0	2.9	-3.2	5.1	-1.9	2.3	2.4	6.2
1	-11.6	25.1	-24.0	46.8	-4.4	13.6	-6.8	20.5

Note: 15 km baselines were compared to differential levelling, 130 km baselines were compared to weekly IGS coordinates.

The results in Table 5.9 are for only two baselines for each distance (the baselines measured on the two days chosen for comparison of the ionospheric effects), and the variations in standard deviation for the 15 km baselines should be seen in the context of the reported differences in Table 5.8 that represent the results from multiple baseline sets.

So, for the standard deviation of 8.5 mm given in Table 5.8, the standard deviation can be expected to increase marginally with decreasing occupation length up until the 1-hour session, when large increases in standard deviation are evident. The results for the 130 km baselines incorporate the estimation of only one parameter, so the standard deviations would be expected to be better than in the 15 km differential case where two rover stations are varying. With the chosen strategy, the effect of high ionospheric activity is minimal until 2 hours for the 15 km baselines, but the effect on the 130 km baseline is evident throughout. So, for baselines of this length it is recommended that the survey be planned on a day of relative inactivity according to on-line data at the Geological Survey Canada (http://www.geolab.nrcan.gc.ca/myservlet/geomag/magnetogram/dataplot_geomagg_e.jsp).

CHAPTER 6

CONCLUSIONS AND RECOMMENDATIONS

The contribution of this research was to find the attainable positioning accuracy of GPS, especially for the height component, in the far North of Canada. By studying the feasibility of replacing precise levelling with GPS for permafrost deformation monitoring, the attainable ‘GPS levelling’ accuracy under poor satellite geometry and intense ionospheric activity was investigated. At the same time this research quantified, for the first time, the stability of monuments in permafrost, which knowledge plays a important role not only in the future analysis of movement due to oil and gas extraction and hence its affect on the environment, but also in the analysis of climate change effects in permafrost areas where stable stations over long periods is required.

The feasibility study of replacing precise levelling with GPS for permafrost deformation monitoring has been carried out by investigating the impact of different error sources on the accuracy of GPS positioning in the target area. An analysis of the results led to the development of an optimised strategy for data capture and processing for the target area.

Based on the research, the following conclusions address the findings in both the long term stability study of different survey monument in permafrost and the feasibility of replacing precise levelling with GPS for permafrost deformation monitoring.

6.1 Conclusions

The following conclusions have been made to the foregoing research:

1. It has been found that the use of solid ground rods founded at 5.5 m or deeper will display similar movement pattern which is independent of the geological conditions in which they are founded. These types of benchmarks are therefore recommended for long-term monitoring.
2. The estimated station height error introduced by the uncorrected antenna PCV in the IF solution for a 5 m baseline measured using different antenna type at base and rover station was at 1 cm level. The influence of this type of error source can be enlarged if different types of antenna were used. To avoid this problem, it is recommended to use only one type of antenna for data collection.
3. Significant loss-of-track problems were found in the Trimble 4000SSI receivers, which adopts codeless technology to track the L2 signal. It is much better in the case of Ashtech Z-12 receivers which adopt semi-codeless technology. It is recommended to use GPS receivers adopting semi-codeless technology for data collection in the target area. Of course, this will be mitigated when the L2C is available.
4. An elevation dependent weighting scheme is not recommended for data processing, since it was found to have insignificant or even deleterious effects on the levelling results.
5. The best cut-off angle used for data processing was found to be 15 degrees, balancing longer-path observations (and higher associated atmospheric errors) against the geometry of the satellite constellation.
6. By processing two 130 km baselines in both a low- and high- ionosphere conditions, no accuracy degradation was found on the station height estimation

- for a 12 hour occupation. However, when shortening the occupation length to 6 hours or less, a degradation in positioning accuracy is evident.
7. The best tropospheric delay estimation strategy was found by making use of measured station height differences from precise levelling to examine the station height estimation from GPS using different tropospheric delay estimation strategies. Mode 3 in Table 5.6 was recommended for data processing. In Mode 3, Saastamoinen tropospheric model and cosZ mapping function are used to model the tropospheric error. The residual tropospheric error is estimated every 2 hours along with other unknown parameters at both base and rover stations.
 8. A multipath mitigation algorithm which uses day-to-day correlation has been implemented and is based on Radovanovic's algorithm. This algorithm has shown its success on short baseline (< 1 km) applications. However, it is not successful on long baselines (> 1 km) under the conditions tested in this research. This algorithm needs to be further investigated for long baseline applications. It is found from the analysis that averaging (or long term filtering) over long period of time is another efficient method for carrier phase multipath mitigation.
 9. Repeatability analysis was used as an external check for GPS positioning accuracy in the target area. It was found from the repeatability analysis that the positioning accuracy of GPS in the target area is approximately 2 mm in the horizontal and 7 mm in the vertical.
 10. By examining the GPS height estimation using precise levelling results, the attainable accuracy of GPS positioning in the height component by adopting the developed best strategy for data collection and processing was found to be 2 mm

with a standard deviation of 8 mm. As has been found in the stability analysis of different survey monuments, the best monument type (conclusion 1) changes only 5-10 mm over 17-year period of time (Tait *et al*, 2004). After applying the error propagation law, the combination of the developed best strategy for ‘GPS levelling’ and the best monument type is capable of detecting 1 cm movement. After applying the same congruency analysis (95% confidence, Fisher test for 1D and assuming a known probability density function [PDF]) as that in Section 3.1, the combination of ‘GPS levelling’ with this 1σ observation accuracy of 1 cm is only capable of finding 28 mm movement on a annual basis. It will take 5-6 years to find movement of 5 mm per year. But it can still be used as an early warning system for subsidence higher than expected.

6.2 Recommendations

Based on the results of this research, the following recommendations regarding improvement of the positioning accuracy of GPS in the target area are drawn:

1. Since the significant impact of uncorrected antenna PCV has been identified, the mitigation of this error source should be further investigated. The latest technology is to calibrate absolute antenna PCV based on the use of an orientated antenna and the use of special observation differences. However, this type of product is not yet available for distribution. The performance of this type of product needs to be evaluated.
2. Since the multipath mitigation via day-to-day correlation algorithm is not successful in long baseline applications, this algorithm need to be further

- investigated. Averaging (or long term filtering) can be used as an alternative for carrier phase multipath mitigation, in which case long term occupation was needed. In addition, if available, it is recommended to use choke ring antenna for data collection.
3. The satellite geometry problem of GPS for the target area has been identified in section 3.2.4. Recent work (O'Keefe, 2001) has shown that the combination of GPS and Galileo can greatly improved the global satellite availability and satellite geometry, especially for the target area. Therefore, it is recommended to investigate the use GPS/Galileo combination in the future.
 4. The current L2 GPS measurements by survey-grade receivers are noisier and less continuous than those expected to be made on the new L2C signal. With the new L2C signal to be launched on Sept 21, 2005, the need to measure L2 using codeless technique will have passed, and the reliability of dual frequency operation will be enhanced (Rizos et al, 2005).

REFERENCES

Alves, P., G. Lachapelle, M.E. Cannon, J. Park, P. Park (2002). Use of Self-constrained Ionospheric Modelling to Enhance Long Baseline Multiple Reference Station RTK Positioning, Proceedings of ION GPS-02, September 24-27, 2002, Portland, Oregon, pp. 1388-1399.

Berry, R.M. (1976). History of Geodetic Levelling in the United States. Surveying and Mapping, Vol. XXXVI, No.2, pp. 137-153.

Beutler, G. (1992). The Impact of the International GPS Service for Geodynamics on the Surveying and Mapping Community. In: International Union of Surveying and Mapping (IUSM) Presented papers of the Working Group Sessions, pp. 84-94.

Biacs, Z.F. (1989). Estimation and Hypothesis Testing for Deformation Analysis in Special Purpose Networks. Master Thesis, Department of Geomatics Engineering, University of Calgary, Alberta, Canada, UCGE Reports Number 20032.

Braasch, M.S. (1996). Multipath Effects, in Global Positioning System: Theory and Applications Volume 1, Eds. Parkinson, B., Spiker, J., Axelrad, P, Enge, P., American Institute of Aeronautics and Astronautics, pp. 547-568.

Brunner F.K., Hartinger H., and Troyer L. (1999). GPS Signal Diffraction Modelling: The Stochastic SIGMA- Δ Model. *Journal of Geodesy* 73: pp. 259-267

Caspary, W. (1987). Concepts of Network and Deformation Analysis. University of New South Wales. Monograph No. 11, Kensington, N.S.W.

Cannon, M.E. and Lachapelle, G. (2003). GPS Positioning, ENGO 561 Lecture Notes, Department of Geomatics Engineering, The University of Calgary, Calgary, Alberta.

Chen, D. and Lachapelle, G. (1994), A Comparison of the FASF and Least-Squares Search Algorithms for On-the-Fly Ambiguity Resolution. *Journal of the Institute of Navigation*, Vol. 42, No.2, pp. 371-390.

Collins, J. (1989). The Satellite Solution to Surveying. *Professional Surveyor*. No. 2. Vol. 6. pp. 12-17.

Counselman, C., Shapiro, I., Greenspan, R., Cox, D. (1979). Astronomical application of differential interferometry. *Science*, No. 178. pp. 607-608.

Francisco, S.G. (1996). GPS Operational Control Segment. In: *Global Positioning System : Theory and Applications : Volume 1*. Parkinson, B. and Spilker, J., eds. American Institute of Aeronautics and Astronautics. pp. 435-465.

Fotopoulos, G. (2003). An Analysis on the Optimal Combination of Geoid, Orthometric and Ellipsoidal Height Data. PhD Thesis, Department of Geomatics Engineering, University of Calgary, Alberta, Canada, UCGE Reports Number 20185.

Fortes, L. (2002). Optimising the Use of GPS Multi-Reference Stations for Kinematic Positioning. PhD Thesis, Department of Geomatics Engineering, University of Calgary, Alberta, Canada, UCGE Reports Number 20158.

Gareau, R.M. (1986): History of Precise Levelling in Canada and The North American Vertical Datum Readjustment. MSc Thesis, Department of Geomatics Engineering, University of Calgary, Alberta, Canada, UCSE Reports Number 20018.

Gili, J.A., Corominas, J. and Rius, J. (2000). Using Global Positioning System Techniques in Landslide Monitoring, Engineering Geology, Vol 55, pp. 167-192.

Guo, J. and Ge, S. (1997). Research of Displacement and Frequency of Tall Building under Wind Load Using GPS. In: Proceedings of the 10th International Technical Meeting of the Satellite Division of the Institute of Navigation. pp. 1385-1388.

Hartinger, H., Brunner, F.K. (1998). Experimental detection of deformations using GPS. In : Kahmen H, Brückl E, Wunderlich T (eds) Geodesy for Geotechnical and Structural Engineering. Proc. IAG Special Commission 4 Symposium Eisenstadt, pp. 145-152.

Hartinger H, Brunner FK (1999) Variances of GPS Phase Observations: The SIGMA- ϵ Model. GPS Solutions 2/4: pp. 35-43.

Hartinger, H., Brunner, F.K. (2000). Development of a monitoring system of landslide motions using GPS. In: Proc 9th FIG Symposium on Deformation Measurements, Olsztyn, Sept. 1999, pp. 29-38.

Hedling, G., Jonsson, B., Lilje, C., and Lilje, M. (2001). SWEPOS – The Swedish Network of Permanent GPS reference Station (Status February 2001). International Conference on New technology for a New Century. FIG Working Week 2001. 6-11 May 2001. Seoul, Korea.

Heiskanen, W.A. and Moritz, H. (1967). Physical Geodesy. W.H. Freeman and Company San Francisco.

Hofmann-Wellenhof, B., Lichtenegger, H. and Collins, J. (2001). GPS: Theory and Practice. Second Edition. Springer-Verlag.

Hopfield, H.S. (1970). Tropospheric Effect on Electromagnetically Measured Range: Prediction from Surface Weather Data, Applied Physics Laboratory, Johns Hopkins University, Baltimore, MD.

Hopfield, H.S. (1972). Tropospheric Range Error Parameters-Further Studies, Applied

Physics Laboratory, Johns Hopkins University, Baltimore, MD.

Hoyle, V.A. (2004). Personal communication.

Hudnut, K.W. (1996). Continuous GPS monitoring of dam deformation. EOS, Trans. AGU, 77, No. 46, pp. F139.

Hudnut, K.W. and Behr, J.A. (1998). Continuous GPS monitoring of structural deformation at Pacoima Dam, California, Seismological Research Letters, 69, No. 4, pp. 299-308.

Hugentobler, U., S. Schaer, P. Fridez (2001). Bernese GPS Software Version 4.2. Astronomical Institute, University of Berne.

ICD-GPS-200C (2003). Navstar GPS Space Segment / Navigation User Interfaces., Revision C. GPS NAVSTAR JPO. January, 2003.

Janssen, V., Roberts, C., Rizos, C., and Abidin, H. (2001). Experiences with a mixed-mode GPS-based volcano monitoring system at Mt. Papandayan, Indonesia. Geomatics Research Australasia, 74, pp. 43-58.

Kaplan, D (1996). Understanding GPS Principles and Applications, Artech House Publishers, Boston, pp. 351.

Kenselaar, F. and Quadvlieg, R. (2001). Trend Signal Modelling of Land Subsidence. Proceedings of the 10th International Symposium on Deformation Measurements, Orange, California, USA, 19-22 March, 2001.

Klobuchar, J.A. (1986). Design and Characteristics of the GPS Ionospheric time-delay algorithm for single-frequency users. In : Proceedings of PLANS'86-Position Location and Navigations symposium, Las Vegas, Nevada, November, pp. 280-286.

Klobuchar, J.A., Doherty, P.H., and El-Arini, M.B. (1995). Potential Ionospheric Limitations to GPS Wide Area Augmentations System. In: Navigation, Journal of the Institute of Navigation, Vol 42. 1995.

Klobuchar, J.A. (1996). Ionospheric Effects on GPS. In: Global Positioning System, Theory and Application, Vol 1, Eds, Parkinson, B. and Spilker, J., American Institute of Aeronautics and Astronautics, Inc., pp. 485-514.

Knight, M., Cervera, M., Finn A. (1999). A comparison of predicted and measured GPS performance in an ionospheric scintillation environment. Proceeding ION GPS-99, September 14-17 Nashville, TN, pp. 1437-1450.

Lachapelle, G. and Cannon, M.E. (2004). GPS Theory and Applications. ENGO 625 Lecture Notes. Department of Geomatics Engineering, The University of Calgary.

Langley, R. (1997). GPS Receiver System Noise. GPS World. June 1997. pp. 40-45.

Lanyi, G. (1984). Tropospheric Delay Effects in Radio Interferometry, Telecommunications and Data Acquisition Progress Rep., Jet Propulsion Lab, Pasadena, CA.

Mackay, J., Ostrick, J., Lewis, C., Machay, D. (1979). Frost heave at ground temperatures below 0 °C, Inuvik, Northwest Territories. Paper- Geological Survey of Canada 79-1A, pp. 403-406.

Mader, G. (1999). GPS Antenna Calibration at the National Geodetic Survey. GPS Solutions, Vol. 3, No. 1, Summer 1999, Wiley.

Meng, X., Roberts, G.W., Dodson, A.H., Cosser, E., Barnes, J., and Rizos, C. (2004). Impact of GPS satellite and pseudolite geometry on structural deformation monitoring: analytical and empirical studies. Journal of geodesy, 77, pp. 809-822.

Menge, F., G. Seeber, C. Völksen, G. Wübbena, M. Schmitz (1998). Results of Absolute Field Calibration of GPS Antenna PCV, In: Proceedings of the 11th International Technical Meeting of the Satellite Division of the Institute of Navigation ION GPS-98, September 15-18, Nashville, Tennessee, 1998.

Moorman, B. and P. Vachon. (1998). Detecting ground ice melt with interferometric synthetic aperture radar. 20th Canadian Symposium on Remote Sensing, Calgary, Alberta, May 10-13, 1998.

Moorman, B., Vachon, P., Sjogren, D. (2003). Monitoring permafrost degradation and ground surface movement with interferometric synthetic aperture radar. Proceedings, 8th International Conference on Permafrost, Zurich, July 21-25, 2003.

Muller, S.W. (1943). Permafrost or permanently frozen ground and related engineering problems. U.S. Army, Office Chief of Engineers, Military Intelligence Div. Strategic Eng. Study 62, pp. 231. (Also 1947, Ann Arbor, Mich., Edwards Bros.)

Nichols, J.A., Hansen, A., Walter, T., Enge, P.K. (1999). High latitude measurements of ionospheric scintillation using the NSTB. Proceeding ION Nat Tech Meeting, January 25-27 San Diego, CA, pp. 789-798.

O'Keefe, K. (2001). Availability and Reliability Advantages of Galileo/GPS Integration. Proceedings of the Satellite Division of the Institute of Navigation 14th International Technical Meeting (September 11-14, 2001, Salt Lake City, Utah), pp. 2096-2104.

Parkinson, B.W. (1996). GPS Error Analysis, in Global Positioning System: Theory and Applications Volume 1, Eds. Parkinson, B., Spiker, J., Axelrad, P., Enge, P., American Institute of Aeronautics and Astronautics, pp. 469-483.

Radovanovic, R.S. (2000). High Precision Deformation Monitoring by Multipath Mitigation via Day-To-Day Correlation Analysis. Proceedings of ION-GPS 2000, Salt Lake City, September 10-15.

Radovanovic, R.S. (2002). Adjustment of satellite-based ranging observations for precise positioning and deformation monitoring. PhD Thesis, Department of Geomatics Engineering, University of Calgary, Alberta, Canada, UCGE Reports Number 20166.

Raquet, J. (1998), Development of a Method for Kinematic GPS Carrier-Phase Ambiguity Resolution Using Multiple Reference Receivers. Ph.D. Thesis, University of Calgary, Department of Geomatics Engineering Report Number 20116, Calgary 1998.

Ray, J.K. (2000). Mitigation of GPS Code and Carrier Phase Multipath Effects Using a Multi-Antenna System. PhD Thesis, Department of Geomatics Engineering, University of Calgary, Alberta, Canada, UCGE Reports Number 20136.

Remondi, B. (1984). Using the Global Positioning System Phase Observable for Relative Geodesy : Modelling, Processing and Results. Ph.D. Dissertation. Austin: Centre for Space Research, University of Texas at Austin.

Rempel, G. (1970). Arctic terrain and oil field development. Proceedings of the American Geological Institute Conference on Productivity, pp. 243-251

Rizos, C. (1999). Satellite Ephemeris Bias. Principles and Practice of GPS Surveying. The University of New South Wales, Sydney, Australia. http://www.gmat.unsw.edu.au/snap/gps/gps_survey/chap6/6212.htm (last updated: 18 January 2000)

Rizos, C., Higgins, M., and Hewitson, S. (2005). New GNSS Developments and their Impact on Survey Service Providers and Surveyors. Proceedings of SSC2005 Spatial Intelligence, Innovation and Praxis: The national biennial Conference of the Spatial Sciences Institute, September 2005. Melbourne: Spatial Sciences Institute. ISBN 0-9581366-2-9.

Roberts, C. and Rizos, C. (2001). Mitigating differential tropospheric effects for GPS-based volcano monitoring. In: proceedings of the 5th Symposium on Satellite Navigation Technology and Applications, Canberra, Australia, 24-27 July, paper 38, CD ROM proceedings.

Rostoker, G. and Skone, S. (1993). Magnetic flux mapping considerations in the auroral oval and the Earth's magnetotail. *J Geophys Res* 98(A2): pp. 1377-1384.

Roulston, A., Nicholas, T., Zhang, k. (2000). An Evaluation of Various GPS Satellite Ephemerides, In Proceedings of ION GPS 00, Salt Lake City, pp. 45-54.

Saastamoinen, J. (1972). Atmospheric Correction for the Troposphere and stratosphere in Radio Ranging of Satellites, Geophysical Monograph 15, American Geophysical Union, Washington DC.

Seeber, G. (1993) Satellite Geodesy, Foundations, Methods, and Applications. Walter de Gruyter.

Skone, S. (1998). Wide Area Ionosphere Grid Modelling in the Auroral Region, Ph.D. thesis, Department of Geomatics Engineering, University of Calgary, Calgary, AB

Skone, S. and M. de Jong (2000). The Impact of Geomagnetic Substorms on GPS Receiver Performance. In: *Earth Planets Space*, 52, pp. 1067–1071.

Skone, S. (2001). The Impact of Magnetic Storms on GPS Receiver Performance. In *Journal of Geodesy*. 75: pp. 457-468.

Skone, S., K. Knudsen and M. de Jong. (2001). Limitations in GPS receiver tracking performance under ionospheric scintillation conditions. In *Physics and Chemistry of the Earth*, vol. Part A, 26/6-8, pp. 613-621.

Skone, S. (2003). Atmospheric Effects on Satellite Navigation Systems. ENGO 633 Lecture Notes, Department of Geomatics Engineering, The University of Calgary.

Smith, S.L., Burgess, M.M., Heginbottom, J.A. (2001). Permafrost in Canada, a challenge to northern development. In: Brooks, G.R. (ED.), *A synthesis of Geological Hazards in Canada*, Geological Survey of Canada, Bulletin, vol. 548, pp. 241-264.

Spilker, J.J., Jr. (1994). Tropospheric Effects on GPS, in *Global Positioning System: Theory and Applications Volume 1*, Eds. Parkinson, B., Spiker, J., Axelrad, P., Enge, P., American Institute of Aeronautics and Astronautics, pp. 517-546.

Tait, M., Moorman, B. (2003). A feasibility study into monitoring deformation in the Niglintgak region of the Machenzie delta. Proceedings of the 11th FIG Symposium on Deformation Measurement, 25-29 May 2003, Santorini, Greece.

Tait, M. (2004). Geomatics Networks. ENGO 519 Lecture Notes. Department of Geomatics Engineering, The University of Calgary.

Tait, M., Sheng, L., Cannon, M.E. (2004) The feasibility of replacing precise levelling with GPS for permafrost deformation monitoring. Proceedings of the FIG 3rd International Conference on Engineering Surveying, Bratislava, Slovakia, November 11-13.

Tait, M., Moorman, B., and Sheng, L. (2005). The long-term stability of survey monuments in permafrost. Engineering Geology, Vol. 79, pp. 61-79.

Teunissen, P.J.G. and Tiberius, C.C.J.M. (1994). Integer Least-Squares Estimation of The GPS Phase Ambiguities. Proceedings of the International Symposium on Kinematic Systems in Geodesy, Geomatics and Navigation, Department of Geomatics Engineering, The University of Calgary, pp. 221-231.

Wang, Z. and S. Li. (1999). Detection of Winter Frost Heaving of the Active Layer of Arctic Permafrost Using SAR Differential Interferometry. Proceedings of IEEE 1999

International Geoscience and Remote Sensing Symposium 1999 (IGARSS '99). 28 June-2 July, 1999, Hamburg, Germany. pp. 1946-1948.

Wieser, A., Brunner, F.K. (2002). Analysis of Bridge Deformations using Continuous GPS Measurements. INCEO2002, 2nd Conference of Engineering Surveying, Kopáčik A and Kyrinovič P (eds), Bratislava, November 2002, pp. 45-52.

Wooden, W.H. (1985). Navstar Global Positioning System: 1985, Proceedings of the First International Symposium on Precise Positioning with the Global Positioning System, Rockville, Maryland, 1985.

Wübbena, G., Schmitz, M., Menge, F., Böder, H., Seeber, G. (2000). Automated Absolute Field Calibration of GPS Antennas in Real-time. Presented at ION GPS-00, 19-22 September, Salt Lake City, Utah, USA.

Wübbena G., Gagge, A., Boettcher, G., Schmitz, M., Andree, P. (2001). Permanent Object Monitoring with GPS with 1 Millimetre Accuracy. Presented at the International Technical Meeting, ION GPS-01, September 11-14, 2001, Salt Lake City, Utah.

Yunck, T.P. (1993). Coping with the atmosphere and ionosphere in precise satellite and ground positioning. In: Geophys. Monograph 73, Environmental effects on spacecraft positioning and trajectories, AGU, IUGG Vol. 13, pp. 1-16.

APPENDIX 1: A SUMMARY OF THE TYPE OF MONUMENT

#	Type	Depth (m)	Method	Drilling report (June 1987)	Permafrost surface Oct 1987 (m)
621	CCGR	15	D	Permafrost from 0.6m Solid ice 3m – 3.6m Very hard clay 6m – 7.5m Fine / dry clay 12m +	0.2
622	AGR	2	J		0.25
623	CCGR	5.5	D	Permafrost from 0.9m Mud-like clay until 2.5m Heavy ice content 2.5m +	0.25
624	CCGR	9	D	Permafrost from 0.6m High content of small gravel throughout	0.18
625	ReeBar (φ19mm)	0.9	J		0.25
626	SFAP	0.6	J		0.2
627	DBM	14.5	D	Permafrost from 1.5m Frozen clay to 4.5m Ice/clay mix 4.5m – 9m Mostly ice to 14m Frozen clay to 14.5m	>0.45
628	CCGR	8.7	J		0.22
629	CCGR	4.5	J		0.2
630	CCGR	2.7	J		0.2
631	DBM	17.5	D	Permafrost from 0.9m Very dry clay throughout	0.45
632	CCGR	1.8	J		0.2
633	CCGR	1.5	J		0.2
634	AGR	5.5	J		0.4
635	AGR	1.5	J		0.15
636	HELIX	2.5	D	Permafrost from 1.2m Very high moisture content throughout	0.15
637	DBM	8	D	Permafrost from 0.6m Very sticky clay throughout	0.15
638	IPBC	1.5	D	None	0.13
639	DBM	6.9	D	Permafrost from 0.6m High ice content 3m – 4.3m Frozen gravel (?) 4.3m – 4.9m	>0.45
640	IPBC	0.75	D	None	0.25
641	IPBC	0.75	D	None	0.25